Petrogenesis and tectonic significance of Neoproterozoic meta-basites and meta-granitoids within the central Dabie UHP zone, China: Geochronological and geochemical constraints

Yuan Li [a], Yi-Can Liu [a, *], Yang Yang [a], F. Rolfo [b, c] and C. Groppo [b]

[a] CAS Key Laboratory of Crust-Mantle Materials and Environments, School of Earth and Space Sciences, University of Science and Technology of China, Hefei 230026, China

[b] Department of Earth Sciences, University of Torino, Via Valperga Caluso 35, 1-10125 Torino, Italy

[c] C.N.R. – I.G.G., Section of Torino, Via Valperga Caluso 35, 1-10125 Torino, Italy

*Corresponding author. Tel./fax: +86 551 63600367.

E-mail address: liuyc@ustc.edu.cn (Y.-C. Liu)

Abstract

A combined geochemical (whole-rock elements and Sr-Nd-Pb isotopes, zircon trace elements and Hf isotopes) and geochronological (zircon U-Pb ages) study was carried out on the relatively low-grade meta-basites and meta-granitoids from Longjingguan within the central Dabie ultrahigh-pressure (UHP) metamorphic zone, east-central China. Zircon investigations indicate that the meta-basites were formed at ~772 Ma and subsequently experienced granulite-facies metamorphism at ~768 Ma and a later thermal overprint at ~746 Ma, while the meta-granitoids recorded three groups of zircon ages at ca. 819 Ma, 784 Ma and 746 Ma. The meta-granitoids can be subdivided into low-Si and high-Si types, and they were derived from mid-Neoproterozoic partial melting of the Neoarchean and Paleoproterozoic metamorphic basement rocks of the South China Block, respectively. These Neoproterozoic zircon ages are consistent with the protolith ages of the Dabie Triassic UHP meta-igneous rocks. In addition, the low-grade rocks have bulk-rock Pb isotope compositions overlapping with the UHP meta-igneous rocks. Therefore, the low-grade meta-basites and meta-granitoids could be interpreted as counterparts of the UHP meta-igneous rocks in this area, suggesting the same petrogenesis for their protoliths in the Neoproterozoic.

Trace element patterns indicate that the low-grade rocks have better preserved their protolith compositions than their equivalent UHP rocks, and thus they are more suitable for elucidating the Neoproterozoic evolution of the northern margin of the South China Block. Zircon ages combined with geochemical features strongly suggest that the protoliths of the meta-granitoids and meta-basites were formed in a magmatic arc and a continental rifting setting, respectively. More specifically, the granitoids derived from partial melting of Neoarchean and Paleoproterozoic basement materials at ~819 Ma in a magmatic arc setting, whereas the precursors of the meta-basites are products of a continental rifting event at about 784 to 772 Ma. The obtained results provide new geochronological and geochemical constraints for the Neoproterozoic evolution of the northern margin of the South China Block, which can further

51 contribute to the understanding of the breakup of the supercontinent Rodinia.

52

55

1. Introduction

The Dabie orogen located in central China is a continental collision belt with the exposed largest area of coesite- and diamond-bearing ultrahigh-pressure (UHP) metamorphic rocks in the world, and thus it has attracted great research interest in the geologic community during the past decades (e.g., Okay et al., 1989, 1993; Wang et al., 1989; Xu et al., 1992a,b, 2003; Li et al., 1993, 2000; Ames et al., 1996; Rowley et al., 1997; Hacker et al., 1998, 2000; Rolfo et al., 2000, 2004; Zheng et al., 2006; Liu et al., 2007a,b, 2011a,b, 2015; Groppo et al., 2015). Previous studies focused mainly on the Triassic UHP metamorphism and related processes, whereas less attention has been paid to the nature and origin of the protoliths of the UHP rocks (e.g., Ames et al., 1996; Hacker et al., 1998; Zheng et al., 2006). U-Pb dating in magmatic zircon cores demonstrated that the protoliths of the UHP meta-igneous rocks in the Dabie orogen were formed in the Neoproterozoic (e.g., Rowley et al., 1997; Hacker et al., 1998; Liu et al., 2007a,b), likely under a continental rifting setting related to the breakup of the supercontinent Rodinia (Li et al., 2003a,b,c). However, the detailed Neoproterozoic evolutional processes of the area have not been well understood, and the precise onset of the continental rifting is still not well constrained. UHP rocks usually experience complex evolution including interaction with melt and/or fluids that can significantly modify the elemental and isotopic characteristics of the rocks (e.g., Kessel et al., 2005; Hermann et al., 2006; Zheng et al., 2011), making it challenging to reveal their protolith nature and origin.

Apart from the UHP rocks, relatively low-grade metamorphosed rocks have been identified in several localities within the UHP metamorphic zone in the Dabie orogen (e.g., Dong et al., 1997; Gao et al., 2006); these rocks occur as interlayers or tectonic blocks within the UHP units, but yield much lower peak-metamorphic temperatures and pressures. If these rocks can be proved to be counterparts of the UHP rocks that escaped UHP metamorphism, they should be good candidates to reveal the Neoproterozoic evolution of the area. Previous studies about the rocks in the Dabie orogen mainly concentrated on geochronology investigations, while their elemental

4

85 and isotopic signatures have not been studied in detail so far, and their petrogenesis

86 and tectonic setting are still not well constrained.

87 Recently, some relatively low-grade meta-basites and meta-granitoids have been

88 for the first time recognized at Longjingguan, within the central Dabie UHP

89 metamorphic zone (Fig. 1). In this paper we perform integrated investigations on their

90 mineral compositions, whole-rock elements and Pb isotopes, as well as zircon

91 SHRIMP U-Pb dating, REE and Hf isotopes. The aim of the study is to investigate

92 whether the rocks are counterparts of the UHP meta-igneous rocks and, if so, whether

93 the rocks preserved their protolith compositions better than the UHP rocks. These new

94 data are crucial for better understanding the formation and tectonic evolution of the

95 Precambrian basement of the South China Block (SCB), especially the events related

96 to the Neoproterozoic breakup of the supercontinent Rodinia.

97

2. Geological setting and samples

2.1. Geological setting

100 The Dabie orogen located in the middle portion of the

101 Qinling–Tongbai–Dabie–Sulu orogenic belt is formed by the Triassic subduction of

102 the SCB beneath the North China Block (NCB) and exposed the largest area of UHP

103 rocks in the world. The widespread occurrence of coesite- (Okay et al., 1989; Wang et

104 al., 1989) and diamond-bearing (Xu et al., 1992b) rocks in the orogen provides an

105 excellent natural laboratory for investigating evolutional processes of the orogen, as

106 well as formation and exhumation mechanisms of UHP rocks. The orogen is generally

107 divided into five fault-bounded rock units with different metamorphic grades and

108 histories, which are from south to north: the Susong complex zone (SZ), the South

109 Dabie low-T eclogite zone (SDZ), the Central Dabie UHP zone (CDZ), the North

110 Dabie complex zone (NDZ) and the Beihuaiyang zone (BZ) (Xu et al., 2003, 2005;

111 Liu et al., 2005, 2007a,b, 2011a,b; Zheng et al., 2005; Liu and Li, 2008; Li et al.,

112 2017). These five units are separated by the near E-W trending Taihu–Shanlong,

113 Hualiangting–Mituo, Wuhe–Shuihou and Xiaotian–Mozitan faults, respectively (Fig.

1). Although the meta-igneous rocks in the five units exhibit different metamorphic histories, they have similar Neoproterozoic protolith ages reflecting a regional-scale magmatism related to the Rodinia break-up (e.g., Ames et al., 1996; Rowley et al., 1997; Hacker et al., 1998; Liu et al., 2007a,b, 2011a).

UHP index minerals like coesite and diamond were found in different lithologies from the CDZ (e.g., Okay et al., 1989; Wang et al., 1989; Xu et al., 1992b; Schertl et al., 1994; Su et al., 1996; Rolfo et al., 2000, 2004), demonstrating that the CDZ was involved in a deep subduction and experienced Triassic UHP metamorphism as a coherent unit (Xu et al., 1992b, 2003; Li et al., 1993, 2000; Hacker et al., 1998; Rolfo et al., 2004; Liu and Li, 2008). Evidence of UHP metamorphism like coesite pseudomorphs were later discovered also in the low-T eclogites from the SDZ (Li et al., 2004). Eclogites (Wei et al., 1998; Xu et al., 2000; Liu et al., 2001) or eclogite relics (Tsai and Liou, 2000; Xiao et al., 2001) were also recognized in the NDZ, together with diamond inclusion within zircon and other clues of UHP metamorphism (Tsai et al., 2000; Xu et al., 2000, 2003, 2005; Liu et al., 2007b, 2011b). Moreover, the NDZ (Liu et al., 2000; Xie et al., 2001; Liu et al., 2005, 2007a,b, 2011a) and the SDZ (Li et al., 2004) were confirmed to be segments of the Triasic subducted continental crust of the SCB. This implies that the three eclogite-bearing units in the Dabie orogen all experienced the Triassic deep subduction, although they have different lithological and isotopic compositions and metamorphic histories (Liu and Li, 2008).

In recent years, relatively low-grade meta-igneous rocks with Neoproterozoic protolith ages and Triassic metamorphic ages have been recognized within the Dabie-Sulu UHP belt. For example, some meta-igneous rocks in Ganghe provided Rb-Sr isochronal ages of 232 ± 8 Ma and Ar-Ar ages of 770-780 Ma, as well as magmatic zircon U-Pb ages of 760−800 Ma (Dong et al., 1997; Gao et al., 2006). These ages indicate that these rocks formed in the Neoproterozoic and experienced Triassic metamorphism, with peak metamorphic temperatures between the closure temperatures of Rb-Sr and Ar-Ar isotopic systems. Different from the UHP rocks, they experienced a relatively low-grade metamorphism (greenschist- to

144 low-amphibolite-facies) during the Triassic (Dong et al., 1997; Liu et al., 2017 and

145 references therein), indicating that they were exhumed from much shallower depths.

146 Similar granitic gneisses/meta-granites, meta-basites with Neoproterozoic protolith

147 ages have also been recognized in the BZ, the northern sector of the Dabie orogen

148 (e.g., Hacker et al., 2000; Xie et al., 2002; Chen et al., 2003; Jiang et al., 2005; Zheng

149 et al., 2005; Liu et al., 2006a, 2010, 2011c, 2017; Wu et al., 2007). These rocks have

150 identical amphibole Ar-Ar (Hacker et al., 2000) and zircon U-Pb ages (Jiang et al.,

151 2005; Liu et al., 2010, 2017) of ~750 Ma, suggesting that their peak metamorphic

152 temperatures during the Triassic were lower than the closure temperatures of the

153 amphibole Ar-Ar dating system (<500 °C). These protolith ages are in agreement with

154 those of the UHP eclogites and orthogneisses (e.g., Ames et al., 1996; Rowley et al.,

155 1997; Hacker et al., 1998; Liu et al., 2007a,b, 2011a), as well as the Neoproterozoic

156 mafic dykes and granites widely distributed along the northern margin of the SCB,

157 thus they are generally considered to be closely related (Zhao and Zhou, 2009; Hong

158 et al., 2009; Xue et al., 2011; Wang et al., 2013). It is consequently thought that these

159 Neoproterozoic meta-granites and meta-basites were once skin layers of the SCB,

160 detached from the subducted slab during the initial stages of the subduction, and

161 overthrusted onto the southern margin of the NCB (e.g., the BZ), or into the UHP

162 metamorphic zone (e.g., Ganghe) during the Triassic continental collision.

163   In addition to the locations described above, the relatively low-grade

164 meta-basites and meta-granitoids have been discovered at Longjingguan within the

165 central Dabie UHP zone (Fig. 1). So far, their petrogenesis, emplacement time and

166 relationship with the adjacent UHP rocks have not been studied in detail.

167

2.2. Petrography and mineral chemistry

169   Fourteen samples were collected from the Longjingguan area, including six

170 meta-basites (samples 11LJG3-4-5-6-7-8) and eight meta-granitoids (samples 11LJG2,

171 1202LJG3, 1209LJG5, 1303LJG2, 1303LJG4, 1209LJG1, 1209LJG3 and 1209LJG4).

172 Their outcrops are concentrated within an area of few tens of square meters marked

173 by the black star in Figure 1. All the samples were collected as far as possible from

7

174   the contact with different lithologies, to avoid possible interaction between them.

175   The meta-basites occur as tectonic lenses within meta-granitoids (Fig. 2), with

176   the margins slightly deformed; the surface is locally charaterized by few

177   light-coloured, weakly deformed spots of about 0.5 mm in size. The meta-basite

178   generally contains fine-grained symplectites mainly consisting of plagioclase and

179   amphibole. The symplectite composed of plagioclase and amphibole points to the

180   replaced former mineral, rather than derived from magma crystallization. Accessory

181   minerals are rutile, titanite, ilmenite and magnetite. A few amphibole porphyroblasts

182   occur in the meta-basites, and they contain inclusions of plagioclase, plagioclase +

183   rutile, rutile, rutile + ilmenite and rutile + titanite (Figs. 3a & b).

184   Electron microprobe analyses were carried out on representative minerals of three

185   samples 11LJG7, 1209LJG5 and 1209LJG1, which represent the meta-basites, low-Si

186   meta-granitoids and high-Si meta-granitoids, respecitively. The results are listed in

187   Supplementary Table 1.

188   The meta-granitoids are subdivided into two types, named low-Si and high-Si

189   meta-granitoids, respectively, according to their bulk-rock SiO_2 content

190   (Supplementary Table 2). The low-Si meta-granitoid is mainly composed of

191   plagioclase (with K-feldspar exsolutions), quartz, and biotite, with minor amphibole

192   and apatite (Fig. 3c-d), while the high-Si meta-granitoid is dominated by quartz and

193   K-feldspar, with rare allanite, muscovite and amphibole (Figs. 3e-f). Minerals in the

194   meta-granitoids vary from few tens of microns to hundreds of microns in size,

195   significantly coarser than those in the matrix of the meta-basites. The structure varies

196   from gneissic, with a poorly developed foliation (Fig. 3c-d), to granoblastic (Figs.

197   3e-f).

198

2.2.1. 11LJG7

200   In this meta-basite sample, amphibole occurs as fine grains in the symplectitic

201   matrix or as porphyroblasts. Both porphyroblasts and the fine-grained amphibole in

202   the matrix are magnesiohornblende: the porphyroblasts have lower $Mg^{\#}$ values

203   (72~73) and higher TiO_2 contents (0.26~0.35 wt%) than the fine grains in the matrix

204 (Mg$^{\#}$=79~81; TiO_2=0.02~0.13 wt%). Plagioclase is an oligoclase (Supplementary

205 Table 1). Two rutile inclusions within amphibole porphyroblast have Zr contents of

206 277 and 735 ppm, respectively. Rutile inclusions in Neoproterozoic metamorphic

207 zircon domains (see Section 4.2) have higher Zr contents, in the range 2107-2519 ppm

208 (Supplementary Table 3).

209

210 *2.2.2. 1209LJG5*

211 This low-Si meta-granitoid sample exhibits a weak foliation defined by biotite

212 and amphibole preferred orientation (Figs. 3c-d). Plagioclase is oligoclase (An_{19-30})

213 and contains K-feldspar (Or_{92-96}) exsolutions. Amphibole is a ferro-edenite /

214 ferropargasite, with X_{Ca}=0.76–0.77 [X_{Ca}=Ca/(Ca+Na+K)] and X_{Fe}=0.66–0.68

215 [X_{Fe}=Fe/(Fe+Mg)]. Biotite has low Mg$^{\#}$ (~36) and variable TiO_2 contents (3.68 to

216 4.12 wt%).

217

218 *2.2.3. 1209LJG1*

219 This high-Si meta-granitoid sample consists mainly of K-feldspar and quartz,

220 with minor allanite (Fig. 3e). The K-feldspar contains about 6% albite end-member

221 component.

222

223 *2.3. Thermobarometry*

224 Thermbarometric methods were applied on the meta-basite sample 11LJG7. The

225 main amphibole–plagioclase symplectititic assemblage gives a P-T range of

226 478-541 °C, 2.2-3.4 kbar (i.e. lower-T boundary of the amphibolite-facies) based on

227 the amphibole-plagioclase thermometer (Holland and Blundy, 1994) and the

228 Al^{Tot}-in-amphibole barometer (Schmidt, 1992).

229 Rutile inclusions within amphibole porphyroblast yield temperatures of

230 651-737 °C based on their Zr contents (Tomkins et al., 2007), with the pressure set to

231 ~12 kbar according to the coexistence of rutile, ilmenite and titanite (Bohlen and

232 Liotta, 1986; Angiboust and Harlov, 2017). Rutile inclusions in Neoproterozoic

233 metamorphic zircon domains (see Section 4.2) yield significantly higher temperatures

234 of about 850-870 °C. In the application of Zr-in-rutile thermometer, rutile

235 measurements with Si > 200 ppm should be excluded from further analysis if the Zr

236 concentration is substantially higher than that of other rutiles in the same sample

237 (Zack et al., 2004); accordingly, data of three analytical spots (No. 2, 3 and 4,

238 Supplementary Table 4) were excluded. In addition, the analytical spot No. 1

239 (Supplementary Table 4) was also excluded because of extremely low total contents.

240 Overall, thermobarometric results suggest that rutile inclusions within

241 Neoproterozoic metamorphic zircon domains preserve evidence of a HT,

242 granulite-facies metamorphic event (840-860°C, ~12 kbar), completely overprinted by

243 a later amphibolite-facies event (480-540 °C, 2.2-3.4 kbar), responsible for the

244 formation of the amphibole + plagioclase symplectites in the matrix. The

245 Neoproterozoic granulite-facies metamorphic event is also supported by the previous

246 investigations from the deeply subducted NDZ in Liu et al. (2007a). Rutile inclusions

247 within amphibole porphyroblasts were likely partially reequilibrated during the late

248 amphibolite-facies metamorphic event, due to the lack of protection by rigid

249 "container" such as zircon, thus indicating temperatures (652-737 °C) lower than

250 those preserved by rutiles included in zircons.

251

3. Analytical methods

253 Rock-crushing and powdering were performed at the Langfang Laboratory,

254 Hebei Bureau of Geological and Mineral Resources. Zircon grains were separated by

255 the procedures of crushing, heavy-liquid separation, magnetic separation. After that,

256 zircon grains were further selected by hand-picking under a binocular microscope,

257 and mounted in an epoxy mount, which was polished to section the crystals for

258 analyses, with a zircon U–Pb standard TEM (417 Ma) (Black et al., 2003) at Beijing

259 SHRIMP Center, Chinese Academy of Geological Sciences (CAGS).

260 Whole-rock major element composition was analyzed by wet chemical methods

261 at the Langfang Laboratory, Hebei Bureau of Geological and Mineral Resources.

262 Analytical uncertainties have a range from ±1 to ±5% for major elements. Trace

263 elements analysis was carried out at the CAS Key Laboratory of Crust-Mantle

264 Materials and Environments, University of Science and Technology of China (USTC)

265 in Hefei, by an Elan DRCII ICP-MS, with analytical uncertainties ranging from ±5%

266 to ±10%. Detailed analytical procedures and instrument parameters for trace element

267 analyses are documented in Hou and Wang (2007). Zircon SHRIMP U–Pb dating was

268 carried out at the Beijing SHRIMP Center, with transmitted and reflected light

269 micrographs and CL imaging as a guide to selection of U–Pb dating spot. The detailed

270 analytical method was described by Compston et al. (1992) and Williams (1998).

271 Common Pb corrections were made using measured ^{204}Pb, and the data were treated

272 following Compston et al. (1992) with the ISOPLOT program of Ludwig (2001).

273 Zircon trace elements analyses were performed by LA-ICP-MS at the CAS Key

274 Laboratory of Crust-Mantle Materials and Environments, USTC in Hefei and the

275 State Key Laboratory of Continental Dynamics, Northwest University in Xi'an. The

276 analyses were carried out with pulse rate of 10 Hz, beam energy of 10 J/cm^2, and spot

277 diameter of 32 μm. The detailed parameters of the instrument are similar to those

278 described by Yuan et al. (2004) and Liu et al. (2011a). Element contents of zircons

279 were calculated by using Pepita software with the zircon SiO_2 as internal standard and

280 the NIST610 as external standard. Precision and accuracy of analyses are 2–5% for

281 REE, Y, Rb, Sr, Nb, Ta, Hf, Th and U at the ppm concentration level, and from 8% to

282 10% for P, Ti and Pb. The detection limit for the different REE varies from 0.02 to

283 0.09 ppm.

284 In situ zircon Lu–Hf isotope analysis were conducted at the Institute of Geology

285 and Geophysics, the Chinese Academy of Sciences in Beijing, and the School of Earth

286 Sciences and Engineering, Nanjing University, each using a Neptune multi-collector

287 ICPMS, with a Geolas 193 nm laser ablation system. Instrumental parameters and

288 data acquisition followed those described by Wu et al. (2006a). The detailed processes

289 were shown in Liu et al. (2012). Initial Hf isotope ratios are denoted as $\varepsilon_{Hf}(t)$ values

290 that are calculated with the reference to the chondritic reservoir (CHUR) at the time of

291 zircon crystallization. Parameters adopted in this study are: 1.865×10^{-11} yr^{-1} for the

292 decay constant of ^{176}Lu (Scherer et al., 2001), 0.282772 and 0.0332 for the ^{176}Hf/^{177}Hf

293 and $^{176}Lu/^{177}Hf$ ratios of the chondrite (Blichert-Toft and Albarede, 1997). Single

294 stage model ages (T_{DM1}) were calculated referred to the depleted mantle with a

295 present day $^{176}Hf/^{177}Hf$ ratio of 0.28325, similar to that of the average MORB (Nowell

296 et al., 1998) and $^{176}Lu/^{177}Hf$ ratio of 0.0384 (Griffin et al., 2000).

297 Mineral inclusions in zircon were identified using Raman spectroscopy at the

298 CAS Key Laboratory of Crust–Mantle Materials and Environments, University of

299 Science and Technology of China in Hefei, and analyzed using the electron

300 microprobe (EMP) at the Institute of Mineral Resources, CAGS in Beijing. The

301 analytical conditions of the Raman and EMP were reported by Liu et al. (2009). The

302 compositions of the representative minerals in thin sections were detected by EMP at

303 the Department of Resource and Environment Engineering, Hefei University of

304 Technology in Hefei. The accelerating voltage and beam current were 15 kV and

305 15nA, respectively.

306 Rb-Sr, Sm-Nd, and Pb isotopic analyses were performed at the Laboratory for

307 Radiogenic Isotope Geochemistry, in USTC according to the methods of Chen et al.

308 (2000, 2007). Sm, Nd, Rb, and Sr concentrations were determined by isotopic dilution

309 using ^{149}Sm, ^{150}Nd, ^{84}Sr, and ^{85}Rb tracers. The isotopic abundance ratios were

310 determined on a Finnigan MAT 262. Sr and Nd isotopic ratios were corrected for mass

311 fractionation relative to $^{86}Sr/^{88}Sr = 0.1194$ and $^{146}Nd/^{144}Nd = 0.7219$, respectively.

312 NBS987 and La Jolla standard solutions analyzed along with samples yielded

313 0.710250 ± 12 (2σ) for $^{87}Sr/^{86}Sr$ and 0.511860 ± 12 (2σ) for $^{143}Nd/^{144}Nd$. Measured Pb

314 isotopic ratios were then corrected for instrumental mass fractionation using a value

315 of 0.11% per atomic mass unit inferred from analysis of the reference material

316 NBS981.

317

4. Results

4.1. Major and trace elements

320 Whole-rock major and trace elemental compositions of the studied meta-basites

321 and meta-granitoids are listed in Supplementary Table 2.

4.1.1. Meta-basites

323

The meta-basite samples 11LJG3-4-5-6-7-8 have uniform bulk-rock

324

compositions. The SiO_2 contents range from 45.72 to 51.81 wt%, Al_2O_3 from 12.46 to

325

14.30 wt%, and MgO from 4.37 to 13.29 wt%. They have high FeO^T (11.47–14.99

326

wt%) and $Mg^{\#}$ values of 34–67. The TiO_2 contents are also relatively high (2.01–3.42

327

wt%). They are alkalic with Na_2O contents of 1.74–3.55 wt%, K_2O contents of

328

0.77–1.80 wt% and Na_2O/K_2O ratios of 1.25–4.14. Element pairs that have similar

329

bulk D values (solid/melt partition coefficient for modal melting), for example Y-Ho

330

and Eu-Sm, are correlated during magmatic processes (e.g., Workman and Hart, 2005).

331

In the Y vs. Ho and Eu vs. Sm plots (no attachment), all the studied meta-mafic rocks

332

fall along a linear trend, suggesting that they were derived from the same source.

333

In the TAS (Le Bas et al., 1986) and Zr/TiO_2 vs Nb/Y (Winchester and Floyd,

334

1977) diagrams (Fig. 4), the meta-mafic rocks plot very close to the boundary

335

between fields of alkaline and sub-alkaline series. The primitive mantle normalized

336

spider diagram (Fig. 5b) shows that they are enriched in incompatible elements

337

compared to MORB, and have negative anomalies of Sr, Nb and Ta, positive or

338

slightly negative Pb anomalies. They have uniform C1 chondrite normalized REE

339

patterns (Fig. 5a) characterized by enrichment in LREE, slight depletion in HREE and

340

weakly positive or negative Eu anomaly (Eu/Eu*=0.80–1.06). Their $(La/Yb)_N$

341

(primitive mantle normalized) ratios range from 2.2 to 7.5 and $(La/Sm)_N$ from 1.3 to

342

2.1. The UHP eclogites derived from basaltic protoliths have similar REE patterns and

343

related trace-element contents (Fig. 5c and d).

344

345

4.1.2. Low-Si meta-granitoids

346

The low-Si meta-granitoids (samples 11LJG2, 1209LJG5 and 1202LJG3) have

347

slightly inhomogeneous bulk compositions. The SiO_2 contents range from 60.45 to

348

61.50 wt%, Al_2O_3 from 14.18 to 14.96 wt%, TiO_2 from 1.16 to 1.38 wt% and MgO

349

from 1.60 to 1.86 wt%. They have high FeO^T (7.78–8.29 wt%) with $Mg^{\#}$ values of

350

0.26–0.31. They have Na_2O ranging from 1.50 to 3.26 wt% and K_2O from 3.11 to

351

352   4.28 wt% with Na_2O/K_2O ratios of 0.35–1.05. In the TAS diagram, these rocks plot in

353   the field of andesite, close to the boundary with trachy-andesite; in the Zr/TiO_2 vs

354   Nb/Y diagram, they are distributed in the fields of dacite + rhyodacite and

355   trachyandesite. They exhibit significant depletion of HFSE including Nb, Ta, Ti and P,

356   as well as enrichment of Pb (Fig. 5b), which are typical features of crustal-sourced

357   rocks (Rudnick and Gao, 2003). They have identical C1 chondrite normalized REE

358   patterns (Fig. 5a) characterized by enrichment of LREE, weak depletion of HREE and

359   positive Eu anomalies (Eu/Eu*=1.12–2.00). Their $(La/Yb)_N$ ratios range from 9.59 to

360   17.49 and $(La/Sm)_N$ from 2.77 to 4.02.

361

362   *4.1.3. High-Si meta-granitoids*

363   Compared to the meta-basites and low-Si meta-granitoids, the high-Si

364   meta-granitoids (samples 1303LJG2, 1303LJG4, 1209LJG1, 1209LJG3 and

365   1209LJG4) have more scattered bulk-rock compositions. The SiO_2 contents range

366   from 67.98 to 80.98 wt%, Al_2O_3 from 8.96 to 11.78 wt%, TiO_2 from 0.17 to 0.54 wt%

367   and MgO from 0.06 to 3.82 wt%. They have low FeO^T (2.09–4.30 wt%) contents with

368   varied $Mg^{\#}$ values of 0.04–0.62. The Na_2O contents range from 1.12 to 2.99 wt% and

369   K_2O from 2.44 to 5.35 wt% with Na_2O/K_2O ratios of 0.29–0.98. In the TAS diagram,

370   four samples plot into the field of sub-alkaline rhyolite and one sample into that of

371   dacite; in the Zr/TiO_2 vs Nb/Y plot, the studied samples scatter among four categories:

372   comendite + pantellerite, rhyolite, rhyodacite + dacite and trachyandesite. They have

373   trace elements patterns comparable to those of the low-Si meta-granitoids (Fig. 5b),

374   and uniform C1 chondrite normalized REE patterns (Fig. 5a) characterized by

375   enrichment of LREE, slight depletion of HREE and strong negative Eu anomalies

376   (Eu/Eu*=0.10–0.75). Their $(La/Yb)_N$ ratios range from 10.29 to 49.87 and $(La/Sm)_N$

377   range from 3.64 to 5.41.

378

379   *4.2. Zircon geochronology*

380   *4.2.1. Zircon morphology and mineral inclusions*

381   Zircons from the meta-basites are anhedral to subhedral in shape with smooth

14

382 outlines, and their length-width ratios are generally smaller than 1.5. CL images show

383 that most of them have core, mantle and rim structures with clear boundaries between

384 them. The cores are grey colored with clear or weak oscillatory zoning while the

385 mantles are light colored and homogeneous (Fig. 6). Some zircon grains have a

386 mantle domain showing gradually darker luminance outwards. The rims are bright,

387 too thin to be analysed. According to the microstructures, the cores with oscillatory

388 zoning are interpreted to be of magmatic origin, while the homogeneous cores and

389 mantles are considered to be metamorphic zircon domains (e.g., Hanchar and Rudnick,

390 1995; Gebauer et al., 1997; Hermann et al., 2001). Most of the zircon cores exhibit

391 rounded shapes, suggesting that they were partially resorbed after crystallization,

392 maybe during the formation of the zircon mantles.

393   As opposed to the meta-basites, zircons from the meta-granitoids exhibit more

394 regular crystal shapes. Some of the zircons from the meta-granitoids are euhedral in

395 shape with clear oscillatory zones, indicative of magmatic origin. Other zircons show

396 core and mantle structures, wherein the cores are dark grey with clear oscillatory

397 zoning or no zoning, while the mantles are light grey with weak or no oscillatory

398 zonings. Similarly, the zircons in the meta-granitoids can also be divided into

399 magmatic (with oscillatory zoning) and metamorphic (no zoning) domains. Generally,

400 the metamorphic zircon domains from both the meta-basites and the meta-granitoids

401 are granular, platy and prismatic in shape with smooth boundaries, and some of them

402 retain plenty of mineral inclusions (Fig. 7), which are powerful tools to link zircon

403 growth to precise metamorphic events (e.g., Gebauer et al., 1997; Hermann et al.,

404 2001; Liu et al., 2007b, 2011a). The metamorphic zircons in the meta-basite sample

405 11LJG3 contain quartz, plagioclase, apatite, hornblende, K-feldspar, chlorite, epidote,

406 biotite, rutile, ilmenite and titanite, while those from the meta-granitoid sample

407 11LJG2 contain K-feldspar, muscovite, epidote and quartz. The compositions of

408 typical mineral inclusions in metamorphic zircons were detected by electron

409 microprobe, with the results listed in Supplementary Table 3. Biphase inclusions

410 composed of rutile + titanite or of titanite + ilmenite are recognized in a few

411 metamorphic zircons from sample 11LJG3.

412

4.2.2. Zircon REE patterns

413

Representative zircon REE contents of the meta-basites (samples 11LJG3 and

414

11LJG7) and the meta-granitoids (samples 11LJG2, 1202LJG3, 1303LJG2 and

415

1209LJG5) are listed in Supplementary Table 5 (all the analyzed results for zircon

416

rare earth elements in Supplementary Table 6). Zircon cores have almost identical

417

steep HREE patterns, positive Ce anomalies and negative Eu anomalies (Fig. 8),

418

typical of magmatic zircon (Hoskin and Ireland, 2000). On the contrary, the REE

419

patterns of metamorphic zircons are varied. In the meta-basites, most metamorphic

420

zircons (the cyan lines, Fig. 8a) exhibit higher REE contents than, but similar REE

421

patterns with, the magmatic zircons, except for one spot that show slightly positive Eu

422

anomaly; besides, a metamorphic zircon (the black line, Fig. 8a) has almost the same

423

La, Ce and HREE contents with the magmatic zircons, but it exhibits significantly

424

higher Pr, Nd, Sm and Eu. In the meta-granitoids, most metamorphic zircons exhibit

425

similar REE patterns with the magmatic cores, whereas some analyses exhibit higher

426

REE contents and/or higher LREE/HREE ratios than the magmatic zircons (Fig. 8b-d),

427

or exhibit no anomaly of Eu.

428

429

4.2.3. Zircon SHRIMP U-Pb ages

430

In-situ analyses have been performed on different zircon domains, with the

431

U-Th-Pb data listed in Supplementary Table 7 and U-Pb concordia diagram illustrated

432

in Figure 9.

433

Magmatic zircon cores from the meta-basite sample 11LJG3 yield a cluster of

434

concordant $^{206}Pb/^{238}U$ age averaging at 772 ± 4 Ma (MSWD=2.0, n=7; Fig. 9a), while

435

the metamorphic domains give a concordant $^{206}Pb/^{238}U$ age group of 768 ± 7 Ma

436

(MSWD=2.9, n=11; Fig. 9a). In another meta-basite sample 11LJG7, magmatic zircon

437

domains yield a cluster of concordant $^{206}Pb/^{238}U$ age of 772 ± 7 Ma (MSWD=2.5, n=5;

438

Fig. 9b), and the metamorphic domains give a concordant $^{206}Pb/^{238}U$ age group of 746

439

± 4 Ma (MSWD=2.6, n=9; Fig. 9b). Summing up, the magmatic zircons yield a

440

cluster of concordant $^{206}Pb/^{238}U$ age at ~772 Ma (Ma domains), and the metamorphic

441

442 zircons yield two groups of concordant ^{206}Pb/^{238}U age at ~768 Ma (Me1 domains) and

443 ~746 Ma (Me2 domains), corresponding to magmatism, metamorphism and thermal

444 overprinting events, respectively.

445   Zircon cores in the low-Si meta-granitoids (samples 11LJG2, 1202LJG3,

446 1209LJG5) have a wide age spectrum spreading from ~800 Ma to ~2500 Ma.

447 Analytical spots on zircon cores in sample 11LJG2 are distributed along the concordia

448 curve or on a Pb loss line, yielding two upper intercept ages of 1940 ± 140 Ma

449 (MSWD=2.1; Fig. 9d) and 2529 ± 38 Ma (MSWD=3.1; Fig. 9d), respectively. Six

450 magmatic zircon spots give a concordant ^{206}Pb/^{238}U age cluster of 838 ± 18 Ma

451 (MSWD=0.73, n=6; Fig. 9e), while twelve metamorphic zircon analyses yield two

452 concordant ^{206}Pb/^{238}U age clusters averaging at 797 ± 7 Ma (MSWD=0.54, n=9; Fig.

453 10e) and 762 ± 22 Ma (MSWD=0.25, n=3; Fig. 9e), respectively. Zircons in sample

454 1209LJG5 plot along the concordia curve, or on a Pb loss line with an upper intercept

455 age of 1999 ± 57 Ma and a lower intercept age of 779 ± 49 Ma (MSWD=4.8; Fig. 9g).

456 Neoproterozoic magmatic zircons give a concordant ^{206}Pb/^{238}U age of 839 ± 7 Ma

457 (MSWD=0.99, n=6; Fig. 9h), and two analyses on metamorphic zircon yield

458 concordant ^{206}Pb/^{238}U ages of 785 ± 6 Ma and 744 ± 16 Ma, respectively. Three near

459 concordant ^{206}Pb/^{238}U age clusters were obtained from sample 1202LJG3: one age of

460 819 ± 12 Ma (MSWD=2.3, n=3; Fig. 9c) from magmatic zircon cores, and two ages

461 of 772 ± 7 Ma (MSWD=1.14, n=3; Fig. 9c) and 751 ± 6 Ma (MSWD=0.39, n=3; Fig.

462 9c) from metamorphic zircon domains.

463   Magmatic zircons from the high-Si meta-granitoid sample 1303LJG2 give an

464 average concordant ^{206}Pb/^{238}U age of 813 ± 5 Ma (MSWD=0.99, n=7; Fig. 9f), while

465 metamorphic zircons yield two concordant age clusters of 784 ± 7 Ma and 732 ± 6 Ma

466 (Fig. 9f). The zircon dating results indicate that the protoliths of the low-Si and

467 high-Si meta-granitoids were formed at about 819 ± 12 Ma and 813 ± 5 Ma,

468 respectively. The zircons yielding older ages are thus inherited from their source rocks,

469 with their original ages preserved or reset by Pb loss, corresponding to the apparent

470 concordant or disconcordant ages.

4.3. Zircon Hf isotopes

Zircon $\varepsilon_{Hf}(t)$ values and T_{DM} ages of two meta-basites (samples 11LJG3 and 11LJG7), three low-Si meta-granitoids (samples 11LJG2, 1209LJG5 and 1202LJG3) and one high-Si meta-granitoid (sample 1303LJG2) are listed in Supplementary Table 8.

The zircons in the meta-basites have $\varepsilon_{Hf}(780\ Ma)$ values from +2.6 to +7.9 (Fig. 10), and corresponded single stage model ages (T_{DM1}) of 1033 to 1248 Ma, slightly older than their zircon U-Pb ages.

Six inherited zircon cores from low-Si meta-granitoids have $\varepsilon_{Hf}(t)$ values of +7.1 to -6.6, with corresponding T_{DM1} ages of 2359 to 2702 Ma, and T_{DM2} ages of 2506 to 2823 Ma, respectively (Fig. 10). The Neoproterozoic zircon domains in the low-Si meta-granitoids yield a relatively wide $\varepsilon_{Hf}(800\ Ma)$ spectrum of -3.2 to -12.0, with T_{DM1} ages of 1513~1819 Ma and T_{DM2} ages of 1893~2446 Ma. Zircons from the high-Si meta-granitoid have $\varepsilon_{Hf}(800\ Ma)$ values ranging from -7.5 to +1.4, with T_{DM1} ages of 1313~1679 Ma, and T_{DM2} ages of 1618~2172 Ma. Neoproterozoic zircons from low-Si and high-Si meta-granitoids have overlapped $\varepsilon_{Hf}(t)$ values and T_{DM} ages, but the high-Si rocks have slightly higher average $\varepsilon_{Hf}(t)$ values and younger Hf model ages.

4.4. Sr-Nd-Pb isotope compositions

The Rb-Sr, Sm-Nd and Pb contents and isotopic compositions of the meta-basites are listed in Supplementary Tables 9 and 10, respectively. The meta-basites have Rb and Sr contents of 16.0–62.9 and 87–320 ppm, and measured $^{87}Rb/^{86}Sr$ and $^{87}Sr/^{86}Sr$ ratios of 0.1423–1.6997 and 0.705386–0.709376, Sm and Nd contents of 4.15–9.64 and 13.1–35.9 ppm, and measured $^{147}Sm/^{144}Nd$ and $^{143}Nd/^{144}Nd$ ratios of 0.1515–0.1888 and 0.512511–0.512674. Sr and Nd isotopic compositions were back calculated to t=230 Ma, and thus the $(^{87}Sr/^{86}Sr)_I$, $\varepsilon_{Nd}(t)$ values and T_{DM2} ages are 0.7023–0.7067, -1.8–+1.8 and 862–1156 Ma. The meta-basites have U, Th

and Pb contents of 0.34–0.70, 1.27–2.34 and 2.36–10.20 ppm, and measured $^{206}Pb/^{204}Pb$, $^{207}Pb/^{204}Pb$ and $^{208}Pb/^{204}Pb$ ratios of 17.046–17.308, 15.403–15.467 and 38.119–38.344. Pb isotopic compositions were back calculated to t=230 Ma, and thus the $(^{206}Pb/^{204}Pb)_i$, $(^{207}Pb/^{204}Pb)_i$ and $(^{208}Pb/^{204}Pb)_i$ values are 16.84–17.11, 15.39–15.46 and 37.81–38.06, respectively. The Dabie orogen experienced two major geological events: the Neoproterozoic rifting-related magmatism and the Triassic subduction-related metamorphism. In deed, we also tried to calculate the Sr, Nd and Pb isotope compositions back to t=800 Ma, but obtained much more scattered results, indicating that the meta-basites experienced metamorphism at the Triassic, during which their isotopes were resetted.

5. Discussion

5.1. The relationship between the studied rocks and the UHP rocks in the CDZ

5.1.1. Low-grade meta-basites and meta-granitoids vs. ± retrograded UHP eclogites and granitic gneisses

The CDZ contains a variety of coesite- and/or diamond-bearing rock types, including eclogites and granitic gneisses; these rocks experienced Triassic UHP metamorphism and post-peak amphibolite-facies retrogression, responsible for the widespread development of amphibolite-facies assemblages in some eclogites in the area (Wang et al., 1989; Cong et al., 1995; Zhang et al., 2003; Rolfo et al., 2004; Liu et al., 2006b). In some strongly retrograded eclogites, most garnets and omphacites are replaced by symplectites or pseudomorphs; even though, mineral inclusions (e.g. coesite, diamond, omphacite and rutile) within relict garnet preserve the evidence of peak metamorphism at UHP conditions. Even in the most retrograded eclogites that do not contain garnet relics, the former occurrence of garnet is suggested by pseudomorphs of Pl + Amp + Bt that exhibit isometric shape typical of garnet (e.g., Zhang et al., 2003). In contrast, no garnet and/or other microstructural evidence that could be related to eclogite-facies metamorphism have been observed in the studied meta-basites, thus suggesting that the studied rocks have not been involved in the

529   deep subduction of the SCB in the Triassic.

530   In addition to the main rock-forming minerals, inclusions in metamorphic zircon

531   can be also used to reveal the peak metamorphic conditions in strongly retrograded

532   metamorphic rocks (e.g., Xu et al., 1992b; Nasdala and Massonne, 2000; Bauer et al.,

533   2007; Liu et al., 2007b, 2011b). This is because zircon behaves as a rigid "container"

534   that can protect the inclusions from the retrogression occurring in the matrix. Mineral

535   inclusions related to UHP conditions (e.g. coesite, diamond, omphacite and rutile)

536   have been identified in Triassic metamorphic zircons from the retrograded eclogites in

537   the CDZ, thus confirming that they experienced UHP metamorphism, although the

538   matrix of the rocks is dominanted by amphibolite-facies mineral assemblages (Liu et

539   al., 2001, 2006a). On the contrary, no Triassic metamorphic zircon and related

540   eclogite-facies mineral inclusions have been identified in the studied meta-basites (see

541   section 4.2.1).

542   Different from UHP eclogites, felsic gneisses that underwent deep subduction

543   and UHP metamorphism commonly do not preserve evidence of the peak

544   metamorphic mineral assemblage. Nevertheless, their metamorphic zircons can trap

545   and preserve peak metamorphic minerals. In the CDZ, UHP inclusions (e.g. coesite

546   and diamond) have been recognized in Triassic metamorphic zircons from the felsic

547   gneisses (Tabata et al., 1998; Liu et al., 2001). On the contrary, no Triassic ages have

548   been obtained from the metamorphic zircons in the studied meta-granitoids, and no

549   eclogite-facies mineral inclusions have been observed therein (see section 4.2.1).

550   The overall observations and data clearly indicate that the studied meta-basites

551   and meta-granitoids were not involved in the Triassic deep subduction and UHP

552   eclogite-facies metamorphism, but underwent lower-grade metamorphism, i.e., at

553   amphibolite-facies conditions as suggested by the mineral assemblages and estimated

554   temperatures of the meta-basites (see sections 2.2 and 2.3). The age of this low-grade

555   metamorphic event has not been directly constrained due to the lack of related

556   metamorphic zircon, which may be attributed to the relatively low temperatures (<541

557   ºC, section 2.3). Nevertheless, similar low-grade rocks from the same region showing

558   identical Neoproterozoic protolith ages, yield Triassic whole-rock Rb-Sr isochronal

20

559   ages of 232 ± 8 Ma (Dong et al., 1997; Gao et al., 2006). We therefore suggest that

560   during the Triassic, the studied meta-basites and meta-granitoids underwent a shallow

561   subduction associated with amphibolite-facies metamorphism, nearly sinchronous

562   with the deep subduction of the CDZ.

563

564   *5.1.2. The same source and crustal levels indicated by zircon Hf and bulk-rock*

565   *Sr-Nd-Pb isotopes*

566   *Zircon Hf isotopes*

567   Because Hf is more incompatible than Lu, the continental crust acquired a

568   Lu/Hf ratio much lower than that in the primitive mantle, when it differentiated from

569   the primitive mantle. As a result, the $^{176}Hf/^{177}Hf$ ratio in the continental crust increases

570   slower than in the depleted mantle and thus its $\varepsilon_{Hf}(t)$ value becomes more and more

571   negative with time, whereas the depleted mantle develops more and more positive

572    $\varepsilon_{Hf}(t)$ values (Rudnick and Gao, 2003; Kelemen et al., 2003; Salters and Stracke, 2004;

573   Palme and O'Neill, 2003). When a zircon crystallized from a crustal-derived melt, the

574    $^{176}Hf/^{177}Hf$ ratio in the melt was timely imprinted in the zircon, because Hf content in

575   zircon is several orders of magnitude higher than Lu content, and thus the change of

576    $^{176}Hf/^{177}Hf$ ratio in zircon with time is negligible; moreover, zircon $^{176}Hf/^{177}Hf$ ratio is

577   resistant to the influence of later processes such as weathering, fluid alteration and

578   metamorphic recrystallization (Patchett et al., 1984; Wu et al., 2006b; Zheng et al.,

579   2008; Hanyu et al., 2006; Carpentier et al., 2009; Hoffmann et al., 2011; Roux et al.,

580   2009; Yu et al., 2009; Chen et al., 2010; Tappe et al., 2011; Choi and Mukasa, 2012).

581   In this way, the $\varepsilon_{Hf}(t)$ value of zircon reflects the mass source of the host rocks: given

582   the same zircon U-Pb age, the more negative zircon $\varepsilon_{Hf}(t)$ value is, the higher

583   proportion of ancient continental crustal material the host rock contains. In principle,

584   the most positive $\varepsilon_{Hf}(t)$ values correspond to the youngest single-stage Hf model ages

585   (T_{DM1}) that represent the maximum time of the emplacement of the mantle-derived

586   magma, while the most negative $\varepsilon_{Hf}(t)$ values correspond to the oldest T_{DM1} ages that

587   represent the minimum time of the formation of the involved crust.

588   The UHP eclogites and gneisses in the CDZ exhibit varied zircon Hf isotope

21

589 compositions, indicating both source mixing and crustal contamination along an

590 active rifting zone, with varying degrees of mixing between different ages of crustal

591 materials at ~750 Ma. Therein, the youngest zircon T_{DM1} ages from the eclogites are

592 in agreement with the Neoproterozoic zircon U-Pb ages of ~750 Ma, while the oldest

593 zircon T_{DM2} ages from the gneisses are close to the Paleoproterozoic zircon U-Pb ages

594 of ~2.15 Ga, indicating growth and immediate reworking of juvenile crust at

595 Paleoproterozoic (~2.15 Ga) and Neoproterozoic (~750 Ma), respectively (e.g., Zheng

596 et al., 2006).

597   The studied meta-basites and meta-granitoids have varied zircon Hf isotope

598 compositions (Supplementary Table 8) which are in agreement with the UHP

599 eclogites and orthogneisses in the CDZ (e.g., Zheng et al., 2006) (Fig. 10), indicating

600 different degrees of mixing between Neoproterozoic depleted mantle materials and

601 Paleoproterozoic crustal components. The meta-basites have positive $\varepsilon_{Hf}(t)$ values of

602 +2.6~+7.9 and young T_{DM1} ages of about 1.2~1.5 Ga, slightly older than their zircon

603 U-Pb ages, reflecting incongruent contamination of crustal materials during the

604 emplacement of their parental magmas. Inherited zircons from the low-Si

605 meta-granitoids exhibit overlapped T_{DM1} ages of 2359~2702 Ma and T_{DM2} ages of

606 2506~2823 Ma from late Archean to Paleoproterozoic, representing the time of the

607 formation of continental crust from the mantle. For the Neoproterozoic zircons with

608 negative $\varepsilon_{Hf}(t)$ values, T_{DM2} can better reflect their origin than T_{DM1}. Neoproterozoic

609 zircons in the low-Si meta-granitoids exhibit negative $\varepsilon_{Hf}(t)$ values of -3.2~-12.0 and

610 younger T_{DM2} ages of 1893~2446 resulting from mixing between depleted mantle

611 materials and late Archean continental crust at Neoproterozoic. Compared to the

612 low-Si meta-granitoids, the high-Si rocks do not contain ancient (late Archean)

613 inherited zircon, and have higher $\varepsilon_{Hf}(t)$ values of -7.5~+1.4 and younger T_{DM2} ages of

614 1618~2172 Ma, indicating that they were mainly derived from remelting of younger

615 continental crust formed at early Paleoproterozoic. These clusters of T_{DM2} age of the

616 meta-granitoids are consistent with multiple episodes of crust growth of the South

617 China Block from the late Archean to Paleoproterozoic (Greentree et al., 2006; Zhang

618 et al., 2006a,b; Liu et al., 2008; Wang et al., 2010; Zhao and Cawood, 2012).

22

As a summary, the studied meta-basites and meta-granitoids derived from the same sources as the UHP eclogites and felsic gneisses in the CDZ. Therein the meta-basites were formed from depleted mantle upwelling and mafic magmatic activities during the Neoproterozoic, with incongruent mixing with the Yangtze crustal materials; the mafic magmatic activities remelted the basement of the South China Block, which comprises the Archean and early Paleoproterozoic crustal rocks, and generated the low-Si and high-Si meta-granitoids.

Bulk-rock Sr-Nd-Pb isotopes

Because Rb is more incompatible than Sr, and Nd is more incompatible than Sm, melts will have higher Rb/Sr but lower Sm/Nd ratios than residues during partial melting. Therefore, when the the primitive mantle differentiated to form the crust and depleted mantle, the crust acquired higher Rb/Sr and lower Sm/Nd ratios than the bulk earth, while the depleted mantle acquired lower Rb/Sr and higher Sm/Nd ratios. Then the $^{87}Sr/^{86}Sr$ of the crust will be more and more higher than the bulk earth, but the $\varepsilon_{Nd}(t)$ will be more and more negative with time; on the contrary, the $^{87}Sr/^{86}Sr$ and $\varepsilon_{Nd}(t)$ of the depleted mantle will evolve in the opposite direction. The meta-basites have initial $^{87}Sr/^{86}Sr$ ratios of 0.7023–0.7067 (calculated to t=230 Ma), $\varepsilon_{Nd}(230\ Ma)$ values from -1.8 to +1.8 and T_{DM2} ages of 862–1156 Ma. In the $\varepsilon_{Nd}(t)$ vs $(^{87}Sr/^{86}Sr)_i$ diagram (Fig. 11), the meta-basites plot around the composition of the bulk silicate earth and slightly toward lower continental crust, indicating that the meta-basites were derived mainly from the mantle, with minor addition of lower continental crust. This conclusion is also supported by their two-stage Nd model ages (T_{DM2}) of 862–1156 Ma, which are slightly older than their magmatic zircon U-Pb ages (~772 Ma).

U is more incompatible than Pb. This being the case, we would therefore predict that continental crust should be more enriched in radiogenic Pb than the average of the bulk-earth, while the depleted mantle should be depleted in radiogenic Pb. Upper continental crustal rocks do have higher $^{206}Pb/^{204}Pb$ and $^{207}Pb/^{204}Pb$ ratios as expected, but surprisingly, most mantle-derived rocks also exhibit higher Pb isotope ratios than the average of the bulk-earth, whereas a majority of lower crustal rocks are relatively

23

649 depleted in radiogenic Pb. This phenomenon is known as the Pb paradox and it implies

650 that other processes apart from magmatism may have played key roles in the

651 differentiation of the U-Pb element pair.

652 In addition, Pb isotopes can be used to trace the crust affinity of given rocks from

653 upper or lower crust, i.e., upper crustal rocks commonly have higher radiogenic Pb

654 isotopes than lower crustal rocks (Zartman and Doe, 1981; Taylor and McLennan, 1985).

655 For example, Liu and Li (2008) concluded that the NDZ is of lower crustal origin, while

656 the CDZ and the SDZ are slices from middle to upper crust, according to their different

657 radiogenic Pb isotope compositions. As shown in Figure 12, the Pb isotope compositions

658 of the studied meta-basites fall into the range of the UHP meta-igneous rocks from the

659 CDZ, and are significantly higher than that of the UHP meta-igneous rocks from the NDZ.

660 This indicates that the studied meta-basites and the associated meta-granitoids were at

661 middle to upper crustal depths, consistent with the UHP meta-igneous rocks from the

662 CDZ.

663 Summing up, both zircon Hf and bulk-rock Sr-Nd-Pb isotopic data demonstrate

664 that the studied meta-basites and meta-granitoids are low-grade metamorphosed

665 counterparts of the UHP eclogites and orthogneisses in the CDZ; these rocks did not

666 experience deep subduction and UHP metamorphism during the Triassic, but were

667 detached from the subducting plate and exhumed from shallower depths, experiencing

668 amphibolite-facies metamorphic peak conditions.

669

670 *5.1.3. The studied rocks as the best candidates for elucidating the Neoproterozoic*

671 *evolution of the South China Block*

672 The UHP meta-igneous rocks in the CDZ consist mainly of granitic gneisses and

673 eclogites, which are generally considered to be transformed from bimodal igneous

674 rocks derived from rift magmatism in Neoproterozoic (e.g., Ames et al., 1996; Rowley

675 et al., 1997; Hacker et al., 1998). The studied meta-basites and meta-granitoids at

676 Longjingguan have consistent Neoproterozoic protolith ages and zircon Hf isotopic

677 compositions with those from the UHP meta-igneous rocks, most likely indicating that

678 they were derived from the same rifting events, during which depleted mantle

24

679 materials were added to the crust, and caused remelting of existing old crust and

680 generated bimodal magmas (Liu et al., 2007a). In addition, the bulk-rock Pb isotopic

681 compositions of the studied rocks fall into the range of the UHP meta-igneous rocks in

682 the CDZ (Fig.12), suggestive of upper crustal origin (Liu et al., 2017). In this regard,

683 the studied rocks are likely counterparts of the UHP rocks in the region, and both of

684 them were formed from partial melting of ancient crust in the Neoproterozoic.

685 Moreover, during the Triassic the studied rocks experienced lower-grade and

686 lower-pressure metamorphism with respect to their UHP counterpart. Therefore, we

687 suggest that the rocks could likely have better preserved their protolith compositions

688 than the UHP rocks, which often experienced interactions with melt and/or

689 supercritical fluids during UHP metamorphism (e.g., Zheng et al., 2011). In order to

690 test this hypothesis, the trace element patterns of the studied meta-basites are

691 compared to those of the UHP eclogites derived from basites (data from Tang et al.,

692 2007), as shown in Fig. 5: the studied meta-basites have identical REE and trace

693 element patterns, while the UHP eclogites exhibit similar REE patterns but

694 significantly varied large ion lithophile element (LILE) contents. This is consistent

695 with the fact that LILE have significantly higher mobilities than REE in hydrous

696 fluids during UHP metamorphism (Kessel et al., 2005; Hermann et al., 2006; Zheng et

697 al., 2011). As a conclusion, the rocks here have better preserved their protolith

698 compositions than their UHP counterparts, and thus they are more suitable for

699 elucidating the Neoproterozoic evolution in the area.

700

5.2. Neoproterozoic magmatic and metamorphic events

701

5.2.1. Meta-basites

702

703 Zircons in the meta-basites (samples 11LJG3 and 11LJG7) give a concordant

704 magmatic age cluster of ~772 Ma (Ma) and two concordant metamorphic age clusters

705 of ~768 Ma (Me1) and ~746 Ma (Me2) (see section 4.2.3). As mentioned above, the

706 magmatic zircons exhibit clear oscillatory zoning and REE patterns typical of

707 magmatic genesis, thus the age of ~772 Ma represents a magmatic event. As to the

708 metamorphic zircons, they formed during metamorphic events characterized by the

709 circulation of REE-enriched fluids controlled by fractures. In addition, most
710 metamorphic zircons exhibit slightly higher Nb + Ta, U and Th contents than the
711 magmatic zircons (Supplementary Table 5), thus suggesting that the metamorphic
712 fluids were also enriched in Nb+Ta, U and Th. These REE-, Nb+Ta-, U- and Th-
713 enriched fluids favoured the precipitation of minerals rich in these elements, such as
714 epidote, rutile, ilmenite and titanite (Figs. 7a-i), observed as inclusions in the
715 metamorphic zircons (e.g., sample 11LJG3; Me1 domains). Thermobarometric
716 estimates (see Section 2.3) based on rutile inclusions indicate that metamorphic zircon
717 domains Me1 grew at about 850-870 °C, 12 kbar. No rutile or other inclusions
718 suitable for themometric estimates have been recognized in the Me2 domain of
719 zircons in sample 11LJG7, thus the temperatures of the late thermal overprinting at
720 ~746 Ma has not been estimated. Summing up, the meta-basites were formed at ca.
721 772 Ma (Ma domains) and experienced subsequent granulite-facies (850-870 °C)
722 metamorphism at ca. 768 Ma (Me1 domains), followed by a thermal overprinting
723 event at ~746 Ma (Me2 domains). The almost overlapped magmatic and metamorphic
724 zircon ages (772 ± 4 and 768 ± 7 Ma, respectively) suggest that the Neoproterozoic
725 magmatism in this area occurred in pulse, and that the later magma underplating
726 warmed the already solidified rocks (e.g., Liu et al., 2007a; Liu et al., 2015) resulting
727 in granulite-facies metamorphism. The thermal overprinting age of ~746 Ma is
728 comparable with the emplacement age of some mafic rocks in the Dabie orogen, for
729 example the meta-basites in the BZ located in the northern part of the Dabie orogen
730 (Liu et al., 2017), indicating that a later magma emplacement at that time in the area
731 may have been the heat source of the thermal overprinting. Moreover, these ages are
732 in agreement with the time of Rodinia breakup indicated by large volumes of mafic
733 and felsic magmatism along the northern margin of the Yangtze Block (Li et al., 2002;
734 Li et al., 2003a,b,c; Zhou et al., 2002a,b, 2006a,b; Zhao and Zhou, 2007a,b, 2008),
735 suggesting that the studied rocks are generated from several episodes of magmatic
736 event related to the Rodinia breakup.

737

738 *5.2.2. Meta-granitoids*

739   Compared to the meta-basites, the low-Si meta-granitoids exhibit a more complex

740   zircon U-Pb age spectrum. Few inherited zircon cores preserve two groups of age at

741   ~2.0 and ~2.5 Ga, timely consistent with two episodes of Precambrian crustal growth

742   and immediate reworking event of the SCB (e.g., Zhang et al., 2006a,b,c; Liu et al.,

743   2008; Wang et al., 2010; Zhao and Cawood, 2012). Safe for these inherited zircon

744   cores, the zircons in the studied rocks are distinguished into two types: magmatic

745   zircon domains yielding concordant ages of ca. 819 Ma (Ma domains) and

746   metamorphic zircon domains with concordant ages at ca. 784 (Me1 domains) and 746

747   Ma (Me2 domains). The latters are discriminated from the formers by weaker or no

748   oscillatory zonings, lighter brightness in CL image and enrichment of mineral

749   inclusion. A typical zircon with magmatic zircon core and metamorphic mantle in

750   meta-granitoid sample 11LJG2 (Me1) is shown (Figs. 7j-l): the core is dark with

751   obvious oscillatory zoning, while the mantle is light and homogeneous in CL image;

752   the core is free of mineral inclusion, while the mantle contains K-feldspar +

753   muscovite inclusion; and there is a clear boundary between the core and the mantle.

754   Two analytical spots on metamorphic zircon domains exhibit significantly higher

755   LREE patterns than the magmatic zircons (Figs. 8b,c), therein a spot also exhibit

756   higher REE contents than the magmatic zircons. Moreover, muscovite + K-feldspar

757   inclusion is identified in metamorphic zircon (Fig. 7k), indicating that the

758   metamorphic zircons were formed in the presence of LREE-enriched fluid, in

759   agreement with the metamorphic zircons in the meta-basites. Therefore, the low-Si

760   meta-granitoids experienced two episodes of metamorphism at ~784 Ma and ~746 Ma,

761   respectively. It is worth noting that, the ~784 Ma metamorphic zircon ages are

762   comparable with the forming (i.e. magmatic) ages of the meta-basites (~772 Ma)

763   within error, suggesting that the emplacement of the basic magmas may be the heat

764   source for the metamorphism of the low-Si meta-granitoids. The thermal overprinting

765   of ~746 Ma is timely in agreement with the ca. 750 Ma forming age of the

766   meta-granitoids and meta-basites in the BZ (Jiang et al., 2005; Wu et al., 2007; Liu et

767   al., 2010, 2017), indicating that the low-Si meta-granitoids and the meta-basites in the

768   region experienced a coeval thermal event as a consequence of the emplacement of

27

769   the meta-basites within the BZ.

770   The high-Si meta-granitoids exhibit nearly the same Neoproterozoic magmatic

771 and metamorphic zircon ages with the low-Si type, indicating that they were

772 generated from the same or adjacent magmatic events and then jointly experienced the

773 same metamorphic processes during the Neoproterozoic. However, the two types of

774 meta-granitoids are likely derived from different sources: (i) the low-Si type contains

775 inherited zircons with two age clusters at ~2.5 Ga and ~2.0 Ga, suggesting that its

776 source could be a late Archean basement that experienced metamorphic reworking

777 during the Paleoproterozoic, whereas (ii) the high-Si type does not contain ancient

778 inherited zircon, and the oldest zircon Hf model age (T_{DM2}) is 2172 Ma, suggesting

779 that a derivation from the juvenile crust formed during the Paleoproterozoic. This

780 hypothesis can well explain the compositional gap, especially the different Si contents,

781 between the two types of meta-granitoids (see section 4.1), and also the slightly higher

782 zircon $\varepsilon_{Hf}(t)$ values and younger Hf model ages of the high-Si meta-granitoids (see

783 section 4.3).

784   The meta-basites and meta-granitoids with similar mid- to late-Neoproterozoic

785 ages have been reported from other localities within the Dabie orogen, for example,

786 Ganghe within the CDZ (Dong et al., 1997), Yuexi within the NDZ (Gao et al., 2006),

787 and Huwan, Sujiahe and Luzhenguan within the BZ (Jiang et al., 2005; Wu et al.,

788 2007; Liu et al., 2010, 2017). In addition, extensive mid- to late-Neoproterozoic mafic

789 dyke swarms and granitic bodies (Zhao and Zhou, 2009; Hong et al., 2009; Xue et al.,

790 2011; Wang et al., 2013) are exposed in Suizhou-Zaoyang of the Hubei province,

791 along the northern margin of the SCB. Moreover, the forming ages of these rocks are

792 clearly comparable with the protolith ages of the UHP eclogites and orthogneisses

793 (Rowley et al., 1997; Hacker et al., 1998; Liu et al., 2007a,b, 2011a; and references

794 therein) in the Dabie orogen. In this regard, these rocks, including those from

795 Longjingguan in this study, should be counterparts of the UHP meta-igneous rocks in

796 the Dabie orogen, implying that the protoliths of the latter could have been formed

797 during the same Neoproterozoic magmatic events, and could have experienced the

798 same Neoproterozoic metamorphism.

799

5.3. Petrogenesis and tectonic setting

5.3.1. Meta-basites

Mantle-normalized trace element patterns are frequently used to infer petrogenesis and tectonic settings of igneous rocks, because the same rock type formed in different tectonic settings can display significantly different trace element patterns. For example, the basites of mid-ocean ridges (MORB) are formed from the depleted mantle within a narrow depth interval, and thus have a uniform chemical composition, while the island-arc basalts (IAB) and within-plate basalts (WPB) exhibit large variation in trace element contents and patterns, and generally enrichment in LILE and LREE compared to MORB, depending on addition component of crustal materials. The strong negative Sr anomalies, together with slightly positive or negative anomalies of HFSE elements of the studied meta-basites (Fig. 5b) indicate that they are unlikely IAB or post-collision basic rocks (PCB), which commonly exhibit positive Sr anomalies and strong depletion of the HFSE. WPB fits better with the studied meta-basites, with respect to the mantle-normalized trace element pattern (e.g., Velikoslavinsky and Krylov, 2014 and references therein), thus the meta-basites were most likely formed in a within-plate environment. To reinforce the hypothesis, the discrimination diagrams proposed by Velikoslavinsky and Krylov (2014) were applied (Fig. 13). Nearly all major elements as well as many trace elements are involved in the discriminant functions of these diagrams; hence they include comprehensive information of the geochemical characteristics of basalts. In this way, the average weighted uncertainty of IAB, MORB, and WPB identification is substantially small as compared with previously elaborated plots. All of the studied meta-basites plot into the category of WPB in the $DF_1(x)$ range (Fig. 13a) and most of them fall into continental WPB field with only a small percentage of OIB in the $DF_3(x)$ range (Fig. 13b). In addition, the $DF_5(x)$ values of the meta-basites are coincident with most WPB but only few post-collision basic rocks (PCB) (Fig. 13c). As a consequence, the studied meta-basites are most likely continental WPB not related to post-collision processes, but rather involved in mantle plume or continental rifting.

29

829   This conclusion is highly in agreement with the zircon Hf isotopic features of the

830   meta-basites (see section 5.1), which demonstrate mixing between the depleted mantle

831   and the crust.

832

833   *5.3.2. Meta-granitoids*

834   Various binary discrimination diagrams were applied to constrain the tectonic

835   setting of the meta-granitoids in Longjingguan. The diagrams employing Ga/Al

836   (Whalen et al., 1987) show that the meta-granitoids have similar geochemical features

837   with A-type granites (Fig. 14). A-type granite was firstly proposed to be related to

838   anorogenic environments (Chappell and White, 1974), but afterwards more and more

839   studies suggest that A-type granite may form under different environments (Whalen et

840   al., 1987; Eby, 1990; Wu et al., 2002; Bonin, 2007). Nevertheless, it is widely

841   accepted that high melting temperatures (>830 °C) are required to generate A-type

842   granite magmas (Clemens et al., 1986), probably through the emplacement of

843   mantle-derived mafic magmas into the lower crust. In this study, the meta-granitoids

844   are spatially and temporally associated with meta-basites, indicating that they were

845   formed under a geodynamic setting characterized by asthenosphere upwelling and

846   basic magmatism, which can provide sufficient heat to generate high-T granitoids.

847   Zircon Hf isotopic compositions of the meta-granitoids (see section 5.1) also suggest

848   addition of the depleted mantle materials into the felsic magmas.

849   Trace elements and REE patterns are frequently used in identifying petrogenesis

850   and tectonic setting of granitoids. The significant depletion of HREE, Nb, Ta, and Ti

851   of the studied meta-granitoids (Fig. 5b) is in agreement with adakite and arc-related

852   ADR (andesite, dacite and rhyolite) (see Castillo, 2006 for an overview). Adakite and

853   arc-related ADR are generally associated to slab subducting and mantle convecting,

854   consistent with the aforementioned high temperature characteristics of the studied

855   meta-granitoids. However, the high Sr, low Yb and high Sr/Y characteristics of

856   adakite are in contrast with the studied meta-granitoids, which exhibit low Sr (13-275

857   ppm), high Y (19-46 ppm) and low Sr/Y (0.34-10.39). In the Sr/Y vs Y diagram (Fig.

858   15), which is usually used to discriminate adakites and TTGs from typical arc

calc-alkaline rocks (Drummond and Defant, 1990), all the studied meta-granitoids plot into the field of typical arc rocks. Therefore, based on the geochemical characteristics, zircon U-Pb ages and Hf isotopic compositions described above, the studied meta-granitoids most likely formed under magmatic arc setting, in agreement with the previous investigations on the Neoproterozoic igneous rocks in the periphery of the SCB (Zheng et al., 2007; Zhao et al., 2018 and references therein); and the low-Si and high-Si types are mainly derived from partial melting of late-Archean and Paleoproterozoic continental crustal materials, respectively, with various degrees of addition of mantle materials.

In summary, the meta-granitoids were formed at ca. 819 Ma by partial melting of ancient continental crustal materials in an arc setting, whereas the meta-basites were derived mainly from the depleted mantle at ca. 772 Ma in a rifting setting. Thus, the studied rocks witness the transition from a convergent to an extensional tectonic setting, and provide new constraints for the beginning of the Neoproterozoic rifting in northern SCB, which can further help to better understand the breakup of the supercontinent Rodinia.

6. Conclusions

(1) The meta-basites and meta-granitoids in Longjingguan are relatively low-grade metamorphosed counterparts of the UHP eclogites and orthogneisses within the CDZ; they were detached from the subducted crust of the SCB and exhumed from shallow depths during subduction, and subsequently thrusted over the CDZ during collisional orogenesis.

(2) The precursors of the studied meta-granitoids and meta-basites were formed at ca. 819 Ma and 772–784 Ma, respectively. They jointly experienced a granulite-facies metamorphism at ca. 768 Ma and a thermal overprinting at ca. 746 Ma resulted from underplating of mafic magmas, strongly pointing to multiple episodes of continental rifting during the Neoproterozoic.

(3) The meta-granitoids are derived mainly from partial melting of ancient continental

crustal materials of the SCB in an arc setting. The low-Si meta-granitoids were derived from the late Archean basement rocks that underwent Paleoproterozoic metamorphic reworking, while the high-Si meta-granitoids mainly come from the Paleoproterozoic juvenile crust. The meta-basites were derived from the depleted mantle in a rifting environment. The studied rocks thus witness the transition from a convergent to an extensional tectonic setting, and provide new time constraints for the beginning of the Neoproterozoic rifting in northern SCB, which can further help to better understand the breakup of the supercontinent Rodinia.

Acknowledgements

References

907 Ames, L., Zhou, G.Z., Xiong, B.C., 1996. Geochronology and isotopic character of
909 ultrahigh-pressure metamorphism with implications for the collision of the
910 Sino-Korean and Yangtze cratons, central China. Tectonics 15, 472–489.

911 Angiboust, S., Harlov, D., 2017. Ilmenite breakdown and rutile-titanite stability in
912 metagranitoids: Natural observations and experimental results. American
913 Mineralogist 102, 1696–1708.

914 Bauer, C., Rubatto, D., Krenn, K., Proyer, A., Hoinkes, G., 2007. A zircon study from
915 the rhodope metamorphic complex, n-greece: time record of a multistage
916 evolution. Lithos 99(3), 207–228.

917 Black, L.P., Kamo, S.L., Allen, C.M., Aleinikoff, J.N., 2003. TEMORA 1: a new
918 zircon standard for phanerozoic U–Pb geochronology. Chemical Geology 200,
919 155–170.

920 Blichert-Toft, J., Albarede, F., 1997. The Lu–Hf isotope geochemistry of chondrites
921 and the evolution of the mantle–crust system. Earth and Planetary Science
922 Letters 148, 243–258.

923 Bohlen, S.R., Liotta, J.J., 1986. A Barometer for Garnet Amphibolites and Garnet
924 Granulites. Journal of Petrology 27, 1025–1034.

925 Bonin, B., 2007. A-type granites and related rocks: evolution of a concept, problems
926 and prospects. Lithos 97(1–2), 1–29.

927 Carpentier, M., Chauvel, C., Maury, R., Mattielli, N., 2009. The "zircon effect" as
928 recorded by the chemical and Hf isotopic compositions of the Lesser Antilles
929 forearc sediments. Earth and Planetary Science Letters 287, 86–99.

930 Castillo, P.R., 2006. An overview of adakite petrogenesis. Chinese Science Bulletin
931 51(3), 257–268.

932 Chappell, B.W., White, A.J.R., 1974. Two contrasting granite types. Pacific Geology 8,
933 173–174.

934 Chemenda, A.I., Mattauer, M., Bokun, A.N., 1996. Continental subduction and a
935 mechanism for exhumation of high-pressure metamorphic rocks: new modelling,

936   field data from Oman. Earth and Planetay Science Letters 143, 173–182.

937   Chen, F., Hegner, E., Todt, W., 2000. Zircon ages and Nd isotopic and chemical

938   compositions of orthogneisses from the Black Forest, Germany: evidence for a

939   Cambrian magmatic arc. International Journal of Earth Sciences 88, 791– 802.

940   Chen, F.K., Guo, J.H., Jiang, L.L., Siebel, W., Cong, B., Satir, M., 2003. Provenance

941   of the Beihuaiyang lower-grade metamorphic zone of the Dabie

942   ultrahigh-pressure collisional orogen, China: evidence from zircon ages. Journal

943   of Asian Earth Science 22(4), 343–352.

944   Chen, F., Li, X.H., Wang, X.L., Li, Q.L., Siebel, W., 2007. Zircon age and Nd-Hf

945   isotopic composition of the Yunnan Tethyan belt, southwestern China.

946   International Journal of Earth Science 96, 1179–1194.

947   Chen, R.X., Zheng, Y.F., Xie, L., 2010. Metamorphic growth and recrystallization of

948   zircon: distinction by simultaneous in-situ analyses of trace elements, U–Th–Pb

949   and Lu–Hf isotopes in zircons from eclogite-facies rocks in the Sulu orogen.

950   Lithos 114, 132–154.

951   Choi, S.H., Mukasa, S.B., 2012. Lu–Hf and Sm–Nd isotope systematic of Korean

952   spinel peridotites: a case for metasomatically induced Nd–Hf decoupling. Lithos

953   154, 263–276.

954   Chopin, C., 1984. Coesite and pure pyrope in high grade blueschists of the western

955   Alps: a first record and some consequences. Contributions to Mineralogy and

956   Petrology 86, 107–118.

957   Clemens, J.D., Holloway, J.R., White, A.J.R., 1986. Origin of an A-type granite:

958   experimental constraints. American Mineralogist 71, 317–324.

959   Compston, W., Williams, I.S., Kirschvink, J.L., 1992. Zircon U–Pb ages for the Early

960   Cambrian time-scale. Journal of the Geological Society 149, 171–184.

961   Cong, B., Zhai, M., Carswell, D.A., Wilson, R.N., Wang, Q., Zhao, Z., Windly, B.F.,

962   1995. Petrogenesis of ultrahigh-pressure rocks and their country rocks at

963   Shuanghe in Dabieshan, central China. European Journal of Mineralogy 7, 119–

964   138.

965   Dong, S.W., Wang, X.F., Huang, D.Z., 1997. Discovery of low grade metamorphic

volcanic rock sheets within UHP in Dabie Mts. and its implications. Chinese Science Bulletin 42, 1199–1203.

Drummond, M.S., Defant, M.J., 1990. A model for trondhjemite–tonalite–dacite genesis and crustal growth via slab melting: Archaean to modern comparisons. Journal of Geophysical Research 95, 21503–21521.

Eby, G.N., 1990. The A-type granitoids: a review of their occurrence and chemical characteristics and speculations on their petrogenesis. Lithos 26, 115–134.

Ernst, W.G., Maruyama, S., Wallis, S., 1997. Buoyancy-driven, rapid exhumation of ultrahigh-pressure metamorphosed continental crust. Proceedings of the National Academy of Science, USA 94, 9532–9537.

Gao, T.S., Tang, J.F., Sang, H.Q., Hu, S.L., Qian, C.C., 2006. Whole-rock Ar-Ar dating for low-grade metavolcanics within the Dabie orogen and its geological implications. Chinese Science Bulletin 51, 1197–1202.

Gebauer, D., Schertl, H.P., Brix, M., Schreyer, W., 1997. 35 Ma old ultrahigh-pressure metamorphism and evidence for very rapid exhumation in the Dora Maira Massif, Western Alps. Lithos 41, 5–24.

Greentree, M.R., Li, Z.X., Li, X.H., Wu, H., 2006. Late mesoproterozoic to earliest neoproterozoic basin record of the sibao orogenesis in western south china and relationship to the assembly of rodinia. Precambrian Research 151(1–2), 79–100.

Griffin, W.L., Pearson, N.J., Belousova, E., Jackson, S.E., van Achterbergh, E., O'Reilly, S.Y., Shee, S.R., 2000. The Hf isotope composition of cratonic mantle: LAM-MC-ICPMS analysis of zircon megacrysts in kimberlites. Geochimica et Cosmochimica Acta 64, 133–147.

Groppo, C., Rolfo, F., Liu, Y.C., Deng, L.P., Wang, A.D., 2015. P-T evolution of elusive UHP eclogites from the Luotian dome (north Dabie zone, China): how far can the thermodynamic modeling lead us? Lithos 226, 183–200.

Hacker, B.R., Ratschbacher, L., Webb, L., Ireland, T., Walker, D., Dong, S.W., 1998. U/Pb zircon ages constrain the architecture of the ultrahigh-pressure Qinling–Dabie orogen, China. Earth and Planetary Science Letters 161, 215–230.

996   Hacker, B.R., Ratschbacher, L., Webb, L., McWiliams, M.O., Ireland, T., Calvert, A.,

997   Dong, S.W., Wenk, H.R., Chateigner, D., 2000. Exhumation of ultrahigh-pressure

998   continental crust in east central China: Late Triassic-Early Jurassic tectonic

999   unroofing. Journal of Geophysical Research 105 (B6), 13339–13364.

1000   Hanchar, J.M., Rudnick, R.L., 1995. Revealing hidden structures: the application of

1001   cathodoluminescence and back-scattered electron imaging to dating zircons from

1002   lower crustal xenoliths. Lithos 36, 289–303.

1003   Hanyu, T., Tatsumi, Y., Nakai, S., Chang, Q., Miyazaki, T., Sato, K., Tani, K., Shi-bata,

1004   T., Yoshida, T., 2006. Contribution of slab melting and slab dehydration to

1005   magmatism in the NE Japan arc for the last 25 Myr: Constraints from

1006   geochemistry. Geochemistry Geophysics Geosystems 7, Q08002.

1007   Hermann, J., Rubatto, D., Korsakov, A., Shatsky, V.S., 2001. Multiple zircon growth

1008   during fast exhumation of diamondiferous, deeply subducted continental crust

1009   (Kokchetav massif, Kazakhstan). Contributions to Mineralogy and Petrology 141,

1010   66–82.

1011   Hermann, J., Spandlera, C., Hacka, A., Korsakovb, A.V., 2006. Aqueous fluids and

1012   hydrous melts in high-pressure and ultra-high pressure rocks: Implications for

1013   element transfer in subduction zones. Lithos 92, 399–417.

1014   Hoffmann, J.E., Münker, C., Polat, A., Rosing, M.T., Schulz, T., 2011. The origin of

1015   decoupled Hf–Nd isotope compositions in Eoarchean rocks from southern West

1016   Greenland. Geochimica et Cosmochimica Acta 75, 6610–6628.

1017   Holland, T., Blundy, J., 1994. Non-ideal interactions in calcic amphiboles and their

1018   bearing on amphibole-plagioclase thermometry. Contributions to Mineralogy and

1019   Petrology 116, 433–447.

1020   Hong, J.A., Ma, B., Huang, Q., 2009. The Dafushan meta-basic/ultrameta-basic

1021   complex and genesis of the related rutile ore deposit at Zaoyang, Hubei (in

1022   Chinese with English abstract). Chinese Journal of Geology 44, 231–244.

1023   Hoskin, P.W., Ireland, T.R., 2000. Rare earth element chemistry of zircon and its use

1024   as a provenance indicator. Geology 28(7), 627–630.

1025   Hou, Z.H., Wang, C.X., 2007. Determination of 35 trace elements in geological

1026   samples by inductively coupled plasma mass spectrometry (in Chinese with

1027   English abstract). Journal of University of Science and Technology of China 37,

1028   940–944.

1029 Jiang, L., Siebel, W., Chen, F., Liu, Y.C., Chu, D., 2005. U-Pb zircon ages for the

1030   Luzhenguan Complex in northern part of the eastern Dabie orogen. Science

1031   China (Series D) 48, 1357–1367.

1032 Kelemen, P.B., Hanghoj, K., Greene, A.R., 2003. One view of the geochemistry of

1033   subducted-related magmatic arcs, with an emphasis on primitive andesites and

1034   lower crust. Treatise of Geochemistry 3, 593–659.

1035 Kessel, R., Schmidt, M.W., Ulmer, P., Pettke, T., 2005. Trace element signature of

1036   subduction-zone fluids, melts and supercritical liquids at 120–180 km depth.

1037   Nature 437, 724–727.

1038 Le Bas, M.J., Le Maitre, R.W., Streckeisen, A., Zanettin, B., 1986. A chemical

1039   classification of volcanic rocks based on the total alkali-silica diagram. Journal

1040   of Petrology 27(3), 745–750.

1041 Lee, C.A., Luffi, P., Plank, T., Dalton, H., Leeman, W.P., 2009. Constraints on the

1042   depths and temperatures of basic magma generation on Earth and other terrestrial

1043   planets using new thermobarometers for mafic magmas. Earth and Planetary

1044   Science Letters 279, 20–33.

1045 Li, S.G., Xiao, Y.L., Liou, D.L., Ge, N.J., Zhang, Z.Q., Sun, S.S., Cong, B.L., Zhang,

1046   R.Y., Hart, S.R., Wang, S.S., 1993. Collision of the North China and Yangtze

1047   blocks and formation of coesite bearing eclogites: timing and processes.

1048   Chemical Geology 109, 89–111.

1049 Li, S.G., Jagoutz, E., Chen, Y.Z., Li, Q.L., 2000. Sm–Nd and Rb–Sr isotope

1050   chronology of ultrahigh-pressure metamorphic rocks and their country rocks at

1051   Shuanghe in the Dabie Mountains, central China. Geochimica et Cosmochimica

1052   Acta 64, 1077–1093.

1053 Li, S.Z., Kusky, T.M., Zhao, G.C., Liu, X.C., Zhang, G.W., Kopp, H., Wang, L., 2010.

1054   Two-stage Triassic exhumation of HP–UHP terranes in the western Dabie orogen

1055   of China: constraints from structural geology. Tectonophysics 490, 267–293.

Li, X.H., Li, Z.X., Ge, W.C., Zhou, H.W., Li, W.X., Liu, Y., Wingate, M.T.D., 2003a. Neoproterozoic granitoids in South China: crustal melting above a mantle plume at ca 825 Ma? Precambrian Research 122, 45–83.

Li, X.H., Li, Z.X., Zhou, H., Liu, Y., Liang, X., Li, W., 2003b. SHRIMP U–Pb zircon age, geochemistry and Nd isotope of the Guandaoshan pluton in SW Sichuan: petrogenesis and tectonic significance. Science China (Series D) 46, 73–83.

Li, X.P., Zheng, Y., Wu, Y., Chen, F., Gong, B., Li, Y.L., 2004. Low-T eclogite in the Dabie terrane of China: petrological and isotopic constrains on fluid activity and radiometric dating. Contributions to Mineralogy and Petrology 148, 443–470.

Li, Z.X., Li, X.H., Kinny, P.D., Wang, J., Zhang, S., Zhou, H., 2003c. Geochronology of Neoproterozoic syn-rift magmatism in the Yangtze Craton, South China and correlations with other continents: evidence for a mantle superplume that broke up Rodinia. Precambrian Research 122, 85–109.

Li, S.G., Huang, F., Zhou, H.Y., Li, H.M., 2003d. U-Pb isotopic compositions of the ultrahigh pressure metamorphic (UHPM) rocks from Shuanghe and gneisses from Northern Dabie zone in the Dabie Mountains, central China: Constraint on the exhumation mechanism of UHPM rocks. Science China (Series D) 46(3), 200–209.

Li, Y., Liu, Y.C., Yang, Y., Deng, L.P., 2017. New U-Pb geochronological constraints on formation and evolution of the Susong complex zone in the Dabie orogen. Acta Geologica Sinica 91, 1915–1918.

Liu, F., Gerdes, A., Xue, H., Liang, F., 2006a. SHRIMP U-Pb zircon dating from eclogite lenses in marble, Dabie-Sulu UHP terrane: restriction on the prograde, UHP and retrograde metamorphic ages. Acta Petrologica Sinica 22, 1761–1778.

Liu, J., Ye, K., Maruyama, S., Cong, B., Fan, H., 2001. Mineral inclusions in zircon from gneisses in the ultrahigh-pressure zone of the Dabie Mountains, China. Journal of Geology 109, 523–535.

Liu, X.C., Jahn, B.-M., Liu, D., Dong, S., Li, S., 2004. SHRIMP U-Pb zircon dating of a metagabbro and eclogites from western Dabieshan (Hong'an Block), China, and its tectonic implications. Tectonophysics 394, 171–192.

1086 Liu, X.M, Gao, S., Diwu, C.R, Ling, W.L., 2008. Precambrian crustal growth of
1087   Yangtze Craton as revealed by detrital zircon studies. American Journal of
1088   Science 308(4), 421–468.

1089 Liu, Y.C., Deng, L.P., Gu, X.F., Groppo, C., Franco, R., 2015. Application of
1090   Ti-in-zircon and Zr-in-rutile thermometers to constrain high-temperature
1091   metamorphism in eclogites from the Dabie orogen, central China. Gondwana
1092   Research 27, 410–423.

1093 Liu, Y.C., Gu, X.F., Li, S.G., Hou, Z.F., Song, B., 2011a. Multistage metamorphic
1094   events in granulitized eclogites from the North Dabie complex zone, central
1095   China: evidence from zircon U-Pb age, trace element and mineral inclusion.
1096   Lithos 122, 107–121.

1097 Liu, Y.C., Gu, X.F., Rolfo, F., Chen, Z.Y., 2011b. Ultrahigh-pressure metamorphism
1098   and multistage exhumation of eclogite from the Luotian dome, North Dabie
1099   Complex Zone (central China): Evidence from mineral inclusions and
1100   decompression texture. Journal of Asian Earth Science 42, 607–617.

1101 Liu, Y.C., Li, S.G, 2005. Lower crustal rocks from the Dabie Mountains and their
1102   subduction. Acta Petrologica Sinica 21, 1059–1066.

1103 Liu, Y.C., Li, S.G., 2008. Detachment within subducted continental crust and
1104   multi-plate successive exhumation of ultrahigh-pressure metamorphic rocks:
1105   Evidence from the Dabie-Sulu orogenic belt. Chinese Science Bulletin 53,
1106   3105–3119.

1107 Liu, Y.C., Li, S.G., Gu, X.F., Hou, Z.H., 2006b. Zircon SHRIMP U-Pb dating for
1108   olivine gabbro at Wangmuguan in the Beihuaiyang zone and its geological
1109   significance. Chinese Science Bulletin 51, 2500–2506.

1110 Liu, Y.C., Li, S.G., Gu, X.F., Xu, S.T., Chen, G.B., 2007a. Ultrahigh-pressure eclogite
1111   transformed from mafic granulite in the Dabie orogen, east-central China.
1112   Journal of Metamorphic Geology 25, 975–989.

1113 Liu, Y.C., Li S.G., Xu, S.T., 2007b. Zircon SHRIMP U-Pb dating for gneiss in
1114   northern Dabie high T/P metamorphic zone, central China: Implication for
1115   decoupling within subducted continental crust. Lithos 96, 170–185.

1116 Liu, Y.C., Li, S.G., Xu, S.T., John, B., Zheng, Y.F., Zhang, Z.Q., Jiang, L.L., Chen,
1117   G.B., Wu, W.P., 2005. Geochemistry and geochronology of eclogites from the
1118   northern Dabie Mountains, central China. Journal of Asian Earth Science 25,
1119   431–443.

1120 Liu, Y.C., Liu, L.X., Gu, X.F., Li, S.G., Liu, J., Song, B., 2010. Occurrence of
1121   Neoproterozoic low-grade metagranite in the western Beihuaiyang zone, the
1122   Dabie orogen. Chinese Science Bulletin 55, 3490–3498.

1123 Liu, Y.C., Liu, L.X., Li, Y., Gu, X.F., Song, B., 2017. Zircon U-Pb geochronology and
1124   petrogenesis of metabasites from the western Beihuaiyang zone in the Hong'an
1125   orogen, central China: Implications for detachment within subducting continental
1126   crust at shallow depths. Journal of Asian Earth Science 145, 74–90.

1127 Liu, Y.C., Wang, A.D., Rolfo, F., Groppo, C., Gu, X.F., Song, B., 2009.
1128   Geochronological and petrological constraints on Palaeoproterozoic granulite
1129   facies metamorphism in southeastern margin of the North China Craton. Journal
1130   of Metamorphic Geology 27, 125–138.

1131 Liu, Y.S., Gao, S., Yuan, H.L., Zhou, L., Liu, X.M., Wang, X.C., Hu, Z.C., Wang, L.S.,
1132   2004. U–Pb zircon ages and Nd, Sr, and Pb isotopes of lower crustal xenoliths
1133   from North China Craton: insights on evolution of lower continental crust.
1134   Chemical Geology 211, 87–109.

1135 Ludwig, K.R., 2001. Users Manual for Isoplot/Ex (rev. 2.49): A Geochronological
1136   Toolkit for Microsoft Excel. Berkeley Geochronology Center, Special
1137   Publication No. 1a, 55 p.

1138 Maruyama, S., Liou, J.G., Terabayashi, M., 1996. Blueschists and eclogites of the
1139   world, and their exhumation. International Geology Review 38, 485–594.

1140 Nasdala, L., Massonne, H.J., 2000. Microdiamonds from the Saxonian Erzgebirge,
1141   Germany: in situ micro-Raman characterisation. European Journal of Mineralogy
1142   12, 495–498.

1143 Nowell, G.M., Kempton, P.D., Noble, S.R., Fitton, J.G., Saunders, A.D., Mahoney, J.J.,
1144   Taylor, R.N., 1998. High precision Hf isotope measurements of MORB and OIB
1145   by thermal ionisation mass spectrometry: insights into the depleted mantle.

1146   Chemical Geology 149, 211–233.

1147 Okay, A.I., Xu, S.T., Sengör, A.M.C., 1989. Coesite from the Dabie Shan eclogites,

1148   central China. European Journal of Mineralogy 1, 595–598.

1149 Okay, A.I., Sengör, A.M.C., 1992. Evidence for intracontinental thrust-related

1150   exhumation of the ultra-high-pressure rocks in China. Geology 20, 411–414.

1151 Okay, A.I., Sengör, A.M.C., Satir, M., 1993. Tectonics of an ultrahigh-pressure

1152   metamorphic terrane: the Dabie Shan/Tongbai orogen, China. Tectonics 12,

1153   1320–1334.

1154 Palme, H., O'Neill, H.St.C., 2003. Cosmochemical constraints of mantle composition.

1155   Treatise of Geochemistry 2, 1–38.

1156 Patchett, P.J., White, W.M., Feldmann, H., Kienlinczuk, S., Hofmann, A.W., 1984.

1157   Hafnium/rare earth element fractionation in the sedimentary system and crustal

1158   recycling into the Earth's mantle. Earth and Planetary Science Letters 1984,

1159   365–378.

1160 Rolfo, F., Compagnoni, R., Xu, S., Jiang, L., 2000. First report of felsic whiteschist in

1161   the ultrahigh-pressure metamorphic belt of Dabie Shan, China. European Journal

1162   of Mineralogy 12, 883–898.

1163 Rolfo, F., Compagnoni, R., Wu, W.P., Xu, S.T., 2004. A coherent lithostratigraphic

1164   unit in the coesite–eclogite complex of Dabie Shan, China: geologic and

1165   petrologic evidence. Lithos 73, 71–94.

1166 Roux, V.L., Bodinier, J.L., Alard, O., O'Reilly, S.Y., Griffin, W.L., 2009. Isotopic

1167   decoupling during porous melt flow: a case-study in the Lherzperidotite. Earth

1168   and Planetary Science Letters 279, 76–85.

1169 Rowley, D.B., Xue, F., Tucker, R.D., Peng, Z.X., Baker, J., Davis, A., 1997. Ages of

1170   ultrahigh pressure metamorphism and protolith orthogneisses from the eastern

1171   Dabie Shan: U/Pb zircon geochronology. Earth and Planetary Science Letters

1172   151, 191–203.

1173 Rudnick, R.L., Gao, S., 2003. Composition of the continental crust. Treatise on

1174   Geochemistry 3, 1–64.

1175 Salters, V.J.M., Stracke, A., 2004. Composition of the depleted mantle. Geochemistry

1176   Geophysics Geosystems 5, Q05004.

1177 Scherer, E., Munker, C., Mezger, K., 2001. Calibration of the lutetium–hafnium clock.

1178   Science 293, 683–687.

1179 Schertl, H.P., Okay, A.I., 1994. A coesite inclusion in dolomite in Dabie Shan, China;

1180   petrological and rheological significance. European Journal of Mineralogy 6,

1181   995–1000.

1182 Schmidt, M.W., 1992. Amphibole composition in tonalite as a function of pressure: an

1183   experimental calibration of the Al-in-hornblende barometer. Contributions to

1184   Mineralogy and Petrology 110, 304–310.

1185 Smith, D.C., 1984. Coesite in clinopyroxene in the Caledonides and its implications

1186   for geodynamics. Nature 310, 641–644.

1187 Sobolev, N.V., Shatsky, V.S., 1990. Diamond inclusions in garnets from metamorphic

1188   rocks: a newenvironment for diamond formation. Nature 343, 742–746.

1189 Su, W., Xu, S., Jiang, L., Liu, Y.C., 1996. Coesite from quartz jadeitite in the Dabie

1190   Mountains, Eastern China. Mineralogical Magazine 60, 659–662.

1191 Sun, S.S., McDonough, W.F., 1989. Chemical and isotopic systematics of oceanic

1192   basalts: implications for mantle composition and processes. In: Saunders, A.D.,

1193   Norry, M.J. (Eds.), Magmatism in the ocean basins. Geological Society, London,

1194   Special Publications 42, pp. 313–345.

1195 Tabata, H., Yamauchi, K., Maruyama, S., Liou, J.G., 1998. Tracing the Extent of a

1196   UHP Metamorphic Terrane: Mineral-Inclusion Study of Zircons in Gneisses from

1197   the Dabie Shan. In: Hacker, B.R., Liou, J.G. (Eds), When Continents Collide:

1198   Geodynamics and Geochemistry of Ultrahigh-Pressure Rocks. Springer

1199   Netherlands 10, pp. 261–273.

1200 Tang, H.F., Liu, C.Q., Nakai, S., Orihashi, Y., 2007. Geochemistry of eclogites from

1201   the Dabie–Sulu terrane, eastern china: new insights into protoliths and trace

1202   element behaviour during UHP metamorphism. Lithos 95, 441–457.

1203 Tang, J., Zheng, Y.F., Wu, Y. B., Gong, B., 2006. Zircon SHRIMP U–Pb dating, C and

1204   O isotopes for impure marbles from the Jiaobei terrane in the Sulu orogen:

1205   Implication for tectonic affinity. Precambrian Research 144, 1–18.

1206 Tappe, S., Pearson, D.G., Nowell, G., Nielsen, T., Milstead, P., Muehlenbachs, K.,
1207   2011. A fresh isotopic look at Greenland kimberlites: cratonic mantle lithosphere
1208   imprint on deep source signal. Earth and Planetary Science Letters 305, 235–248.

1209 Taylor, S.R., McLennan, S.M., 1985. The Continental Crust: Its Composition and
1210   Evolution. Blackwell Scientific Publications, Oxford.

1211 Tomkins, H.S., Powell, R., Ellis, D.J., 2007. The pressure dependence of the
1212   zirconium-in-rutile thermometer. Journal of Metamorphic Geology 25, 703–713.

1213 Tsai, C.H., Liou, J.G., 2000. Eclogite-facies relics and inferred ultrahigh-pressure
1214   metamorphism in the North Dabie Complex, central-eastern China. American
1215   Mineralogist 85, 1–8.

1216 Velikoslavinsky, S.D., Krylov, D.P. 2014. Geochemical discrimination of basalts
1217   formed in major geodynamic settings. Geotectonics 48(6), 427–439.

1218 Wang, L.J., Griffin, W.L., Yu, J.H., O'Reilly, S.Y., 2010. Precambrian crustal
1219   evolution of the Yangtze Block tracked by detrital zircons from Neoproterozoic
1220   sedimentary rocks. Precambrian Research 177(1), 131–144.

1221 Wang, M.X., Wang, C.Y., Zhao, J.H., 2013. Zircon U/Pb dating and Hf-O isotopes of
1222   the Zhouan ultramafic intrusion in the northern margin of the Yangtze Block, SW
1223   China: Constraints on the nature of mantle source and timing of the
1224   supercontinent Rodinia breakup. Chinese Science Bulletin 58(7), 777–787.

1225 Wang, X., Liou, J.G., Mao, H.K., 1989. Coesite-bearing eclogites from the Dabie
1226   Mountains in central China. Geology 17, 1085–1088.

1227 Whalen, J.B., Currie, K.L., Chappell, B.W., 1987. A-type granites: geochemical
1228   characteristics, discrimination and petrogenesis. Contributions to Mineralogy and
1229   Petrology 95, 407–419.

1230 Whitney, J.A., Stormer, J.C., 1977. Two-feldspar geothermometry, geobarometry in
1231   mesozonal granitic intrusions: three examples from the Piedmont of Georgia.
1232   Contributions to Mineralogy and Petrology 63(1), 51–64.

1233 Williams, I.S., 1998. U–Th–Pb geochronology by ion microprobe. Applications of
1234   Microanalytical Techniques to Understanding Mineralizing Processes. In:
1235   McKibben, M.A., Shanks III, W.C., Ridley, W.I. (Eds.), Reviews in Economic

1236   Geology 7, pp. 1–35.

1237   Winchester, J.A., Floyd, P.A., 1977. Geochemical discrimination of different magma

1238   series and their differentiation products using immobile elements. Chemical

1239   Geology 20, 325–343.

1240   Workman, R.K., Hart, S.R., 2005. Major and trace element composition of the

1241   depleted MORB mantle (DMM). Earth and Planetary Science Letters 231,

1242   53–72.

1243   Wu, F.Y., Sun, D.Y., Li, H., Jahn, B.M., Wilde, S., 2002. A-type granites in

1244   northeastern china: age and geochemical constraints on their petrogenesis.

1245   Chemical Geology 187, 143–173.

1246   Wu, Y.B., Zheng, Y.F., Zhao, Z.F., Gong, B., Liu, X.M., Wu, F.Y., 2006a. U–Pb, Hf

1247   and O isotope evidence for two episodes of fluid-assisted zircon growth in

1248   marble-hosted eclogites from the Dabie orogen. Geochimica et Cosmochimica

1249   Acta 70, 3743–3761.

1250   Wu, R.X., Zheng, Y.F., Wu, Y.B., Zhao, Z.F., Zhang, S.B., Liu, X.M., Wu, F.Y., 2006b.

1251   Reworking of juvenile crust: element and isotope evidence from Neoproterozoic

1252   granodiorite in South China. Precambrian Research 146, 179–212.

1253   Wu, Y.B., Zheng, Y.F., Tang, J., Gong, B., Zhao, Z.F., Liu, X., 2007. Zircon U–Pb

1254   dating of water–rock interaction during Neoproterozoic rift magmatism in South

1255   China. Chemical Geology 246, 65–86.

1256   Xiao, Y., Hoefs, J., van den Kerkhof, A.M., Li, S.G., 2001. Geochemical constraints of

1257   the eclogite and granulite facies metamorphism as recognized in the Raobazhai

1258   complex from North DabieShan, China. Journal of Metamorphic Geology 19,

1259   3–19.

1260   Xu, S.T., Jiang, L.L., Liu, Y.C., Zhang, Y., 1992a. Tectonic Framework and Evolution

1261   of the Dabie Mountains in Anhui, Eastern China. Acta Geologica Sinica 5,

1262   221–238.

1263   Xu, S.T, Okay, A.I., Ji, S.Y., Sengör, A.M.C., Su, W., Liu, Y.C., Jiang, L.L., 1992b.

1264   Diamond from the Dabie Shan metamorphic rocks and its implication for

1265   tectonic setting. Science 256, 80–82.

1266 Xu, S.T., Liu, Y.C., Su, W., Wang, R.C., Jiang, L.L., Wu, W.P., 2000. Discovery of the
1267   eclogite and its petrography in the Northern Dabie Mountains. Chinese Science
1268   Bulletin 45, 273–278.

1269 Xu, S.T., Liu, Y.C., Chen, G.B., Compagnoni, R., Rolfo, F., He, M.C., Liu, H.F., 2003.
1270   New finding of micro-diamonds in eclogites from Dabie-Sulu region in
1271   central-eastern China. Chinese Science Bulletin 48, 988–994.

1272 Xu, S.T., Liu, Y.C., Chen, G.B., Ji, S.Y., Ni, P., Xiao, W.S., 2005. Microdiamonds,
1273   their classification and tectonic implications for the host eclogites from the Dabie
1274   and Su-Lu regions in central eastern China. Mineralogical Magazine 69,
1275   509–520.

1276 Xue, H.M., Ma, F., Song, Y.Q., 2011. Geochemistry and SHRIMP zircon U-Pb data of
1277   Neoproterozoic meta-magmatic rocks in the Suizhou-Zaoyang area, northern
1278   margin of the Yangtze Craton, Central China. Acta Petrologica Sinica 27,
1279   1116–1130.

1280 Yu, S.Y., Xu, Y.G., Huang, X.L., Ma, J.L., Ge, W.C., Zhang, H.H., Qin, X.F., 2009.
1281   Hf–Nd isotopic decoupling in continental mantle lithosphere beneath Northeast
1282   China: effects of pervasive mantle metasomatism. Journal of Asian Earth Science
1283   35, 554–570.

1284 Yuan, H.L., Gao, S., Liu, X.M., Gunther, D., Wu, F.Y., 2004. Accurate U–Pb age and
1285   trace element determinations of zircon by laser ablation-inductively coupled
1286   plasma mass spectrometry. Geostandards and Geoanalytical Research 28,
1287   353–370.

1288 Zack, T., Moraes, R., Kronz, A., 2004. Temperature dependence of Zr in rutile:
1289   empirical calibration of a rutile thermometer. Contributions to Mineralogy and
1290   Petrology, 148, 471–488.

1291 Zartman, R.E., 1981. PIumbotectonics—the model. Tectonophysics 75, 135–162.

1292 Zhang, H.F., Gao, S., Zhang, Z.Q., Zhang, B.R., Zhang, L., Hu, S.H., 2002.
1293   Geochemical and Sr-Nd-Pb isotopic compositions of Cretaceous granitoids:
1294   constraints on tectonic framework and crustal structure of the Dabieshan
1295   ultrahigh-pressure metamorphic belt, China. Chemical Geology 186, 281–299.

1296 Zhang, R.Y., Liou, J.G., Zheng, Y.F., Fu, B., 2003. Transition of UHP eclogites to
1297   gneissic rocks of low-amphibolite facies during exhumation: evidence from the
1298   dabie terrane, central China. Lithos, 70, 269–291.

1299 Zhang, S.B., Zheng, Y.F., Wu, Y.B., Zhao, Z.F., Gao, S., Wu, F.Y., 2006a. Zircon
1300   isotope evidence for ≥3.5 Ga continental crust in the Yangtze craton of China.
1301   Precambrian Research 146, 16–34.

1302 Zhang, S.B., Zheng, Y.F., Wu, Y.B., Zhao, Z.F., Gao, S., Wu, F.Y., 2006b. Zircon
1303   U–Pb age and Hf–O isotope evidence for Paleoproterozoic metamorphic event in
1304   South China. Precambrian Research 151, 265–288.

1305 Zhang, S.B., Zheng, Y.F., Wu, Y.B., Zhao, Z.F., Gao, S., Wu, F.Y., 2006c. Zircon
1306   U–Pb age and Hf isotope evidence for 3.8 Ga crustal remnant and episodic
1307   reworking of Archean crust in South China. Earth and Planetary Science Letters
1308   252, 56–71.

1309 Zhao, G.C., Cawood, P.A., 2012. Precambrian geology of China. Precambrian
1310   Research 222–223, 13–54.

1311 Zhao, J.H., Zhou, M.F., 2009. Secular evolution of the Neoproterozoic lithospheric
1312   mantle underneath the northern margin of the Yangtze Block, South China.
1313   Lithos 107, 152–168.

1314 Zhao, J.H., Li, Q.W., Liu, H., Wang, W., 2018. Neoproterozoic magmatism in the
1315   western and northern margins of the Yangtze Block (South China) controlled by
1316   slab subduction and subduction-transform-edge-propagator. Earth-Science
1317   Reviews 187, 1–18.

1318 Zheng, Y.F., Zhou, J.B., Wu, Y.B., Xie, Z., 2005. Low-grade metamorphic rocks in the
1319   Dabie-Sulu orogenic belt: a passive-margin accretionary wedge deformed during
1320   continent subduction. International Geology Review 47, 851–871.

1321 Zheng, Y.F., Zhao, Z.F., Wu, Y.B., Zhang, S.B., Liu, X.M., Wu, F.Y., 2006. Zircon
1322   U–Pb age, Hf and O isotope constraints on protolith origin of ultrahigh-pressure
1323   eclogite and gneiss in the Dabie orogen. Chemical Geology 231, 135–158.

1324 Zheng, Y.F., Zhang, S.B., Zhao, Z.F., Wu, Y.B., Li, X.H., Li, Z.X., Wu, F.Y., 2007.
1325   Contrasting zircon Hf and O isotopes in the two episodes of Neoproterozoic

1326 granitoids in South China: implications for growth and reworking of continental

1327 crust. Lithos 96, 127–150.

1328 Zheng, Y.F., Wu, R.X., Wu, Y.B., Zhang, S.B., Yuan, H.L., Wu, F.Y., 2008. Rift

1329 melting of juvenile arc-derived crust: geochemical evidence from

1330 Neoproterozoic volcanic and granitic rocks in the Jiangnan Orogen, South China.

1331 Precambrian Research163, 351–383.

1332 Zheng, Y.F., Xia, Q.X., Chen, R.X., Gao, X.Y., 2011. Partial melting, fluid

1333 supercriticality and element mobility in ultrahigh-pressure metamorphic rocks

1334 during continental collision. Earth Science Reviews 107, 342–374.

1335 Zhou, M.F., Kennedy, A.K., Sun, M., Malpas, J., Lesher, C.M., 2002a. Neoproterozoic

1336 arc-related mafic intrusions in the northern margin of South China: implications

1337 for accretion of Rodinia. The Journal of Geology 110, 611–618.

1338 Zhou, M.F., Yan, D.P., Kennedy, A.K., Li, Y.Q., Ding, J., 2002b. SHRIMP zircon

1339 geochronological and geochemical evidence for Neo-proterozoic arc-related

1340 magmatism along the western margin of the Yangtze Block, South China. Earth

1341 and Planetary Science Letters 196, 51–67.

1342 Zhou, M.F., Ma, Y.X., Yan, D.P., Xia, X.P., Zhao, J.H., Sun, M., 2006a. The Yanbian

1343 Terrane (Southern Sichuan Province, SW China): a Neoproterozoic arc

1344 assemblage in the western margin of the Yangtze Block. Precambrian Research

1345 144, 19–38.

1346 Zhou, M.F., Yan, D.P., Wang, C.L., Qi, L., Kennedy, A., 2006b. Subduction related

1347 origin of the 750 Ma Xuelongbao adakitic complex (Sichuan Province, China):

1348 implications for the tectonic setting of the giant Neoproterozoic magmatic event

1349 in South China. Earth and Planetary Science Letters 248, 286–300.

1350 Zindler, A., Hart, S., 1986. Chemical geodynamics. Annual Review of Earth and

1351 Planetary Science 14, 493–571.

1352

Figure captions

1354 **Figure 1** Schematic geological map of the Dabie orogen. The inset shows its location

1355 within the Triassic Qinling–Dabie–Sulu collision orogen in central China (modified

1356 from Liu et al., 2007a). Sample locality is marked by a red star. BZ = Beihuaiyang

1357 zone, NDZ = North Dabie high-T/UHP complex zone, CDZ = Central Dabie

1358 mid-T/UHP metamorphic zone, SDZ = South Dabie low-T eclogite zone, SZ =

1359 Susong complex zone, HMZ = Huwan mélange zone, HZ = Hong'an low-T eclogite

1360 zone, DC = amphibolite-facies Dabie complex, XMF = Xiaotian-Mozitan fault, WSF

1361 = Wuhe-Shuihou fault, HMF = Hualiangting-Mituo fault, TSF = Taihu-Shanlong fault,

1362 TLF = Tan-Lu fault.

1363

1364 **Figure 2** Field photograph showing meta-basite lens tectonically enclosed within

1365 meta-granitoid.

1366

1367 **Figure 3** Photomicrographs of plane- and corresponding cross-polarized images for

1368 the meta-basite sample 11LJG7 (a & b), low-Si meta-granitoid sample 1209LJG5 (c

1369 & d), high-Si meta-granitoid sample 1209LJG1 (e & f). Pl: plagioclase; Rt: rutile;

1370 Amp: amphibole; Bt: biotite; Qz: quartz; Ap: apatite; Kfs: K-feldspar; Aln: allanite.

1371

1372 **Figure 4** TAS (total alkalies versus silica) diagram (Le Bas et al., 1986) (a) and

1373 Zr/TiO_2 vs Nb/Y (Winchester and Floyd, 1977) (b) plots for the studied rocks in

1374 Longjingguan. Green circles: meta-basites; red circles: low-Si granitoids; blue circles:

1375 high-Si granitoids; Pc: picrobasalt; B: basalt; O1: basaltic andesite; O2: andesite; O3:

1376 dacite; R: rhyolite; S1: trachybasalt; S2: basaltic trachyandesite; S3: trachyandesite; T:

1377 trachyte; U1: basanite; U2: phonotephrite; U3: tephriphonolite; Ph: phonolite; F:

1378 foidite. Symbols used for different types of samples are the same as in the following

1379 figures.

1380

1381 **Figure 5** Chondrite-normalized REE patterns (a) and primitive mantle-normalized

trace element patterns (b) for the studied rocks in Longjingguan and for the UHP eclogites (c & d) in the CDZ. Normalized values and the data of the N-MORB and E-MORB are from Sun and McDonough (1989), the elemental data of the UHP eclogites are from Tang et al. (2007).

Figure 6 Representative CL images of zircons from the meta-basites (samples 11LJG3 and 11LJG7), low-Si meta-granitoids (samples 11LJG2, 1209LJG5 and 1202LJG3) and high-Si meta-granitoid (sample 1303LJG2) in Longjingguan. The red circles locate the SHRIMP analysis spots, and the red numbers are the corresponding $^{206}Pb/^{238}U$ ages.

Figure 7 Mineral inclusions within metamorphic zircon domains from samples 11LJG3 (a-i) and 11LJG2 (j-l). Hbl, hornblende; Rt, rutile; Qz, quartz; Ap, apatite; Kfs, K-feldspar; Mus, muscovite; Ep, epidote; Ttn, titanite; Ilm, ilmenite.

Figure 8 Zircon rare earth element (REE) patterns for the meta-basites (samples 11LJG3 and 11LJG7) and meta-granitoids (samples 1209LJG5, 11LJG2, 1303LJG2 and 1202LJG3) in Longjingguan. Normalized values are from Sun and McDonough (1989).

Figure 9 SHRIMP zircon U-Pb ages for the meta-basites (a & b), low-Si meta-granitoids (c, d, e, g & h) and high-Si meta-granitoid (f) in Longjingguan. (e) and (h) correspond to the dashed squares in (d) and (g), respectively.

Figure 10 Zircon ε_{Hf} (t) vs U-Pb age of the studied meta-basites and meta-granitoids, as well as the UHP eclogites and gneisses (data from Zheng et al., 2006) from the CDZ. The evolution trendlines of the depleted mantle (DMM) and chondrite are from Griffin et al. (2000).

1412 **Figure 11** Plot of Nd vs Sr isotopes for the meta-basites (samples 11LJG3 to 11LJG8)

1413 from Longjingguan. MORB: mid-ocean ridge basalt; UCC: upper continental crust;

1414 LCC: lower continental crust.

1415

1416 **Figure 12** $(^{207}Pb/^{204}Pb)_i$ vs $(^{206}Pb/^{204}Pb)_i$ and $(^{208}Pb/^{204}Pb)_i$ vs $(^{206}Pb/^{204}Pb)_i$ plots for

1417 the meta-basites (samples 11LJG3 to 11LJG8) from Longjingguan. The initial Pb

1418 isotopes data of the meta-basites are calibrated with t=230 Ma, the blue-green and

1419 grey areas in the diagrams represent the UHP orthogneiss and eclogites in the North

1420 Dabie (NDZ) and Central Dabie (CDZ) terranes, respectively (data from Zhang et al.,

1421 2002; Li et al., 2003d). The initial Pb isotope data of MORB, EMI and EMII are from

1422 Zindler and Hart. (1986), and that of lower crust (LC) is from Liu et al. (2004).

1423 $(^{207}Pb/^{204}Pb)_{NHRL}=0.1084\times(^{206}Pb/^{204}Pb)_i + 13.401$; $(^{208}Pb/^{204}Pb)_{NHRL}=1.209\times(^{206}Pb/$

1424 $^{204}Pb)_i + 15.627$.

1425

1426 **Figure 13** Tectonic discrimination diagrams (Velikoslavinsky and Krylov, 2014) for

1427 the meta-basites in Longjingguan. Values of the discriminant functions $DF_1(x)$, $DF_2(x)$,

1428 $DF_3(x)$ and $DF_5(x)$ have been calculated from formula: $D(x) = \Sigma a_i*x_i +$ constant,

1429 where a_i is coefficient at corresponding variable; x_i is value of variable (oxide content,

1430 wt %; trace element content, ppm). In the $DF_1(x)-DF_2(x)$ diagram (a), the

1431 meta-basites (green circles) plot in the field of WPB. In the $DF_3(x)-$ frequency (%) (b)

1432 and $DF_5(x)-$ frequency (%) (c) diagrams, the rocks (the red rectangles with dashed

1433 oblique lines) have function values coincident with the majority population of WPB.

1434

1435 **Figure 14** Plots employing Ga/Al (Whalen et al., 1987) for the meta-granitoids in

1436 Longjingguan. I & S: I-type and S-type granite; A: A-type granite.

1437

1438 **Figure 15** (Sr/Y) vs. Y diagram discriminating adakite and TTG from typical arc

1439 calc-alkaline rocks (Drummond and Defant, 1990).

1440

Petrogenesis and tectonic significance of Neoproterozoic meta-basites and meta-granitoids within the central Dabie UHP zone, China: Geochronological and geochemical constraints

Yuan Li [a], Yi-Can Liu [a, *], Yang Yang [a], F. Rolfo [b, c] and C. Groppo [b]

[a] CAS Key Laboratory of Crust-Mantle Materials and Environments, School of Earth and Space

Sciences, University of Science and Technology of China, Hefei 230026, China

[b] Department of Earth Sciences, University of Torino, Via Valperga Caluso 35, 1-10125 Torino,

Italy

[c] C.N.R. – I.G.G., Section of Torino, Via Valperga Caluso 35, 1-10125 Torino, Italy

*Corresponding author. Tel./fax: +86 551 63600367.

E-mail address: liuyc@ustc.edu.cn (Y.-C. Liu)

Abstract

A combined geochemical (whole-rock elements and Sr-Nd-Pb isotopes, zircon trace elements and Hf isotopes) and geochronological (zircon U-Pb ages) study was carried out on the relatively low-grade meta-basites and meta-granitoids from Longjingguan within the central Dabie ultrahigh-pressure (UHP) metamorphic zone, east-central China. Zircon investigations indicate that the meta-basites were formed at ~772 Ma and subsequently experienced granulite-facies metamorphism at ~768 Ma and a later thermal overprint at ~746 Ma, while the meta-granitoids recorded three groups of zircon ages at ca. 819 Ma, 784 Ma and 746 Ma. The meta-granitoids can be subdivided into low-Si and high-Si types, and they were derived from mid-Neoproterozoic partial melting of the Neoarchean and Paleoproterozoic metamorphic basement rocks of the South China Block, respectively. These Neoproterozoic zircon ages are consistent with the protolith ages of the Dabie Triassic UHP meta-igneous rocks. In addition, the low-grade rocks have bulk-rock Pb isotope compositions overlapping with the UHP meta-igneous rocks. Therefore, the low-grade meta-basites and meta-granitoids could be interpreted as counterparts of the UHP meta-igneous rocks in this area, suggesting the same petrogenesis for their protoliths in the Neoproterozoic.

Trace element patterns indicate that the low-grade rocks have better preserved their protolith compositions than their equivalent UHP rocks, and thus they are more suitable for elucidating the Neoproterozoic evolution of the northern margin of the South China Block. Zircon ages combined with geochemical features strongly suggest that the protoliths of the meta-granitoids and meta-basites were formed in a magmatic arc and a continental rifting setting, respectively. More specifically, the granitoids derived from partial melting of Neoarchean and Paleoproterozoic basement materials at ~819 Ma in a magmatic arc setting, whereas the precursors of the meta-basites are products of a continental rifting event at about 784 to 772 Ma. The obtained results provide new geochronological and geochemical constraints for the Neoproterozoic evolution of the northern margin of the South China Block, which can further

51 contribute to the understanding of the breakup of the supercontinent Rodinia.

52

55

1. Introduction

The Dabie orogen located in central China is a continental collision belt with the exposed largest area of coesite- and diamond-bearing ultrahigh-pressure (UHP) metamorphic rocks in the world, and thus it has attracted great research interest in the geologic community during the past decades (e.g., Okay et al., 1989, 1993; Wang et al., 1989; Xu et al., 1992a,b, 2003; Li et al., 1993, 2000; Ames et al., 1996; Rowley et al., 1997; Hacker et al., 1998, 2000; Rolfo et al., 2000, 2004; Zheng et al., 2006; Liu et al., 2007a,b, 2011a,b, 2015; Groppo et al., 2015). Previous studies focused mainly on the Triassic UHP metamorphism and related processes, whereas less attention has been paid to the nature and origin of the protoliths of the UHP rocks (e.g., Ames et al., 1996; Hacker et al., 1998; Zheng et al., 2006). U-Pb dating in magmatic zircon cores demonstrated that the protoliths of the UHP meta-igneous rocks in the Dabie orogen were formed in the Neoproterozoic (e.g., Rowley et al., 1997; Hacker et al., 1998; Liu et al., 2007a,b), likely under a continental rifting setting related to the breakup of the supercontinent Rodinia (Li et al., 2003a,b,c). However, the detailed Neoproterozoic evolutional processes of the area have not been well understood, and the precise onset of the continental rifting is still not well constrained. UHP rocks usually experience complex evolution including interaction with melt and/or fluids that can significantly modify the elemental and isotopic characteristics of the rocks (e.g., Kessel et al., 2005; Hermann et al., 2006; Zheng et al., 2011), making it challenging to reveal their protolith nature and origin.

Apart from the UHP rocks, relatively low-grade metamorphosed rocks have been identified in several localities within the UHP metamorphic zone in the Dabie orogen (e.g., Dong et al., 1997; Gao et al., 2006); these rocks occur as interlayers or tectonic blocks within the UHP units, but yield much lower peak-metamorphic temperatures and pressures. If these rocks can be proved to be counterparts of the UHP rocks that escaped UHP metamorphism, they should be good candidates to reveal the Neoproterozoic evolution of the area. Previous studies about the rocks in the Dabie orogen mainly concentrated on geochronology investigations, while their elemental

85 and isotopic signatures have not been studied in detail so far, and their petrogenesis

86 and tectonic setting are still not well constrained.

87 Recently, some relatively low-grade meta-basites and meta-granitoids have been

88 for the first time recognized at Longjingguan, within the central Dabie UHP

89 metamorphic zone (Fig. 1). In this paper we perform integrated investigations on their

90 mineral compositions, whole-rock elements and Pb isotopes, as well as zircon

91 SHRIMP U-Pb dating, REE and Hf isotopes. The aim of the study is to investigate

92 whether the rocks are counterparts of the UHP meta-igneous rocks and, if so, whether

93 the rocks preserved their protolith compositions better than the UHP rocks. These new

94 data are crucial for better understanding the formation and tectonic evolution of the

95 Precambrian basement of the South China Block (SCB), especially the events related

96 to the Neoproterozoic breakup of the supercontinent Rodinia.

97

2. Geological setting and samples

2.1. Geological setting

100 The Dabie orogen located in the middle portion of the

101 Qinling–Tongbai–Dabie–Sulu orogenic belt is formed by the Triassic subduction of

102 the SCB beneath the North China Block (NCB) and exposed the largest area of UHP

103 rocks in the world. The widespread occurrence of coesite- (Okay et al., 1989; Wang et

104 al., 1989) and diamond-bearing (Xu et al., 1992b) rocks in the orogen provides an

105 excellent natural laboratory for investigating evolutional processes of the orogen, as

106 well as formation and exhumation mechanisms of UHP rocks. The orogen is generally

107 divided into five fault-bounded rock units with different metamorphic grades and

108 histories, which are from south to north: the Susong complex zone (SZ), the South

109 Dabie low-T eclogite zone (SDZ), the Central Dabie UHP zone (CDZ), the North

110 Dabie complex zone (NDZ) and the Beihuaiyang zone (BZ) (Xu et al., 2003, 2005;

111 Liu et al., 2005, 2007a,b, 2011a,b; Zheng et al., 2005; Liu and Li, 2008; Li et al.,

112 2017). These five units are separated by the near E-W trending Taihu–Shanlong,

113 Hualiangting–Mituo, Wuhe–Shuihou and Xiaotian–Mozitan faults, respectively (Fig.

1). Although the meta-igneous rocks in the five units exhibit different metamorphic histories, they have similar Neoproterozoic protolith ages reflecting a regional-scale magmatism related to the Rodinia break-up (e.g., Ames et al., 1996; Rowley et al., 1997; Hacker et al., 1998; Liu et al., 2007a,b, 2011a).

UHP index minerals like coesite and diamond were found in different lithologies from the CDZ (e.g., Okay et al., 1989; Wang et al., 1989; Xu et al., 1992b; Schertl et al., 1994; Su et al., 1996; Rolfo et al., 2000, 2004), demonstrating that the CDZ was involved in a deep subduction and experienced Triassic UHP metamorphism as a coherent unit (Xu et al., 1992b, 2003; Li et al., 1993, 2000; Hacker et al., 1998; Rolfo et al., 2004; Liu and Li, 2008). Evidence of UHP metamorphism like coesite pseudomorphs were later discovered also in the low-T eclogites from the SDZ (Li et al., 2004). Eclogites (Wei et al., 1998; Xu et al., 2000; Liu et al., 2001) or eclogite relics (Tsai and Liou, 2000; Xiao et al., 2001) were also recognized in the NDZ, together with diamond inclusion within zircon and other clues of UHP metamorphism (Tsai et al., 2000; Xu et al., 2000, 2003, 2005; Liu et al., 2007b, 2011b). Moreover, the NDZ (Liu et al., 2000; Xie et al., 2001; Liu et al., 2005, 2007a,b, 2011a) and the SDZ (Li et al., 2004) were confirmed to be segments of the Triasic subducted continental crust of the SCB. This implies that the three eclogite-bearing units in the Dabie orogen all experienced the Triassic deep subduction, although they have different lithological and isotopic compositions and metamorphic histories (Liu and Li, 2008).

In recent years, relatively low-grade meta-igneous rocks with Neoproterozoic protolith ages and Triassic metamorphic ages have been recognized within the Dabie-Sulu UHP belt. For example, some meta-igneous rocks in Ganghe provided Rb-Sr isochronal ages of 232 ± 8 Ma and Ar-Ar ages of 770-780 Ma, as well as magmatic zircon U-Pb ages of 760−800 Ma (Dong et al., 1997; Gao et al., 2006). These ages indicate that these rocks formed in the Neoproterozoic and experienced Triassic metamorphism, with peak metamorphic temperatures between the closure temperatures of Rb-Sr and Ar-Ar isotopic systems. Different from the UHP rocks, they experienced a relatively low-grade metamorphism (greenschist- to

low-amphibolite-facies) during the Triassic (Dong et al., 1997; Liu et al., 2017 and references therein), indicating that they were exhumed from much shallower depths. Similar granitic gneisses/meta-granites, meta-basites with Neoproterozoic protolith ages have also been recognized in the BZ, the northern sector of the Dabie orogen (e.g., Hacker et al., 2000; Xie et al., 2002; Chen et al., 2003; Jiang et al., 2005; Zheng et al., 2005; Liu et al., 2006a, 2010, 2011c, 2017; Wu et al., 2007). These rocks have identical amphibole Ar-Ar (Hacker et al., 2000) and zircon U-Pb ages (Jiang et al., 2005; Liu et al., 2010, 2017) of ~750 Ma, suggesting that their peak metamorphic temperatures during the Triassic were lower than the closure temperatures of the amphibole Ar-Ar dating system (<500 °C). These protolith ages are in agreement with those of the UHP eclogites and orthogneisses (e.g., Ames et al., 1996; Rowley et al., 1997; Hacker et al., 1998; Liu et al., 2007a,b, 2011a), as well as the Neoproterozoic mafic dykes and granites widely distributed along the northern margin of the SCB, thus they are generally considered to be closely related (Zhao and Zhou, 2009; Hong et al., 2009; Xue et al., 2011; Wang et al., 2013). It is consequently thought that these Neoproterozoic meta-granites and meta-basites were once skin layers of the SCB, detached from the subducted slab during the initial stages of the subduction, and overthrusted onto the southern margin of the NCB (e.g., the BZ), or into the UHP metamorphic zone (e.g., Ganghe) during the Triassic continental collision.

In addition to the locations described above, the relatively low-grade meta-basites and meta-granitoids have been discovered at Longjingguan within the central Dabie UHP zone (Fig. 1). So far, their petrogenesis, emplacement time and relationship with the adjacent UHP rocks have not been studied in detail.

2.2. Petrography and mineral chemistry

Fourteen samples were collected from the Longjingguan area, including six meta-basites (samples 11LJG3-4-5-6-7-8) and eight meta-granitoids (samples 11LJG2, 1202LJG3, 1209LJG5, 1303LJG2, 1303LJG4, 1209LJG1, 1209LJG3 and 1209LJG4). Their outcrops are concentrated within an area of few tens of square meters marked by the black star in Figure 1. All the samples were collected as far as possible from

174 the contact with different lithologies, to avoid possible interaction between them.

175   The meta-basites occur as tectonic lenses within meta-granitoids (Fig. 2), with

176 the margins slightly deformed; the surface is locally charaterized by few

177 light-coloured, weakly deformed spots of about 0.5 mm in size. The meta-basite

178 generally contains fine-grained symplectites mainly consisting of plagioclase and

179 amphibole. The symplectite composed of plagioclase and amphibole points to the

180 replaced former mineral, rather than derived from magma crystallization. Accessory

181 minerals are rutile, titanite, ilmenite and magnetite. A few amphibole porphyroblasts

182 occur in the meta-basites, and they contain inclusions of plagioclase, plagioclase +

183 rutile, rutile, rutile + ilmenite and rutile + titanite (Figs. 3a & b).

184   Electron microprobe analyses were carried out on representative minerals of three

185 samples 11LJG7, 1209LJG5 and 1209LJG1, which represent the meta-basites, low-Si

186 meta-granitoids and high-Si meta-granitoids, respecitively. The results are listed in

187 Supplementary Table 1.

188   The meta-granitoids are subdivided into two types, named low-Si and high-Si

189 meta-granitoids, respectively, according to their bulk-rock SiO_2 content

190 (Supplementary Table 2). The low-Si meta-granitoid is mainly composed of

191 plagioclase (with K-feldspar exsolutions), quartz, and biotite, with minor amphibole

192 and apatite (Fig. 3c-d), while the high-Si meta-granitoid is dominated by quartz and

193 K-feldspar, with rare allanite, muscovite and amphibole (Figs. 3e-f). Minerals in the

194 meta-granitoids vary from few tens of microns to hundreds of microns in size,

195 significantly coarser than those in the matrix of the meta-basites. The structure varies

196 from gneissic, with a poorly developed foliation (Fig. 3c-d), to granoblastic (Figs.

197 3e-f).

198

199 *2.2.1. 11LJG7*

200   In this meta-basite sample, amphibole occurs as fine grains in the symplectitic

201 matrix or as porphyroblasts. Both porphyroblasts and the fine-grained amphibole in

202 the matrix are magnesiohornblende: the porphyroblasts have lower $Mg^{\#}$ values

203 (72~73) and higher TiO_2 contents (0.26~0.35 wt%) than the fine grains in the matrix

204    $(Mg^{\#}=79\sim81$; $TiO_2=0.02\sim0.13$ wt%). Plagioclase is an oligoclase (Supplementary

205   Table 1). Two rutile inclusions within amphibole porphyroblast have Zr contents of

206   277 and 735 ppm, respectively. Rutile inclusions in Neoproterozoic metamorphic

207   zircon domains (see Section 4.2) have higher Zr contents, in the range 2107-2519 ppm

208   (Supplementary Table 3).

209

210   *2.2.2. 1209LJG5*

211   This low-Si meta-granitoid sample exhibits a weak foliation defined by biotite

212   and amphibole preferred orientation (Figs. 3c-d). Plagioclase is oligoclase (An_{19-30})

213   and contains K-feldspar (Or_{92-96}) exsolutions. Amphibole is a ferro-edenite /

214   ferropargasite, with $X_{Ca}=0.76–0.77$ [$X_{Ca}=Ca/(Ca+Na+K)$] and $X_{Fe}=0.66–0.68$

215   [$X_{Fe}=Fe/(Fe+Mg)$]. Biotite has low $Mg^{\#}$ (~36) and variable TiO_2 contents (3.68 to

216   4.12 wt%).

217

218   *2.2.3. 1209LJG1*

219   This high-Si meta-granitoid sample consists mainly of K-feldspar and quartz,

220   with minor allanite (Fig. 3e). The K-feldspar contains about 6% albite end-member

221   component.

222

223   *2.3. Thermobarometry*

224   Thermbarometric methods were applied on the meta-basite sample 11LJG7. The

225   main amphibole–plagioclase symplectititic assemblage gives a P-T range of

226   478-541 °C, 2.2-3.4 kbar (i.e. lower-T boundary of the amphibolite-facies) based on

227   the amphibole-plagioclase thermometer (Holland and Blundy, 1994) and the

228   Al^{Tot}-in-amphibole barometer (Schmidt, 1992).

229   Rutile inclusions within amphibole porphyroblast yield temperatures of

230   651-737 °C based on their Zr contents (Tomkins et al., 2007), with the pressure set to

231   ~12 kbar according to the coexistence of rutile, ilmenite and titanite (Bohlen and

232   Liotta, 1986; Angiboust and Harlov, 2017). Rutile inclusions in Neoproterozoic

233   metamorphic zircon domains (see Section 4.2) yield significantly higher temperatures

9

234 of about 850-870 °C. In the application of Zr-in-rutile thermometer, rutile

235 measurements with Si > 200 ppm should be excluded from further analysis if the Zr

236 concentration is substantially higher than that of other rutiles in the same sample

237 (Zack et al., 2004); accordingly, data of three analytical spots (No. 2, 3 and 4,

238 Supplementary Table 4) were excluded. In addition, the analytical spot No. 1

239 (Supplementary Table 4) was also excluded because of extremely low total contents.

240 Overall, thermobarometric results suggest that rutile inclusions within

241 Neoproterozoic metamorphic zircon domains preserve evidence of a HT,

242 granulite-facies metamorphic event (840-860°C, ~12 kbar), completely overprinted by

243 a later amphibolite-facies event (480-540 °C, 2.2-3.4 kbar), responsible for the

244 formation of the amphibole + plagioclase symplectites in the matrix. The

245 Neoproterozoic granulite-facies metamorphic event is also supported by the previous

246 investigations from the deeply subducted NDZ in Liu et al. (2007a). Rutile inclusions

247 within amphibole porphyroblasts were likely partially reequilibrated during the late

248 amphibolite-facies metamorphic event, due to the lack of protection by rigid

249 "container" such as zircon, thus indicating temperatures (652-737 °C) lower than

250 those preserved by rutiles included in zircons.

251

3. Analytical methods

253 Rock-crushing and powdering were performed at the Langfang Laboratory,

254 Hebei Bureau of Geological and Mineral Resources. Zircon grains were separated by

255 the procedures of crushing, heavy-liquid separation, magnetic separation. After that,

256 zircon grains were further selected by hand-picking under a binocular microscope,

257 and mounted in an epoxy mount, which was polished to section the crystals for

258 analyses, with a zircon U–Pb standard TEM (417 Ma) (Black et al., 2003) at Beijing

259 SHRIMP Center, Chinese Academy of Geological Sciences (CAGS).

260 Whole-rock major element composition was analyzed by wet chemical methods

261 at the Langfang Laboratory, Hebei Bureau of Geological and Mineral Resources.

262 Analytical uncertainties have a range from ±1 to ±5% for major elements. Trace

263 elements analysis was carried out at the CAS Key Laboratory of Crust-Mantle

264 Materials and Environments, University of Science and Technology of China (USTC)

265 in Hefei, by an Elan DRCII ICP-MS, with analytical uncertainties ranging from ±5%

266 to ±10%. Detailed analytical procedures and instrument parameters for trace element

267 analyses are documented in Hou and Wang (2007). Zircon SHRIMP U–Pb dating was

268 carried out at the Beijing SHRIMP Center, with transmitted and reflected light

269 micrographs and CL imaging as a guide to selection of U–Pb dating spot. The detailed

270 analytical method was described by Compston et al. (1992) and Williams (1998).

271 Common Pb corrections were made using measured ^{204}Pb, and the data were treated

272 following Compston et al. (1992) with the ISOPLOT program of Ludwig (2001).

273 Zircon trace elements analyses were performed by LA-ICP-MS at the CAS Key

274 Laboratory of Crust-Mantle Materials and Environments, USTC in Hefei and the

275 State Key Laboratory of Continental Dynamics, Northwest University in Xi'an. The

276 analyses were carried out with pulse rate of 10 Hz, beam energy of 10 J/cm^2, and spot

277 diameter of 32 μm. The detailed parameters of the instrument are similar to those

278 described by Yuan et al. (2004) and Liu et al. (2011a). Element contents of zircons

279 were calculated by using Pepita software with the zircon SiO$_2$ as internal standard and

280 the NIST610 as external standard. Precision and accuracy of analyses are 2–5% for

281 REE, Y, Rb, Sr, Nb, Ta, Hf, Th and U at the ppm concentration level, and from 8% to

282 10% for P, Ti and Pb. The detection limit for the different REE varies from 0.02 to

283 0.09 ppm.

284 In situ zircon Lu–Hf isotope analysis were conducted at the Institute of Geology

285 and Geophysics, the Chinese Academy of Sciences in Beijing, and the School of Earth

286 Sciences and Engineering, Nanjing University, each using a Neptune multi-collector

287 ICPMS, with a Geolas 193 nm laser ablation system. Instrumental parameters and

288 data acquisition followed those described by Wu et al. (2006a). The detailed processes

289 were shown in Liu et al. (2012). Initial Hf isotope ratios are denoted as $\varepsilon_{Hf}(t)$ values

290 that are calculated with the reference to the chondritic reservoir (CHUR) at the time of

291 zircon crystallization. Parameters adopted in this study are: 1.865×10^{-11} yr^{-1} for the

292 decay constant of ^{176}Lu (Scherer et al., 2001), 0.282772 and 0.0332 for the ^{176}Hf/^{177}Hf

293 and $^{176}Lu/^{177}Hf$ ratios of the chondrite (Blichert-Toft and Albarede, 1997). Single

294 stage model ages (T_{DM1}) were calculated referred to the depleted mantle with a

295 present day $^{176}Hf/^{177}Hf$ ratio of 0.28325, similar to that of the average MORB (Nowell

296 et al., 1998) and $^{176}Lu/^{177}Hf$ ratio of 0.0384 (Griffin et al., 2000).

297   Mineral inclusions in zircon were identified using Raman spectroscopy at the

298 CAS Key Laboratory of Crust–Mantle Materials and Environments, University of

299 Science and Technology of China in Hefei, and analyzed using the electron

300 microprobe (EMP) at the Institute of Mineral Resources, CAGS in Beijing. The

301 analytical conditions of the Raman and EMP were reported by Liu et al. (2009). The

302 compositions of the representative minerals in thin sections were detected by EMP at

303 the Department of Resource and Environment Engineering, Hefei University of

304 Technology in Hefei. The accelerating voltage and beam current were 15 kV and

305 15nA, respectively.

306   Rb-Sr, Sm-Nd, and Pb isotopic analyses were performed at the Laboratory for

307 Radiogenic Isotope Geochemistry, in USTC according to the methods of Chen et al.

308 (2000, 2007). Sm, Nd, Rb, and Sr concentrations were determined by isotopic dilution

309 using ^{149}Sm, ^{150}Nd, ^{84}Sr, and ^{85}Rb tracers. The isotopic abundance ratios were

310 determined on a Finnigan MAT 262. Sr and Nd isotopic ratios were corrected for mass

311 fractionation relative to $^{86}Sr/^{88}Sr = 0.1194$ and $^{146}Nd/^{144}Nd = 0.7219$, respectively.

312 NBS987 and La Jolla standard solutions analyzed along with samples yielded

313 0.710250 ± 12 (2σ) for $^{87}Sr/^{86}Sr$ and 0.511860 ± 12 (2σ) for $^{143}Nd/^{144}Nd$. Measured Pb

314 isotopic ratios were then corrected for instrumental mass fractionation using a value

315 of 0.11% per atomic mass unit inferred from analysis of the reference material

316 NBS981.

317

4. Results

319 *4.1. Major and trace elements*

320   Whole-rock major and trace elemental compositions of the studied meta-basites

321 and meta-granitoids are listed in Supplementary Table 2.

4.1.1. Meta-basites

323

324　The meta-basite samples 11LJG3-4-5-6-7-8 have uniform bulk-rock

325　compositions. The SiO_2 contents range from 45.72 to 51.81 wt%, Al_2O_3 from 12.46 to

326　14.30 wt%, and MgO from 4.37 to 13.29 wt%. They have high FeO^T (11.47–14.99

327　wt%) and $Mg^{\#}$ values of 34–67. The TiO_2 contents are also relatively high (2.01–3.42

328　wt%). They are alkalic with Na_2O contents of 1.74–3.55 wt%, K_2O contents of

329　0.77–1.80 wt% and Na_2O/K_2O ratios of 1.25–4.14. Element pairs that have similar

330　bulk D values (solid/melt partition coefficient for modal melting), for example Y-Ho

331　and Eu-Sm, are correlated during magmatic processes (e.g., Workman and Hart, 2005).

332　In the Y vs. Ho and Eu vs. Sm plots (no attachment), all the studied meta-mafic rocks

333　fall along a linear trend, suggesting that they were derived from the same source.

334　In the TAS (Le Bas et al., 1986) and Zr/TiO_2 vs Nb/Y (Winchester and Floyd,

335　1977) diagrams (Fig. 4), the meta-mafic rocks plot very close to the boundary

336　between fields of alkaline and sub-alkaline series. The primitive mantle normalized

337　spider diagram (Fig. 5b) shows that they are enriched in incompatible elements

338　compared to MORB, and have negative anomalies of Sr, Nb and Ta, positive or

339　slightly negative Pb anomalies. They have uniform C1 chondrite normalized REE

340　patterns (Fig. 5a) characterized by enrichment in LREE, slight depletion in HREE and

341　weakly positive or negative Eu anomaly (Eu/Eu*=0.80–1.06). Their $(La/Yb)_N$

342　(primitive mantle normalized) ratios range from 2.2 to 7.5 and $(La/Sm)_N$ from 1.3 to

343　2.1. The UHP eclogites derived from basaltic protoliths have similar REE patterns and

344　related trace-element contents (Fig. 5c and d).

345

4.1.2. Low-Si meta-granitoids

346

347　The low-Si meta-granitoids (samples 11LJG2, 1209LJG5 and 1202LJG3) have

348　slightly inhomogeneous bulk compositions. The SiO_2 contents range from 60.45 to

349　61.50 wt%, Al_2O_3 from 14.18 to 14.96 wt%, TiO_2 from 1.16 to 1.38 wt% and MgO

350　from 1.60 to 1.86 wt%. They have high FeO^T (7.78–8.29 wt%) with $Mg^{\#}$ values of

351　0.26–0.31. They have Na_2O ranging from 1.50 to 3.26 wt% and K_2O from 3.11 to

352
353
354
355
356
357
358
359
360
361
362
363
364
365
366
367
368
369
370
371
372
373
374
375
376
377
378
379
380
381

4.28 wt% with Na_2O/K_2O ratios of 0.35–1.05. In the TAS diagram, these rocks plot in the field of andesite, close to the boundary with trachy-andesite; in the Zr/TiO_2 vs Nb/Y diagram, they are distributed in the fields of dacite + rhyodacite and trachyandesite. They exhibit significant depletion of HFSE including Nb, Ta, Ti and P, as well as enrichment of Pb (Fig. 5b), which are typical features of crustal-sourced rocks (Rudnick and Gao, 2003). They have identical C1 chondrite normalized REE patterns (Fig. 5a) characterized by enrichment of LREE, weak depletion of HREE and positive Eu anomalies (Eu/Eu*=1.12–2.00). Their $(La/Yb)_N$ ratios range from 9.59 to 17.49 and $(La/Sm)_N$ from 2.77 to 4.02.

4.1.3. High-Si meta-granitoids

Compared to the meta-basites and low-Si meta-granitoids, the high-Si meta-granitoids (samples 1303LJG2, 1303LJG4, 1209LJG1, 1209LJG3 and 1209LJG4) have more scattered bulk-rock compositions. The SiO_2 contents range from 67.98 to 80.98 wt%, Al_2O_3 from 8.96 to 11.78 wt%, TiO_2 from 0.17 to 0.54 wt% and MgO from 0.06 to 3.82 wt%. They have low FeO^T (2.09–4.30 wt%) contents with varied $Mg^\#$ values of 0.04–0.62. The Na_2O contents range from 1.12 to 2.99 wt% and K_2O from 2.44 to 5.35 wt% with Na_2O/K_2O ratios of 0.29–0.98. In the TAS diagram, four samples plot into the field of sub-alkaline rhyolite and one sample into that of dacite; in the Zr/TiO_2 vs Nb/Y plot, the studied samples scatter among four categories: comendite + pantellerite, rhyolite, rhyodacite + dacite and trachyandesite. They have trace elements patterns comparable to those of the low-Si meta-granitoids (Fig. 5b), and uniform C1 chondrite normalized REE patterns (Fig. 5a) characterized by enrichment of LREE, slight depletion of HREE and strong negative Eu anomalies (Eu/Eu*=0.10–0.75). Their $(La/Yb)_N$ ratios range from 10.29 to 49.87 and $(La/Sm)_N$ range from 3.64 to 5.41.

4.2. Zircon geochronology

4.2.1. Zircon morphology and mineral inclusions

Zircons from the meta-basites are anhedral to subhedral in shape with smooth

382 outlines, and their length-width ratios are generally smaller than 1.5. CL images show

383 that most of them have core, mantle and rim structures with clear boundaries between

384 them. The cores are grey colored with clear or weak oscillatory zoning while the

385 mantles are light colored and homogeneous (Fig. 6). Some zircon grains have a

386 mantle domain showing gradually darker luminance outwards. The rims are bright,

387 too thin to be analysed. According to the microstructures, the cores with oscillatory

388 zoning are interpreted to be of magmatic origin, while the homogeneous cores and

389 mantles are considered to be metamorphic zircon domains (e.g., Hanchar and Rudnick,

390 1995; Gebauer et al., 1997; Hermann et al., 2001). Most of the zircon cores exhibit

391 rounded shapes, suggesting that they were partially resorbed after crystallization,

392 maybe during the formation of the zircon mantles.

393 As opposed to the meta-basites, zircons from the meta-granitoids exhibit more

394 regular crystal shapes. Some of the zircons from the meta-granitoids are euhedral in

395 shape with clear oscillatory zones, indicative of magmatic origin. Other zircons show

396 core and mantle structures, wherein the cores are dark grey with clear oscillatory

397 zoning or no zoning, while the mantles are light grey with weak or no oscillatory

398 zonings. Similarly, the zircons in the meta-granitoids can also be divided into

399 magmatic (with oscillatory zoning) and metamorphic (no zoning) domains. Generally,

400 the metamorphic zircon domains from both the meta-basites and the meta-granitoids

401 are granular, platy and prismatic in shape with smooth boundaries, and some of them

402 retain plenty of mineral inclusions (Fig. 7), which are powerful tools to link zircon

403 growth to precise metamorphic events (e.g., Gebauer et al., 1997; Hermann et al.,

404 2001; Liu et al., 2007b, 2011a). The metamorphic zircons in the meta-basite sample

405 11LJG3 contain quartz, plagioclase, apatite, hornblende, K-feldspar, chlorite, epidote,

406 biotite, rutile, ilmenite and titanite, while those from the meta-granitoid sample

407 11LJG2 contain K-feldspar, muscovite, epidote and quartz. The compositions of

408 typical mineral inclusions in metamorphic zircons were detected by electron

409 microprobe, with the results listed in Supplementary Table 3. Biphase inclusions

410 composed of rutile + titanite or of titanite + ilmenite are recognized in a few

411 metamorphic zircons from sample 11LJG3.

4.2.2. Zircon REE patterns

Representative zircon REE contents of the meta-basites (samples 11LJG3 and 11LJG7) and the meta-granitoids (samples 11LJG2, 1202LJG3, 1303LJG2 and 1209LJG5) are listed in Supplementary Table 5 (all the analyzed results for zircon rare earth elements in Supplementary Table 6). Zircon cores have almost identical steep HREE patterns, positive Ce anomalies and negative Eu anomalies (Fig. 8), typical of magmatic zircon (Hoskin and Ireland, 2000). On the contrary, the REE patterns of metamorphic zircons are varied. In the meta-basites, most metamorphic zircons (the cyan lines, Fig. 8a) exhibit higher REE contents than, but similar REE patterns with, the magmatic zircons, except for one spot that show slightly positive Eu anomaly; besides, a metamorphic zircon (the black line, Fig. 8a) has almost the same La, Ce and HREE contents with the magmatic zircons, but it exhibits significantly higher Pr, Nd, Sm and Eu. In the meta-granitoids, most metamorphic zircons exhibit similar REE patterns with the magmatic cores, whereas some analyses exhibit higher REE contents and/or higher LREE/HREE ratios than the magmatic zircons (Fig. 8b-d), or exhibit no anomaly of Eu.

4.2.3. Zircon SHRIMP U-Pb ages

In-situ analyses have been performed on different zircon domains, with the U-Th-Pb data listed in Supplementary Table 7 and U-Pb concordia diagram illustrated in Figure 9.

Magmatic zircon cores from the meta-basite sample 11LJG3 yield a cluster of concordant $^{206}Pb/^{238}U$ age averaging at 772 ± 4 Ma (MSWD=2.0, n=7; Fig. 9a), while the metamorphic domains give a concordant $^{206}Pb/^{238}U$ age group of 768 ± 7 Ma (MSWD=2.9, n=11; Fig. 9a). In another meta-basite sample 11LJG7, magmatic zircon domains yield a cluster of concordant $^{206}Pb/^{238}U$ age of 772 ± 7 Ma (MSWD=2.5, n=5; Fig. 9b), and the metamorphic domains give a concordant $^{206}Pb/^{238}U$ age group of 746 ± 4 Ma (MSWD=2.6, n=9; Fig. 9b). Summing up, the magmatic zircons yield a cluster of concordant $^{206}Pb/^{238}U$ age at ~772 Ma (Ma domains), and the metamorphic

442 zircons yield two groups of concordant $^{206}Pb/^{238}U$ age at ~768 Ma (Me1 domains) and

443 ~746 Ma (Me2 domains), corresponding to magmatism, metamorphism and thermal

444 overprinting events, respectively.

445   Zircon cores in the low-Si meta-granitoids (samples 11LJG2, 1202LJG3,

446 1209LJG5) have a wide age spectrum spreading from ~800 Ma to ~2500 Ma.

447 Analytical spots on zircon cores in sample 11LJG2 are distributed along the concordia

448 curve or on a Pb loss line, yielding two upper intercept ages of 1940 ± 140 Ma

449 (MSWD=2.1; Fig. 9d) and 2529 ± 38 Ma (MSWD=3.1; Fig. 9d), respectively. Six

450 magmatic zircon spots give a concordant $^{206}Pb/^{238}U$ age cluster of 838 ± 18 Ma

451 (MSWD=0.73, n=6; Fig. 9e), while twelve metamorphic zircon analyses yield two

452 concordant $^{206}Pb/^{238}U$ age clusters averaging at 797 ± 7 Ma (MSWD=0.54, n=9; Fig.

453 10e) and 762 ± 22 Ma (MSWD=0.25, n=3; Fig. 9e), respectively. Zircons in sample

454 1209LJG5 plot along the concordia curve, or on a Pb loss line with an upper intercept

455 age of 1999 ± 57 Ma and a lower intercept age of 779 ± 49 Ma (MSWD=4.8; Fig. 9g).

456 Neoproterozoic magmatic zircons give a concordant $^{206}Pb/^{238}U$ age of 839 ± 7 Ma

457 (MSWD=0.99, n=6; Fig. 9h), and two analyses on metamorphic zircon yield

458 concordant $^{206}Pb/^{238}U$ ages of 785 ± 6 Ma and 744 ± 16 Ma, respectively. Three near

459 concordant $^{206}Pb/^{238}U$ age clusters were obtained from sample 1202LJG3: one age of

460 819 ± 12 Ma (MSWD=2.3, n=3; Fig. 9c) from magmatic zircon cores, and two ages

461 of 772 ± 7 Ma (MSWD=1.14, n=3; Fig. 9c) and 751 ± 6 Ma (MSWD=0.39, n=3; Fig.

462 9c) from metamorphic zircon domains.

463   Magmatic zircons from the high-Si meta-granitoid sample 1303LJG2 give an

464 average concordant $^{206}Pb/^{238}U$ age of 813 ± 5 Ma (MSWD=0.99, n=7; Fig. 9f), while

465 metamorphic zircons yield two concordant age clusters of 784 ± 7 Ma and 732 ± 6 Ma

466 (Fig. 9f). The zircon dating results indicate that the protoliths of the low-Si and

467 high-Si meta-granitoids were formed at about 819 ± 12 Ma and 813 ± 5 Ma,

468 respectively. The zircons yielding older ages are thus inherited from their source rocks,

469 with their original ages preserved or reset by Pb loss, corresponding to the apparent

470 concordant or disconcordant ages.

4.3. Zircon Hf isotopes

472

473   Zircon $\varepsilon_{Hf}(t)$ values and T_{DM} ages of two meta-basites (samples 11LJG3 and

474   11LJG7), three low-Si meta-granitoids (samples 11LJG2, 1209LJG5 and 1202LJG3)

475   and one high-Si meta-granitoid (sample 1303LJG2) are listed in Supplementary Table

476   8.

477   The zircons in the meta-basites have $\varepsilon_{Hf}(780\ Ma)$ values from +2.6 to +7.9 (Fig.

478   10), and corresponded single stage model ages (T_{DM1}) of 1033 to 1248 Ma, slightly

479   older than their zircon U-Pb ages.

480   Six inherited zircon cores from low-Si meta-granitoids have $\varepsilon_{Hf}(t)$ values of +7.1

481   to -6.6, with corresponding T_{DM1} ages of 2359 to 2702 Ma, and T_{DM2} ages of 2506 to

482   2823 Ma, respectively (Fig. 10). The Neoproterozoic zircon domains in the low-Si

483   meta-granitoids yield a relatively wide $\varepsilon_{Hf}(800\ Ma)$ spectrum of -3.2 to -12.0, with

484   T_{DM1} ages of 1513~1819 Ma and T_{DM2} ages of 1893~2446 Ma. Zircons from the

485   high-Si meta-granitoid have $\varepsilon_{Hf}(800\ Ma)$ values ranging from -7.5 to +1.4, with T_{DM1}

486   ages of 1313~1679 Ma, and T_{DM2} ages of 1618~2172 Ma. Neoproterozoic zircons

487   from low-Si and high-Si meta-granitoids have overlapped $\varepsilon_{Hf}(t)$ values and T_{DM} ages,

488   but the high-Si rocks have slightly higher average $\varepsilon_{Hf}(t)$ values and younger Hf model

489   ages.

490

4.4. Sr-Nd-Pb isotope compositions

491

492   The Rb-Sr, Sm-Nd and Pb contents and isotopic compositions of the

493   meta-basites are listed in Supplementary Tables 9 and 10, respectively. The

494   meta-basites have Rb and Sr contents of 16.0–62.9 and 87–320 ppm, and measured

495    $^{87}Rb/^{86}Sr$ and $^{87}Sr/^{86}Sr$ ratios of 0.1423–1.6997 and 0.705386–0.709376, Sm and Nd

496   contents of 4.15–9.64 and 13.1–35.9 ppm, and measured $^{147}Sm/^{144}Nd$ and $^{143}Nd/^{144}Nd$

497   ratios of 0.1515–0.1888 and 0.512511–0.512674. Sr and Nd isotopic compositions

498   were back calculated to t=230 Ma, and thus the $(^{87}Sr/^{86}Sr)_I$, $\varepsilon_{Nd}(t)$ values and T_{DM2}

499   ages are 0.7023–0.7067, -1.8–+1.8 and 862–1156 Ma. The meta-basites have U, Th

500 and Pb contents of 0.34–0.70, 1.27–2.34 and 2.36–10.20 ppm, and measured

501 $^{206}Pb/^{204}Pb$, $^{207}Pb/^{204}Pb$ and $^{208}Pb/^{204}Pb$ ratios of 17.046–17.308, 15.403–15.467 and

502 38.119–38.344. Pb isotopic compositions were back calculated to t=230 Ma, and thus

503 the $(^{206}Pb/^{204}Pb)_i$, $(^{207}Pb/^{204}Pb)_i$ and $(^{208}Pb/^{204}Pb)_i$ values are 16.84–17.11, 15.39–15.46

504 and 37.81–38.06, respectively. The Dabie orogen experienced two major geological

505 events: the Neoproterozoic rifting-related magmatism and the Triassic

506 subduction-related metamorphism. In deed, we also tried to calculate the Sr, Nd and

507 Pb isotope compositions back to t=800 Ma, but obtained much more scattered results,

508 indicating that the meta-basites experienced metamorphism at the Triassic, during

509 which their isotopes were resetted.

510

5. Discussion

511

5.1. The relationship between the studied rocks and the UHP rocks in the CDZ

512

5.1.1. Low-grade meta-basites and meta-granitoids vs. ± retrograded UHP eclogites

513

and granitic gneisses

514

515 The CDZ contains a variety of coesite- and/or diamond-bearing rock types,

516 including eclogites and granitic gneisses; these rocks experienced Triassic UHP

517 metamorphism and post-peak amphibolite-facies retrogression, responsible for the

518 widespread development of amphibolite-facies assemblages in some eclogites in the

519 area (Wang et al., 1989; Cong et al., 1995; Zhang et al., 2003; Rolfo et al., 2004; Liu

520 et al., 2006b). In some strongly retrograded eclogites, most garnets and omphacites

521 are replaced by symplectites or pseudomorphs; even though, mineral inclusions (e.g.

522 coesite, diamond, omphacite and rutile) within relict garnet preserve the evidence of

523 peak metamorphism at UHP conditions. Even in the most retrograded eclogites that

524 do not contain garnet relics, the former occurrence of garnet is suggested by

525 pseudomorphs of Pl + Amp + Bt that exhibit isometric shape typical of garnet (e.g.,

526 Zhang et al., 2003). In contrast, no garnet and/or other microstructural evidence that

527 could be related to eclogite-facies metamorphism have been observed in the studied

528 meta-basites, thus suggesting that the studied rocks have not been involved in the

529   deep subduction of the SCB in the Triassic.

530   In addition to the main rock-forming minerals, inclusions in metamorphic zircon

531   can be also used to reveal the peak metamorphic conditions in strongly retrograded

532   metamorphic rocks (e.g., Xu et al., 1992b; Nasdala and Massonne, 2000; Bauer et al.,

533   2007; Liu et al., 2007b, 2011b). This is because zircon behaves as a rigid "container"

534   that can protect the inclusions from the retrogression occurring in the matrix. Mineral

535   inclusions related to UHP conditions (e.g. coesite, diamond, omphacite and rutile)

536   have been identified in Triassic metamorphic zircons from the retrograded eclogites in

537   the CDZ, thus confirming that they experienced UHP metamorphism, although the

538   matrix of the rocks is dominanted by amphibolite-facies mineral assemblages (Liu et

539   al., 2001, 2006a). On the contrary, no Triassic metamorphic zircon and related

540   eclogite-facies mineral inclusions have been identified in the studied meta-basites (see

541   section 4.2.1).

542   Different from UHP eclogites, felsic gneisses that underwent deep subduction

543   and UHP metamorphism commonly do not preserve evidence of the peak

544   metamorphic mineral assemblage. Nevertheless, their metamorphic zircons can trap

545   and preserve peak metamorphic minerals. In the CDZ, UHP inclusions (e.g. coesite

546   and diamond) have been recognized in Triassic metamorphic zircons from the felsic

547   gneisses (Tabata et al., 1998; Liu et al., 2001). On the contrary, no Triassic ages have

548   been obtained from the metamorphic zircons in the studied meta-granitoids, and no

549   eclogite-facies mineral inclusions have been observed therein (see section 4.2.1).

550   The overall observations and data clearly indicate that the studied meta-basites

551   and meta-granitoids were not involved in the Triassic deep subduction and UHP

552   eclogite-facies metamorphism, but underwent lower-grade metamorphism, i.e., at

553   amphibolite-facies conditions as suggested by the mineral assemblages and estimated

554   temperatures of the meta-basites (see sections 2.2 and 2.3). The age of this low-grade

555   metamorphic event has not been directly constrained due to the lack of related

556   metamorphic zircon, which may be attributed to the relatively low temperatures (<541

557   ºC, section 2.3). Nevertheless, similar low-grade rocks from the same region showing

558   identical Neoproterozoic protolith ages, yield Triassic whole-rock Rb-Sr isochronal

20

559   ages of 232 ± 8 Ma (Dong et al., 1997; Gao et al., 2006). We therefore suggest that

560   during the Triassic, the studied meta-basites and meta-granitoids underwent a shallow

561   subduction associated with amphibolite-facies metamorphism, nearly sinchronous

562   with the deep subduction of the CDZ.

563

564   *5.1.2. The same source and crustal levels indicated by zircon Hf and bulk-rock*

565   *Sr-Nd-Pb isotopes*

566   *Zircon Hf isotopes*

567   Because Hf is more incompatible than Lu, the continental crust acquired a

568   Lu/Hf ratio much lower than that in the primitive mantle, when it differentiated from

569   the primitive mantle. As a result, the $^{176}Hf/^{177}Hf$ ratio in the continental crust increases

570   slower than in the depleted mantle and thus its $\varepsilon_{Hf}(t)$ value becomes more and more

571   negative with time, whereas the depleted mantle develops more and more positive

572     $\varepsilon_{Hf}(t)$ values (Rudnick and Gao, 2003; Kelemen et al., 2003; Salters and Stracke, 2004;

573   Palme and O'Neill, 2003). When a zircon crystallized from a crustal-derived melt, the

574     $^{176}Hf/^{177}Hf$ ratio in the melt was timely imprinted in the zircon, because Hf content in

575   zircon is several orders of magnitude higher than Lu content, and thus the change of

576     $^{176}Hf/^{177}Hf$ ratio in zircon with time is negligible; moreover, zircon $^{176}Hf/^{177}Hf$ ratio is

577   resistant to the influence of later processes such as weathering, fluid alteration and

578   metamorphic recrystallization (Patchett et al., 1984; Wu et al., 2006b; Zheng et al.,

579   2008; Hanyu et al., 2006; Carpentier et al., 2009; Hoffmann et al., 2011; Roux et al.,

580   2009; Yu et al., 2009; Chen et al., 2010; Tappe et al., 2011; Choi and Mukasa, 2012).

581   In this way, the $\varepsilon_{Hf}(t)$ value of zircon reflects the mass source of the host rocks: given

582   the same zircon U-Pb age, the more negative zircon $\varepsilon_{Hf}(t)$ value is, the higher

583   proportion of ancient continental crustal material the host rock contains. In principle,

584   the most positive $\varepsilon_{Hf}(t)$ values correspond to the youngest single-stage Hf model ages

585   (T_{DM1}) that represent the maximum time of the emplacement of the mantle-derived

586   magma, while the most negative $\varepsilon_{Hf}(t)$ values correspond to the oldest T_{DM1} ages that

587   represent the minimum time of the formation of the involved crust.

588   The UHP eclogites and gneisses in the CDZ exhibit varied zircon Hf isotope

589   compositions, indicating both source mixing and crustal contamination along an

590   active rifting zone, with varying degrees of mixing between different ages of crustal

591   materials at ~750 Ma. Therein, the youngest zircon T_{DM1} ages from the eclogites are

592   in agreement with the Neoproterozoic zircon U-Pb ages of ~750 Ma, while the oldest

593   zircon T_{DM2} ages from the gneisses are close to the Paleoproterozoic zircon U-Pb ages

594   of ~2.15 Ga, indicating growth and immediate reworking of juvenile crust at

595   Paleoproterozoic (~2.15 Ga) and Neoproterozoic (~750 Ma), respectively (e.g., Zheng

596   et al., 2006).

597   The studied meta-basites and meta-granitoids have varied zircon Hf isotope

598   compositions (Supplementary Table 8) which are in agreement with the UHP

599   eclogites and orthogneisses in the CDZ (e.g., Zheng et al., 2006) (Fig. 10), indicating

600   different degrees of mixing between Neoproterozoic depleted mantle materials and

601   Paleoproterozoic crustal components. The meta-basites have positive $\varepsilon_{Hf}(t)$ values of

602   +2.6~+7.9 and young T_{DM1} ages of about 1.2~1.5 Ga, slightly older than their zircon

603   U-Pb ages, reflecting incongruent contamination of crustal materials during the

604   emplacement of their parental magmas. Inherited zircons from the low-Si

605   meta-granitoids exhibit overlapped T_{DM1} ages of 2359~2702 Ma and T_{DM2} ages of

606   2506~2823 Ma from late Archean to Paleoproterozoic, representing the time of the

607   formation of continental crust from the mantle. For the Neoproterozoic zircons with

608   negative $\varepsilon_{Hf}(t)$ values, T_{DM2} can better reflect their origin than T_{DM1}. Neoproterozoic

609   zircons in the low-Si meta-granitoids exhibit negative $\varepsilon_{Hf}(t)$ values of -3.2~-12.0 and

610   younger T_{DM2} ages of 1893~2446 resulting from mixing between depleted mantle

611   materials and late Archean continental crust at Neoproterozoic. Compared to the

612   low-Si meta-granitoids, the high-Si rocks do not contain ancient (late Archean)

613   inherited zircon, and have higher $\varepsilon_{Hf}(t)$ values of -7.5~+1.4 and younger T_{DM2} ages of

614   1618~2172 Ma, indicating that they were mainly derived from remelting of younger

615   continental crust formed at early Paleoproterozoic. These clusters of T_{DM2} age of the

616   meta-granitoids are consistent with multiple episodes of crust growth of the South

617   China Block from the late Archean to Paleoproterozoic (Greentree et al., 2006; Zhang

618   et al., 2006a,b; Liu et al., 2008; Wang et al., 2010; Zhao and Cawood, 2012).

619   As a summary, the studied meta-basites and meta-granitoids derived from the

620   same sources as the UHP eclogites and felsic gneisses in the CDZ. Therein the

621   meta-basites were formed from depleted mantle upwelling and mafic magmatic

622   activities during the Neoproterozoic, with incongruent mixing with the Yangtze

623   crustal materials; the mafic magmatic activities remelted the basement of the South

624   China Block, which comprises the Archean and early Paleoproterozoic crustal rocks,

625   and generated the low-Si and high-Si meta-granitoids.

626

627   *Bulk-rock Sr-Nd-Pb isotopes*

628   Because Rb is more incompatible than Sr, and Nd is more incompatible than Sm,

629   melts will have higher Rb/Sr but lower Sm/Nd ratios than residues during partial

630   melting. Therefore, when the the primitive mantle differentiated to form the crust and

631   depleted mantle, the crust acquired higher Rb/Sr and lower Sm/Nd ratios than the bulk

632   earth, while the depleted mantle acquired lower Rb/Sr and higher Sm/Nd ratios. Then

633   the $^{87}Sr/^{86}Sr$ of the crust will be more and more higher than the bulk earth, but the

634    $\varepsilon_{Nd}(t)$ will be more and more negative with time; on the contrary, the $^{87}Sr/^{86}Sr$ and

635    $\varepsilon_{Nd}(t)$ of the depleted mantle will evolve in the opposite direction. The meta-basites

636   have initial $^{87}Sr/^{86}Sr$ ratios of 0.7023–0.7067 (calculated to t=230 Ma), $\varepsilon_{Nd}(230\ Ma)$

637   values from -1.8 to +1.8 and T_{DM2} ages of 862–1156 Ma. In the $\varepsilon_{Nd}(t)$ vs $(^{87}Sr/^{86}Sr)_i$

638   diagram (Fig. 11), the meta-basites plot around the composition of the bulk silicate

639   earth and slightly toward lower continental crust, indicating that the meta-basites were

640   derived mainly from the mantle, with minor addition of lower continental crust. This

641   conclusion is also supported by their two-stage Nd model ages (T_{DM2}) of 862–1156

642   Ma, which are slightly older than their magmatic zircon U-Pb ages (~772 Ma).

643   U is more incompatible than Pb. This being the case, we would therefore predict

644   that continental crust should be more enriched in radiogenic Pb than the average of the

645   bulk-earth, while the depleted mantle should be depleted in radiogenic Pb. Upper

646   continental crustal rocks do have higher $^{206}Pb/^{204}Pb$ and $^{207}Pb/^{204}Pb$ ratios as expected, but

647   surprisingly, most mantle-derived rocks also exhibit higher Pb isotope ratios than the

648   average of the bulk-earth, whereas a majority of lower crustal rocks are relatively

23

649　depleted in radiogenic Pb. This phenomenon is known as the Pb paradox and it implies

650　that other processes apart from magmatism may have played key roles in the

651　differentiation of the U-Pb element pair.

652　　In addition, Pb isotopes can be used to trace the crust affinity of given rocks from

653　upper or lower crust, i.e., upper crustal rocks commonly have higher radiogenic Pb

654　isotopes than lower crustal rocks (Zartman and Doe, 1981; Taylor and McLennan, 1985).

655　For example, Liu and Li (2008) concluded that the NDZ is of lower crustal origin, while

656　the CDZ and the SDZ are slices from middle to upper crust, according to their different

657　radiogenic Pb isotope compositions. As shown in Figure 12, the Pb isotope compositions

658　of the studied meta-basites fall into the range of the UHP meta-igneous rocks from the

659　CDZ, and are significantly higher than that of the UHP meta-igneous rocks from the NDZ.

660　This indicates that the studied meta-basites and the associated meta-granitoids were at

661　middle to upper crustal depths, consistent with the UHP meta-igneous rocks from the

662　CDZ.

663　　Summing up, both zircon Hf and bulk-rock Sr-Nd-Pb isotopic data demonstrate

664　that the studied meta-basites and meta-granitoids are low-grade metamorphosed

665　counterparts of the UHP eclogites and orthogneisses in the CDZ; these rocks did not

666　experience deep subduction and UHP metamorphism during the Triassic, but were

667　detached from the subducting plate and exhumed from shallower depths, experiencing

668　amphibolite-facies metamorphic peak conditions.

669

670　*5.1.3. The studied rocks as the best candidates for elucidating the Neoproterozoic*

671　*evolution of the South China Block*

672　　The UHP meta-igneous rocks in the CDZ consist mainly of granitic gneisses and

673　eclogites, which are generally considered to be transformed from bimodal igneous

674　rocks derived from rift magmatism in Neoproterozoic (e.g., Ames et al., 1996; Rowley

675　et al., 1997; Hacker et al., 1998). The studied meta-basites and meta-granitoids at

676　Longjingguan have consistent Neoproterozoic protolith ages and zircon Hf isotopic

677　compositions with those from the UHP meta-igneous rocks, most likely indicating that

678　they were derived from the same rifting events, during which depleted mantle

679 materials were added to the crust, and caused remelting of existing old crust and

680 generated bimodal magmas (Liu et al., 2007a). In addition, the bulk-rock Pb isotopic

681 compositions of the studied rocks fall into the range of the UHP meta-igneous rocks in

682 the CDZ (Fig.12), suggestive of upper crustal origin (Liu et al., 2017). In this regard,

683 the studied rocks are likely counterparts of the UHP rocks in the region, and both of

684 them were formed from partial melting of ancient crust in the Neoproterozoic.

685 Moreover, during the Triassic the studied rocks experienced lower-grade and

686 lower-pressure metamorphism with respect to their UHP counterpart. Therefore, we

687 suggest that the rocks could likely have better preserved their protolith compositions

688 than the UHP rocks, which often experienced interactions with melt and/or

689 supercritical fluids during UHP metamorphism (e.g., Zheng et al., 2011). In order to

690 test this hypothesis, the trace element patterns of the studied meta-basites are

691 compared to those of the UHP eclogites derived from basites (data from Tang et al.,

692 2007), as shown in Fig. 5: the studied meta-basites have identical REE and trace

693 element patterns, while the UHP eclogites exhibit similar REE patterns but

694 significantly varied large ion lithophile element (LILE) contents. This is consistent

695 with the fact that LILE have significantly higher mobilities than REE in hydrous

696 fluids during UHP metamorphism (Kessel et al., 2005; Hermann et al., 2006; Zheng et

697 al., 2011). As a conclusion, the rocks here have better preserved their protolith

698 compositions than their UHP counterparts, and thus they are more suitable for

699 elucidating the Neoproterozoic evolution in the area.

700

701 *5.2. Neoproterozoic magmatic and metamorphic events*

702 *5.2.1. Meta-basites*

703 Zircons in the meta-basites (samples 11LJG3 and 11LJG7) give a concordant

704 magmatic age cluster of ~772 Ma (Ma) and two concordant metamorphic age clusters

705 of ~768 Ma (Me1) and ~746 Ma (Me2) (see section 4.2.3). As mentioned above, the

706 magmatic zircons exhibit clear oscillatory zoning and REE patterns typical of

707 magmatic genesis, thus the age of ~772 Ma represents a magmatic event. As to the

708 metamorphic zircons, they formed during metamorphic events characterized by the

709 circulation of REE-enriched fluids controlled by fractures. In addition, most
710 metamorphic zircons exhibit slightly higher Nb + Ta, U and Th contents than the
711 magmatic zircons (Supplementary Table 5), thus suggesting that the metamorphic
712 fluids were also enriched in Nb+Ta, U and Th. These REE-, Nb+Ta-, U- and Th-
713 enriched fluids favoured the precipitation of minerals rich in these elements, such as
714 epidote, rutile, ilmenite and titanite (Figs. 7a-i), observed as inclusions in the
715 metamorphic zircons (e.g., sample 11LJG3; Me1 domains). Thermobarometric
716 estimates (see Section 2.3) based on rutile inclusions indicate that metamorphic zircon
717 domains Me1 grew at about 850-870 °C, 12 kbar. No rutile or other inclusions
718 suitable for themometric estimates have been recognized in the Me2 domain of
719 zircons in sample 11LJG7, thus the temperatures of the late thermal overprinting at
720 ~746 Ma has not been estimated. Summing up, the meta-basites were formed at ca.
721 772 Ma (Ma domains) and experienced subsequent granulite-facies (850-870 °C)
722 metamorphism at ca. 768 Ma (Me1 domains), followed by a thermal overprinting
723 event at ~746 Ma (Me2 domains). The almost overlapped magmatic and metamorphic
724 zircon ages (772 ± 4 and 768 ± 7 Ma, respectively) suggest that the Neoproterozoic
725 magmatism in this area occurred in pulse, and that the later magma underplating
726 warmed the already solidified rocks (e.g., Liu et al., 2007a; Liu et al., 2015) resulting
727 in granulite-facies metamorphism. The thermal overprinting age of ~746 Ma is
728 comparable with the emplacement age of some mafic rocks in the Dabie orogen, for
729 example the meta-basites in the BZ located in the northern part of the Dabie orogen
730 (Liu et al., 2017), indicating that a later magma emplacement at that time in the area
731 may have been the heat source of the thermal overprinting. Moreover, these ages are
732 in agreement with the time of Rodinia breakup indicated by large volumes of mafic
733 and felsic magmatism along the northern margin of the Yangtze Block (Li et al., 2002;
734 Li et al., 2003a,b,c; Zhou et al., 2002a,b, 2006a,b; Zhao and Zhou, 2007a,b, 2008),
735 suggesting that the studied rocks are generated from several episodes of magmatic
736 event related to the Rodinia breakup.

737

738 *5.2.2. Meta-granitoids*

739   Compared to the meta-basites, the low-Si meta-granitoids exhibit a more complex

740   zircon U-Pb age spectrum. Few inherited zircon cores preserve two groups of age at

741   ~2.0 and ~2.5 Ga, timely consistent with two episodes of Precambrian crustal growth

742   and immediate reworking event of the SCB (e.g., Zhang et al., 2006a,b,c; Liu et al.,

743   2008; Wang et al., 2010; Zhao and Cawood, 2012). Safe for these inherited zircon

744   cores, the zircons in the studied rocks are distinguished into two types: magmatic

745   zircon domains yielding concordant ages of ca. 819 Ma (Ma domains) and

746   metamorphic zircon domains with concordant ages at ca. 784 (Me1 domains) and 746

747   Ma (Me2 domains). The latters are discriminated from the formers by weaker or no

748   oscillatory zonings, lighter brightness in CL image and enrichment of mineral

749   inclusion. A typical zircon with magmatic zircon core and metamorphic mantle in

750   meta-granitoid sample 11LJG2 (Me1) is shown (Figs. 7j-l): the core is dark with

751   obvious oscillatory zoning, while the mantle is light and homogeneous in CL image;

752   the core is free of mineral inclusion, while the mantle contains K-feldspar +

753   muscovite inclusion; and there is a clear boundary between the core and the mantle.

754   Two analytical spots on metamorphic zircon domains exhibit significantly higher

755   LREE patterns than the magmatic zircons (Figs. 8b,c), therein a spot also exhibit

756   higher REE contents than the magmatic zircons. Moreover, muscovite + K-feldspar

757   inclusion is identified in metamorphic zircon (Fig. 7k), indicating that the

758   metamorphic zircons were formed in the presence of LREE-enriched fluid, in

759   agreement with the metamorphic zircons in the meta-basites. Therefore, the low-Si

760   meta-granitoids experienced two episodes of metamorphism at ~784 Ma and ~746 Ma,

761   respectively. It is worth noting that, the ~784 Ma metamorphic zircon ages are

762   comparable with the forming (i.e. magmatic) ages of the meta-basites (~772 Ma)

763   within error, suggesting that the emplacement of the basic magmas may be the heat

764   source for the metamorphism of the low-Si meta-granitoids. The thermal overprinting

765   of ~746 Ma is timely in agreement with the ca. 750 Ma forming age of the

766   meta-granitoids and meta-basites in the BZ (Jiang et al., 2005; Wu et al., 2007; Liu et

767   al., 2010, 2017), indicating that the low-Si meta-granitoids and the meta-basites in the

768   region experienced a coeval thermal event as a consequence of the emplacement of

27

769   the meta-basites within the BZ.

770   The high-Si meta-granitoids exhibit nearly the same Neoproterozoic magmatic

771   and metamorphic zircon ages with the low-Si type, indicating that they were

772   generated from the same or adjacent magmatic events and then jointly experienced the

773   same metamorphic processes during the Neoproterozoic. However, the two types of

774   meta-granitoids are likely derived from different sources: (i) the low-Si type contains

775   inherited zircons with two age clusters at ~2.5 Ga and ~2.0 Ga, suggesting that its

776   source could be a late Archean basement that experienced metamorphic reworking

777   during the Paleoproterozoic, whereas (ii) the high-Si type does not contain ancient

778   inherited zircon, and the oldest zircon Hf model age (T_{DM2}) is 2172 Ma, suggesting

779   that a derivation from the juvenile crust formed during the Paleoproterozoic. This

780   hypothesis can well explain the compositional gap, especially the different Si contents,

781   between the two types of meta-granitoids (see section 4.1), and also the slightly higher

782   zircon $\varepsilon_{Hf}(t)$ values and younger Hf model ages of the high-Si meta-granitoids (see

783   section 4.3).

784   The meta-basites and meta-granitoids with similar mid- to late-Neoproterozoic

785   ages have been reported from other localities within the Dabie orogen, for example,

786   Ganghe within the CDZ (Dong et al., 1997), Yuexi within the NDZ (Gao et al., 2006),

787   and Huwan, Sujiahe and Luzhenguan within the BZ (Jiang et al., 2005; Wu et al.,

788   2007; Liu et al., 2010, 2017). In addition, extensive mid- to late-Neoproterozoic mafic

789   dyke swarms and granitic bodies (Zhao and Zhou, 2009; Hong et al., 2009; Xue et al.,

790   2011; Wang et al., 2013) are exposed in Suizhou-Zaoyang of the Hubei province,

791   along the northern margin of the SCB. Moreover, the forming ages of these rocks are

792   clearly comparable with the protolith ages of the UHP eclogites and orthogneisses

793   (Rowley et al., 1997; Hacker et al., 1998; Liu et al., 2007a,b, 2011a; and references

794   therein) in the Dabie orogen. In this regard, these rocks, including those from

795   Longjingguan in this study, should be counterparts of the UHP meta-igneous rocks in

796   the Dabie orogen, implying that the protoliths of the latter could have been formed

797   during the same Neoproterozoic magmatic events, and could have experienced the

798   same Neoproterozoic metamorphism.

799

5.3. Petrogenesis and tectonic setting

5.3.1. Meta-basites

Mantle-normalized trace element patterns are frequently used to infer

petrogenesis and tectonic settings of igneous rocks, because the same rock type

formed in different tectonic settings can display significantly different trace element

patterns. For example, the basites of mid-ocean ridges (MORB) are formed from the

depleted mantle within a narrow depth interval, and thus have a uniform chemical

composition, while the island-arc basalts (IAB) and within-plate basalts (WPB)

exhibit large variation in trace element contents and patterns, and generally

enrichment in LILE and LREE compared to MORB, depending on addition

component of crustal materials. The strong negative Sr anomalies, together with

slightly positive or negative anomalies of HFSE elements of the studied meta-basites

(Fig. 5b) indicate that they are unlikely IAB or post-collision basic rocks (PCB),

which commonly exhibit positive Sr anomalies and strong depletion of the HFSE.

WPB fits better with the studied meta-basites, with respect to the mantle-normalized

trace element pattern (e.g., Velikoslavinsky and Krylov, 2014 and references therein),

thus the meta-basites were most likely formed in a within-plate environment. To

reinforce the hypothesis, the discrimination diagrams proposed by Velikoslavinsky

and Krylov (2014) were applied (Fig. 13). Nearly all major elements as well as many

trace elements are involved in the discriminant functions of these diagrams; hence

they include comprehensive information of the geochemical characteristics of basalts.

In this way, the average weighted uncertainty of IAB, MORB, and WPB identification

is substantially small as compared with previously elaborated plots. All of the studied

meta-basites plot into the category of WPB in the $DF_1(x)$ range (Fig. 13a) and most of

them fall into continental WPB field with only a small percentage of OIB in the $DF_3(x)$

range (Fig. 13b). In addition, the $DF_5(x)$ values of the meta-basites are coincident with

most WPB but only few post-collision basic rocks (PCB) (Fig. 13c). As a

consequence, the studied meta-basites are most likely continental WPB not related to

post-collision processes, but rather involved in mantle plume or continental rifting.

29

829 This conclusion is highly in agreement with the zircon Hf isotopic features of the

830 meta-basites (see section 5.1), which demonstrate mixing between the depleted mantle

831 and the crust.

832

833 *5.3.2. Meta-granitoids*

834 Various binary discrimination diagrams were applied to constrain the tectonic

835 setting of the meta-granitoids in Longjingguan. The diagrams employing Ga/Al

836 (Whalen et al., 1987) show that the meta-granitoids have similar geochemical features

837 with A-type granites (Fig. 14). A-type granite was firstly proposed to be related to

838 anorogenic environments (Chappell and White, 1974), but afterwards more and more

839 studies suggest that A-type granite may form under different environments (Whalen et

840 al., 1987; Eby, 1990; Wu et al., 2002; Bonin, 2007). Nevertheless, it is widely

841 accepted that high melting temperatures (>830 °C) are required to generate A-type

842 granite magmas (Clemens et al., 1986), probably through the emplacement of

843 mantle-derived mafic magmas into the lower crust. In this study, the meta-granitoids

844 are spatially and temporally associated with meta-basites, indicating that they were

845 formed under a geodynamic setting characterized by asthenosphere upwelling and

846 basic magmatism, which can provide sufficient heat to generate high-T granitoids.

847 Zircon Hf isotopic compositions of the meta-granitoids (see section 5.1) also suggest

848 addition of the depleted mantle materials into the felsic magmas.

849 Trace elements and REE patterns are frequently used in identifying petrogenesis

850 and tectonic setting of granitoids. The significant depletion of HREE, Nb, Ta, and Ti

851 of the studied meta-granitoids (Fig. 5b) is in agreement with adakite and arc-related

852 ADR (andesite, dacite and rhyolite) (see Castillo, 2006 for an overview). Adakite and

853 arc-related ADR are generally associated to slab subducting and mantle convecting,

854 consistent with the aforementioned high temperature characteristics of the studied

855 meta-granitoids. However, the high Sr, low Yb and high Sr/Y characteristics of

856 adakite are in contrast with the studied meta-granitoids, which exhibit low Sr (13-275

857 ppm), high Y (19-46 ppm) and low Sr/Y (0.34-10.39). In the Sr/Y vs Y diagram (Fig.

858 15), which is usually used to discriminate adakites and TTGs from typical arc

30

calc-alkaline rocks (Drummond and Defant, 1990), all the studied meta-granitoids plot into the field of typical arc rocks. Therefore, based on the geochemical characteristics, zircon U-Pb ages and Hf isotopic compositions described above, the studied meta-granitoids most likely formed under magmatic arc setting, in agreement with the previous investigations on the Neoproterozoic igneous rocks in the periphery of the SCB (Zheng et al., 2007; Zhao et al., 2018 and references therein); and the low-Si and high-Si types are mainly derived from partial melting of late-Archean and Paleoproterozoic continental crustal materials, respectively, with various degrees of addition of mantle materials.

In summary, the meta-granitoids were formed at ca. 819 Ma by partial melting of ancient continental crustal materials in an arc setting, whereas the meta-basites were derived mainly from the depleted mantle at ca. 772 Ma in a rifting setting. Thus, the studied rocks witness the transition from a convergent to an extensional tectonic setting, and provide new constraints for the beginning of the Neoproterozoic rifting in northern SCB, which can further help to better understand the breakup of the supercontinent Rodinia.

6. Conclusions

(1) The meta-basites and meta-granitoids in Longjingguan are relatively low-grade metamorphosed counterparts of the UHP eclogites and orthogneisses within the CDZ; they were detached from the subducted crust of the SCB and exhumed from shallow depths during subduction, and subsequently thrusted over the CDZ during collisional orogenesis.

(2) The precursors of the studied meta-granitoids and meta-basites were formed at ca. 819 Ma and 772–784 Ma, respectively. They jointly experienced a granulite-facies metamorphism at ca. 768 Ma and a thermal overprinting at ca. 746 Ma resulted from underplating of mafic magmas, strongly pointing to multiple episodes of continental rifting during the Neoproterozoic.

(3) The meta-granitoids are derived mainly from partial melting of ancient continental

crustal materials of the SCB in an arc setting. The low-Si meta-granitoids were derived from the late Archean basement rocks that underwent Paleoproterozoic metamorphic reworking, while the high-Si meta-granitoids mainly come from the Paleoproterozoic juvenile crust. The meta-basites were derived from the depleted mantle in a rifting environment. The studied rocks thus witness the transition from a convergent to an extensional tectonic setting, and provide new time constraints for the beginning of the Neoproterozoic rifting in northern SCB, which can further help to better understand the breakup of the supercontinent Rodinia.

Acknowledgements

References

907   **References**

908   Ames, L., Zhou, G.Z., Xiong, B.C., 1996. Geochronology and isotopic character of

909   ultrahigh-pressure metamorphism with implications for the collision of the

910   Sino-Korean and Yangtze cratons, central China. Tectonics 15, 472–489.

911   Angiboust, S., Harlov, D., 2017. Ilmenite breakdown and rutile-titanite stability in

912   metagranitoids: Natural observations and experimental results. American

913   Mineralogist 102, 1696–1708.

914   Bauer, C., Rubatto, D., Krenn, K., Proyer, A., Hoinkes, G., 2007. A zircon study from

915   the rhodope metamorphic complex, n-greece: time record of a multistage

916   evolution. Lithos 99(3), 207–228.

917   Black, L.P., Kamo, S.L., Allen, C.M., Aleinikoff, J.N., 2003. TEMORA 1: a new

918   zircon standard for phanerozoic U–Pb geochronology. Chemical Geology 200,

919   155–170.

920   Blichert-Toft, J., Albarede, F., 1997. The Lu–Hf isotope geochemistry of chondrites

921   and the evolution of the mantle–crust system. Earth and Planetary Science

922   Letters 148, 243–258.

923   Bohlen, S.R., Liotta, J.J., 1986. A Barometer for Garnet Amphibolites and Garnet

924   Granulites. Journal of Petrology 27, 1025–1034.

925   Bonin, B., 2007. A-type granites and related rocks: evolution of a concept, problems

926   and prospects. Lithos 97(1–2), 1–29.

927   Carpentier, M., Chauvel, C., Maury, R., Mattielli, N., 2009. The "zircon effect" as

928   recorded by the chemical and Hf isotopic compositions of the Lesser Antilles

929   forearc sediments. Earth and Planetary Science Letters 287, 86–99.

930   Castillo, P.R., 2006. An overview of adakite petrogenesis. Chinese Science Bulletin

931   51(3), 257–268.

932   Chappell, B.W., White, A.J.R., 1974. Two contrasting granite types. Pacific Geology 8,

933   173–174.

934   Chemenda, A.I., Mattauer, M., Bokun, A.N., 1996. Continental subduction and a

935   mechanism for exhumation of high-pressure metamorphic rocks: new modelling,

936   field data from Oman. Earth and Planetay Science Letters 143, 173–182.

937 Chen, F., Hegner, E., Todt, W., 2000. Zircon ages and Nd isotopic and chemical

938   compositions of orthogneisses from the Black Forest, Germany: evidence for a

939   Cambrian magmatic arc. International Journal of Earth Sciences 88, 791– 802.

940 Chen, F.K., Guo, J.H., Jiang, L.L., Siebel, W., Cong, B., Satir, M., 2003. Provenance

941   of the Beihuaiyang lower-grade metamorphic zone of the Dabie

942   ultrahigh-pressure collisional orogen, China: evidence from zircon ages. Journal

943   of Asian Earth Science 22(4), 343–352.

944 Chen, F., Li, X.H., Wang, X.L., Li, Q.L., Siebel, W., 2007. Zircon age and Nd-Hf

945   isotopic composition of the Yunnan Tethyan belt, southwestern China.

946   International Journal of Earth Science 96, 1179–1194.

947 Chen, R.X., Zheng, Y.F., Xie, L., 2010. Metamorphic growth and recrystallization of

948   zircon: distinction by simultaneous in-situ analyses of trace elements, U–Th–Pb

949   and Lu–Hf isotopes in zircons from eclogite-facies rocks in the Sulu orogen.

950   Lithos 114, 132–154.

951 Choi, S.H., Mukasa, S.B., 2012. Lu–Hf and Sm–Nd isotope systematic of Korean

952   spinel peridotites: a case for metasomatically induced Nd–Hf decoupling. Lithos

953   154, 263–276.

954 Chopin, C., 1984. Coesite and pure pyrope in high grade blueschists of the western

955   Alps: a first record and some consequences. Contributions to Mineralogy and

956   Petrology 86, 107–118.

957 Clemens, J.D., Holloway, J.R., White, A.J.R., 1986. Origin of an A-type granite:

958   experimental constraints. American Mineralogist 71, 317–324.

959 Compston, W., Williams, I.S., Kirschvink, J.L., 1992. Zircon U–Pb ages for the Early

960   Cambrian time-scale. Journal of the Geological Society 149, 171–184.

961 Cong, B., Zhai, M., Carswell, D.A., Wilson, R.N., Wang, Q., Zhao, Z., Windly, B.F.,

962   1995. Petrogenesis of ultrahigh-pressure rocks and their country rocks at

963   Shuanghe in Dabieshan, central China. European Journal of Mineralogy 7, 119–

964   138.

965 Dong, S.W., Wang, X.F., Huang, D.Z., 1997. Discovery of low grade metamorphic

966 volcanic rock sheets within UHP in Dabie Mts. and its implications. Chinese

967 Science Bulletin 42, 1199–1203.

968 Drummond, M.S., Defant, M.J., 1990. A model for trondhjemite–tonalite–dacite

969 genesis and crustal growth via slab melting: Archaean to modern comparisons.

970 Journal of Geophysical Research 95, 21503–21521.

971 Eby, G.N., 1990. The A-type granitoids: a review of their occurrence and chemical

972 characteristics and speculations on their petrogenesis. Lithos 26, 115–134.

973 Ernst, W.G., Maruyama, S., Wallis, S., 1997. Buoyancy-driven, rapid exhumation of

974 ultrahigh-pressure metamorphosed continental crust. Proceedings of the National

975 Academy of Science, USA 94, 9532–9537.

976 Gao, T.S., Tang, J.F., Sang, H.Q., Hu, S.L., Qian, C.C., 2006. Whole-rock Ar-Ar

977 dating for low-grade metavolcanics within the Dabie orogen and its geological

978 implications. Chinese Science Bulletin 51, 1197–1202.

979 Gebauer, D., Schertl, H.P., Brix, M., Schreyer, W., 1997. 35 Ma old ultrahigh-pressure

980 metamorphism and evidence for very rapid exhumation in the Dora Maira Massif,

981 Western Alps. Lithos 41, 5–24.

982 Greentree, M.R., Li, Z.X., Li, X.H., Wu, H., 2006. Late mesoproterozoic to earliest

983 neoproterozoic basin record of the sibao orogenesis in western south china and

984 relationship to the assembly of rodinia. Precambrian Research 151(1–2), 79–100.

985 Griffin, W.L., Pearson, N.J., Belousova, E., Jackson, S.E., van Achterbergh, E.,

986 O'Reilly, S.Y., Shee, S.R., 2000. The Hf isotope composition of cratonic mantle:

987 LAM-MC-ICPMS analysis of zircon megacrysts in kimberlites. Geochimica et

988 Cosmochimica Acta 64, 133–147.

989 Groppo, C., Rolfo, F., Liu, Y.C., Deng, L.P., Wang, A.D., 2015. P-T evolution of

990 elusive UHP eclogites from the Luotian dome (north Dabie zone, China): how

991 far can the thermodynamic modeling lead us? Lithos 226, 183–200.

992 Hacker, B.R., Ratschbacher, L., Webb, L., Ireland, T., Walker, D., Dong, S.W., 1998.

993 U/Pb zircon ages constrain the architecture of the ultrahigh-pressure

994 Qinling–Dabie orogen, China. Earth and Planetary Science Letters 161,

995 215–230.

35

996   Hacker, B.R., Ratschbacher, L., Webb, L., McWiliams, M.O., Ireland, T., Calvert, A.,
997   Dong, S.W., Wenk, H.R., Chateigner, D., 2000. Exhumation of ultrahigh-pressure
998   continental crust in east central China: Late Triassic-Early Jurassic tectonic
999   unroofing. Journal of Geophysical Research 105 (B6), 13339–13364.

1000 Hanchar, J.M., Rudnick, R.L., 1995. Revealing hidden structures: the application of
1001   cathodoluminescence and back-scattered electron imaging to dating zircons from
1002   lower crustal xenoliths. Lithos 36, 289–303.

1003 Hanyu, T., Tatsumi, Y., Nakai, S., Chang, Q., Miyazaki, T., Sato, K., Tani, K., Shi-bata,
1004   T., Yoshida, T., 2006. Contribution of slab melting and slab dehydration to
1005   magmatism in the NE Japan arc for the last 25 Myr: Constraints from
1006   geochemistry. Geochemistry Geophysics Geosystems 7, Q08002.

1007 Hermann, J., Rubatto, D., Korsakov, A., Shatsky, V.S., 2001. Multiple zircon growth
1008   during fast exhumation of diamondiferous, deeply subducted continental crust
1009   (Kokchetav massif, Kazakhstan). Contributions to Mineralogy and Petrology 141,
1010   66–82.

1011 Hermann, J., Spandlera, C., Hacka, A., Korsakovb, A.V., 2006. Aqueous fluids and
1012   hydrous melts in high-pressure and ultra-high pressure rocks: Implications for
1013   element transfer in subduction zones. Lithos 92, 399–417.

1014 Hoffmann, J.E., Münker, C., Polat, A., Rosing, M.T., Schulz, T., 2011. The origin of
1015   decoupled Hf–Nd isotope compositions in Eoarchean rocks from southern West
1016   Greenland. Geochimica et Cosmochimica Acta 75, 6610–6628.

1017 Holland, T., Blundy, J., 1994. Non-ideal interactions in calcic amphiboles and their
1018   bearing on amphibole-plagioclase thermometry. Contributions to Mineralogy and
1019   Petrology 116, 433–447.

1020 Hong, J.A., Ma, B., Huang, Q., 2009. The Dafushan meta-basic/ultrameta-basic
1021   complex and genesis of the related rutile ore deposit at Zaoyang, Hubei (in
1022   Chinese with English abstract). Chinese Journal of Geology 44, 231–244.

1023 Hoskin, P.W., Ireland, T.R., 2000. Rare earth element chemistry of zircon and its use
1024   as a provenance indicator. Geology 28(7), 627–630.

1025 Hou, Z.H., Wang, C.X., 2007. Determination of 35 trace elements in geological

1026   samples by inductively coupled plasma mass spectrometry (in Chinese with

1027   English abstract). Journal of University of Science and Technology of China 37,

1028   940–944.

1029   Jiang, L., Siebel, W., Chen, F., Liu, Y.C., Chu, D., 2005. U-Pb zircon ages for the

1030   Luzhenguan Complex in northern part of the eastern Dabie orogen. Science

1031   China (Series D) 48, 1357–1367.

1032   Kelemen, P.B., Hanghoj, K., Greene, A.R., 2003. One view of the geochemistry of

1033   subducted-related magmatic arcs, with an emphasis on primitive andesites and

1034   lower crust. Treatise of Geochemistry 3, 593–659.

1035   Kessel, R., Schmidt, M.W., Ulmer, P., Pettke, T., 2005. Trace element signature of

1036   subduction-zone fluids, melts and supercritical liquids at 120–180 km depth.

1037   Nature 437, 724–727.

1038   Le Bas, M.J., Le Maitre, R.W., Streckeisen, A., Zanettin, B., 1986. A chemical

1039   classification of volcanic rocks based on the total alkali-silica diagram. Journal

1040   of Petrology 27(3), 745–750.

1041   Lee, C.A., Luffi, P., Plank, T., Dalton, H., Leeman, W.P., 2009. Constraints on the

1042   depths and temperatures of basic magma generation on Earth and other terrestrial

1043   planets using new thermobarometers for mafic magmas. Earth and Planetary

1044   Science Letters 279, 20–33.

1045   Li, S.G., Xiao, Y.L., Liou, D.L., Ge, N.J., Zhang, Z.Q., Sun, S.S., Cong, B.L., Zhang,

1046   R.Y., Hart, S.R., Wang, S.S., 1993. Collision of the North China and Yangtze

1047   blocks and formation of coesite bearing eclogites: timing and processes.

1048   Chemical Geology 109, 89–111.

1049   Li, S.G., Jagoutz, E., Chen, Y.Z., Li, Q.L., 2000. Sm–Nd and Rb–Sr isotope

1050   chronology of ultrahigh-pressure metamorphic rocks and their country rocks at

1051   Shuanghe in the Dabie Mountains, central China. Geochimica et Cosmochimica

1052   Acta 64, 1077–1093.

1053   Li, S.Z., Kusky, T.M., Zhao, G.C., Liu, X.C., Zhang, G.W., Kopp, H., Wang, L., 2010.

1054   Two-stage Triassic exhumation of HP–UHP terranes in the western Dabie orogen

1055   of China: constraints from structural geology. Tectonophysics 490, 267–293.

Li, X.H., Li, Z.X., Ge, W.C., Zhou, H.W., Li, W.X., Liu, Y., Wingate, M.T.D., 2003a. Neoproterozoic granitoids in South China: crustal melting above a mantle plume at ca 825 Ma? Precambrian Research 122, 45–83.

Li, X.H., Li, Z.X., Zhou, H., Liu, Y., Liang, X., Li, W., 2003b. SHRIMP U–Pb zircon age, geochemistry and Nd isotope of the Guandaoshan pluton in SW Sichuan: petrogenesis and tectonic significance. Science China (Series D) 46, 73–83.

Li, X.P., Zheng, Y., Wu, Y., Chen, F., Gong, B., Li, Y.L., 2004. Low-T eclogite in the Dabie terrane of China: petrological and isotopic constrains on fluid activity and radiometric dating. Contributions to Mineralogy and Petrology 148, 443–470.

Li, Z.X., Li, X.H., Kinny, P.D., Wang, J., Zhang, S., Zhou, H., 2003c. Geochronology of Neoproterozoic syn-rift magmatism in the Yangtze Craton, South China and correlations with other continents: evidence for a mantle superplume that broke up Rodinia. Precambrian Research 122, 85–109.

Li, S.G., Huang, F., Zhou, H.Y., Li, H.M., 2003d. U-Pb isotopic compositions of the ultrahigh pressure metamorphic (UHPM) rocks from Shuanghe and gneisses from Northern Dabie zone in the Dabie Mountains, central China: Constraint on the exhumation mechanism of UHPM rocks. Science China (Series D) 46(3), 200–209.

Li, Y., Liu, Y.C., Yang, Y., Deng, L.P., 2017. New U-Pb geochronological constraints on formation and evolution of the Susong complex zone in the Dabie orogen. Acta Geologica Sinica 91, 1915–1918.

Liu, F., Gerdes, A., Xue, H., Liang, F., 2006a. SHRIMP U-Pb zircon dating from eclogite lenses in marble, Dabie-Sulu UHP terrane: restriction on the prograde, UHP and retrograde metamorphic ages. Acta Petrologica Sinica 22, 1761–1778.

Liu, J., Ye, K., Maruyama, S., Cong, B., Fan, H., 2001. Mineral inclusions in zircon from gneisses in the ultrahigh-pressure zone of the Dabie Mountains, China. Journal of Geology 109, 523–535.

Liu, X.C., Jahn, B.-M., Liu, D., Dong, S., Li, S., 2004. SHRIMP U-Pb zircon dating of a metagabbro and eclogites from western Dabieshan (Hong'an Block), China, and its tectonic implications. Tectonophysics 394, 171–192.

1086   Liu, X.M, Gao, S., Diwu, C.R, Ling, W.L., 2008. Precambrian crustal growth of
1087   Yangtze Craton as revealed by detrital zircon studies. American Journal of
1088   Science 308(4), 421–468.

1089   Liu, Y.C., Deng, L.P., Gu, X.F., Groppo, C., Franco, R., 2015. Application of
1090   Ti-in-zircon and Zr-in-rutile thermometers to constrain high-temperature
1091   metamorphism in eclogites from the Dabie orogen, central China. Gondwana
1092   Research 27, 410–423.

1093   Liu, Y.C., Gu, X.F., Li, S.G., Hou, Z.F., Song, B., 2011a. Multistage metamorphic
1094   events in granulitized eclogites from the North Dabie complex zone, central
1095   China: evidence from zircon U-Pb age, trace element and mineral inclusion.
1096   Lithos 122, 107–121.

1097   Liu, Y.C., Gu, X.F., Rolfo, F., Chen, Z.Y., 2011b. Ultrahigh-pressure metamorphism
1098   and multistage exhumation of eclogite from the Luotian dome, North Dabie
1099   Complex Zone (central China): Evidence from mineral inclusions and
1100   decompression texture. Journal of Asian Earth Science 42, 607–617.

1101   Liu, Y.C., Li, S.G, 2005. Lower crustal rocks from the Dabie Mountains and their
1102   subduction. Acta Petrologica Sinica 21, 1059–1066.

1103   Liu, Y.C., Li, S.G, 2008. Detachment within subducted continental crust and
1104   multi-plate successive exhumation of ultrahigh-pressure metamorphic rocks:
1105   Evidence from the Dabie-Sulu orogenic belt. Chinese Science Bulletin 53,
1106   3105–3119.

1107   Liu, Y.C., Li, S.G., Gu, X.F., Hou, Z.H., 2006b. Zircon SHRIMP U-Pb dating for
1108   olivine gabbro at Wangmuguan in the Beihuaiyang zone and its geological
1109   significance. Chinese Science Bulletin 51, 2500–2506.

1110   Liu, Y.C., Li, S.G., Gu, X.F., Xu, S.T., Chen, G.B., 2007a. Ultrahigh-pressure eclogite
1111   transformed from mafic granulite in the Dabie orogen, east-central China.
1112   Journal of Metamorphic Geology 25, 975–989.

1113   Liu, Y.C., Li S.G., Xu, S.T., 2007b. Zircon SHRIMP U-Pb dating for gneiss in
1114   northern Dabie high T/P metamorphic zone, central China: Implication for
1115   decoupling within subducted continental crust. Lithos 96, 170–185.

1116   Liu, Y.C., Li, S.G., Xu, S.T., John, B., Zheng, Y.F., Zhang, Z.Q., Jiang, L.L., Chen,

1117   G.B., Wu, W.P., 2005. Geochemistry and geochronology of eclogites from the

1118   northern Dabie Mountains, central China. Journal of Asian Earth Science 25,

1119   431–443.

1120   Liu, Y.C., Liu, L.X., Gu, X.F., Li, S.G., Liu, J., Song, B., 2010. Occurrence of

1121   Neoproterozoic low-grade metagranite in the western Beihuaiyang zone, the

1122   Dabie orogen. Chinese Science Bulletin 55, 3490–3498.

1123   Liu, Y.C., Liu, L.X., Li, Y., Gu, X.F., Song, B., 2017. Zircon U-Pb geochronology and

1124   petrogenesis of metabasites from the western Beihuaiyang zone in the Hong'an

1125   orogen, central China: Implications for detachment within subducting continental

1126   crust at shallow depths. Journal of Asian Earth Science 145, 74–90.

1127   Liu, Y.C., Wang, A.D., Rolfo, F., Groppo, C., Gu, X.F., Song, B., 2009.

1128   Geochronological and petrological constraints on Palaeoproterozoic granulite

1129   facies metamorphism in southeastern margin of the North China Craton. Journal

1130   of Metamorphic Geology 27, 125–138.

1131   Liu, Y.S., Gao, S., Yuan, H.L., Zhou, L., Liu, X.M., Wang, X.C., Hu, Z.C., Wang, L.S.,

1132   2004. U–Pb zircon ages and Nd, Sr, and Pb isotopes of lower crustal xenoliths

1133   from North China Craton: insights on evolution of lower continental crust.

1134   Chemical Geology 211, 87–109.

1135   Ludwig, K.R., 2001. Users Manual for Isoplot/Ex (rev. 2.49): A Geochronological

1136   Toolkit for Microsoft Excel. Berkeley Geochronology Center, Special

1137   Publication No. 1a, 55 p.

1138   Maruyama, S., Liou, J.G., Terabayashi, M., 1996. Blueschists and eclogites of the

1139   world, and their exhumation. International Geology Review 38, 485–594.

1140   Nasdala, L., Massonne, H.J., 2000. Microdiamonds from the Saxonian Erzgebirge,

1141   Germany: in situ micro-Raman characterisation. European Journal of Mineralogy

1142   12, 495–498.

1143   Nowell, G.M., Kempton, P.D., Noble, S.R., Fitton, J.G., Saunders, A.D., Mahoney, J.J.,

1144   Taylor, R.N., 1998. High precision Hf isotope measurements of MORB and OIB

1145   by thermal ionisation mass spectrometry: insights into the depleted mantle.

1146   Chemical Geology 149, 211–233.

1147 Okay, A.I., Xu, S.T., Sengör, A.M.C., 1989. Coesite from the Dabie Shan eclogites,

1148   central China. European Journal of Mineralogy 1, 595–598.

1149 Okay, A.I., Sengör, A.M.C., 1992. Evidence for intracontinental thrust-related

1150   exhumation of the ultra-high-pressure rocks in China. Geology 20, 411–414.

1151 Okay, A.I., Sengör, A.M.C., Satir, M., 1993. Tectonics of an ultrahigh-pressure

1152   metamorphic terrane: the Dabie Shan/Tongbai orogen, China. Tectonics 12,

1153   1320–1334.

1154 Palme, H., O'Neill, H.St.C., 2003. Cosmochemical constraints of mantle composition.

1155   Treatise of Geochemistry 2, 1–38.

1156 Patchett, P.J., White, W.M., Feldmann, H., Kienlinczuk, S., Hofmann, A.W., 1984.

1157   Hafnium/rare earth element fractionation in the sedimentary system and crustal

1158   recycling into the Earth's mantle. Earth and Planetary Science Letters 1984,

1159   365–378.

1160 Rolfo, F., Compagnoni, R., Xu, S., Jiang, L., 2000. First report of felsic whiteschist in

1161   the ultrahigh-pressure metamorphic belt of Dabie Shan, China. European Journal

1162   of Mineralogy 12, 883–898.

1163 Rolfo, F., Compagnoni, R., Wu, W.P., Xu, S.T., 2004. A coherent lithostratigraphic

1164   unit in the coesite–eclogite complex of Dabie Shan, China: geologic and

1165   petrologic evidence. Lithos 73, 71–94.

1166 Roux, V.L., Bodinier, J.L., Alard, O., O'Reilly, S.Y., Griffin, W.L., 2009. Isotopic

1167   decoupling during porous melt flow: a case-study in the Lherzperidotite. Earth

1168   and Planetary Science Letters 279, 76–85.

1169 Rowley, D.B., Xue, F., Tucker, R.D., Peng, Z.X., Baker, J., Davis, A., 1997. Ages of

1170   ultrahigh pressure metamorphism and protolith orthogneisses from the eastern

1171   Dabie Shan: U/Pb zircon geochronology. Earth and Planetary Science Letters

1172   151, 191–203.

1173 Rudnick, R.L., Gao, S., 2003. Composition of the continental crust. Treatise on

1174   Geochemistry 3, 1–64.

1175 Salters, V.J.M., Stracke, A., 2004. Composition of the depleted mantle. Geochemistry

1176   Geophysics Geosystems 5, Q05004.

1177 Scherer, E., Munker, C., Mezger, K., 2001. Calibration of the lutetium–hafnium clock.

1178   Science 293, 683–687.

1179 Schertl, H.P., Okay, A.I., 1994. A coesite inclusion in dolomite in Dabie Shan, China;

1180   petrological and rheological significance. European Journal of Mineralogy 6,

1181   995–1000.

1182 Schmidt, M.W., 1992. Amphibole composition in tonalite as a function of pressure: an

1183   experimental calibration of the Al-in-hornblende barometer. Contributions to

1184   Mineralogy and Petrology 110, 304–310.

1185 Smith, D.C., 1984. Coesite in clinopyroxene in the Caledonides and its implications

1186   for geodynamics. Nature 310, 641–644.

1187 Sobolev, N.V., Shatsky, V.S., 1990. Diamond inclusions in garnets from metamorphic

1188   rocks: a newenvironment for diamond formation. Nature 343, 742–746.

1189 Su, W., Xu, S., Jiang, L., Liu, Y.C., 1996. Coesite from quartz jadeitite in the Dabie

1190   Mountains, Eastern China. Mineralogical Magazine 60, 659–662.

1191 Sun, S.S., McDonough, W.F., 1989. Chemical and isotopic systematics of oceanic

1192   basalts: implications for mantle composition and processes. In: Saunders, A.D.,

1193   Norry, M.J. (Eds.), Magmatism in the ocean basins. Geological Society, London,

1194   Special Publications 42, pp. 313–345.

1195 Tabata, H., Yamauchi, K., Maruyama, S., Liou, J.G., 1998. Tracing the Extent of a

1196   UHP Metamorphic Terrane: Mineral-Inclusion Study of Zircons in Gneisses from

1197   the Dabie Shan. In: Hacker, B.R., Liou, J.G. (Eds), When Continents Collide:

1198   Geodynamics and Geochemistry of Ultrahigh-Pressure Rocks. Springer

1199   Netherlands 10, pp. 261–273.

1200 Tang, H.F., Liu, C.Q., Nakai, S., Orihashi, Y., 2007. Geochemistry of eclogites from

1201   the Dabie–Sulu terrane, eastern china: new insights into protoliths and trace

1202   element behaviour during UHP metamorphism. Lithos 95, 441–457.

1203 Tang, J., Zheng, Y.F., Wu, Y. B., Gong, B., 2006. Zircon SHRIMP U–Pb dating, C and

1204   O isotopes for impure marbles from the Jiaobei terrane in the Sulu orogen:

1205   Implication for tectonic affinity. Precambrian Research 144, 1–18.

1206   Tappe, S., Pearson, D.G., Nowell, G., Nielsen, T., Milstead, P., Muehlenbachs, K.,

1207   2011. A fresh isotopic look at Greenland kimberlites: cratonic mantle lithosphere

1208   imprint on deep source signal. Earth and Planetary Science Letters 305, 235–248.

1209   Taylor, S.R., McLennan, S.M., 1985. The Continental Crust: Its Composition and

1210   Evolution. Blackwell Scientific Publications, Oxford.

1211   Tomkins, H.S., Powell, R., Ellis, D.J., 2007. The pressure dependence of the

1212   zirconium-in-rutile thermometer. Journal of Metamorphic Geology 25, 703–713.

1213   Tsai, C.H., Liou, J.G., 2000. Eclogite-facies relics and inferred ultrahigh-pressure

1214   metamorphism in the North Dabie Complex, central-eastern China. American

1215   Mineralogist 85, 1–8.

1216   Velikoslavinsky, S.D., Krylov, D.P. 2014. Geochemical discrimination of basalts

1217   formed in major geodynamic settings. Geotectonics 48(6), 427–439.

1218   Wang, L.J., Griffin, W.L., Yu, J.H., O'Reilly, S.Y., 2010. Precambrian crustal

1219   evolution of the Yangtze Block tracked by detrital zircons from Neoproterozoic

1220   sedimentary rocks. Precambrian Research 177(1), 131–144.

1221   Wang, M.X., Wang, C.Y., Zhao, J.H., 2013. Zircon U/Pb dating and Hf-O isotopes of

1222   the Zhouan ultramafic intrusion in the northern margin of the Yangtze Block, SW

1223   China: Constraints on the nature of mantle source and timing of the

1224   supercontinent Rodinia breakup. Chinese Science Bulletin 58(7), 777–787.

1225   Wang, X., Liou, J.G., Mao, H.K., 1989. Coesite-bearing eclogites from the Dabie

1226   Mountains in central China. Geology 17, 1085–1088.

1227   Whalen, J.B., Currie, K.L., Chappell, B.W., 1987. A-type granites: geochemical

1228   characteristics, discrimination and petrogenesis. Contributions to Mineralogy and

1229   Petrology 95, 407–419.

1230   Whitney, J.A., Stormer, J.C., 1977. Two-feldspar geothermometry, geobarometry in

1231   mesozonal granitic intrusions: three examples from the Piedmont of Georgia.

1232   Contributions to Mineralogy and Petrology 63(1), 51–64.

1233   Williams, I.S., 1998. U–Th–Pb geochronology by ion microprobe. Applications of

1234   Microanalytical Techniques to Understanding Mineralizing Processes. In:

1235   McKibben, M.A., Shanks III, W.C., Ridley, W.I. (Eds.), Reviews in Economic

1236   Geology 7, pp. 1–35.

1237 Winchester, J.A., Floyd, P.A., 1977. Geochemical discrimination of different magma

1238   series and their differentiation products using immobile elements. Chemical

1239   Geology 20, 325–343.

1240 Workman, R.K., Hart, S.R., 2005. Major and trace element composition of the

1241   depleted MORB mantle (DMM). Earth and Planetary Science Letters 231,

1242   53–72.

1243 Wu, F.Y., Sun, D.Y., Li, H., Jahn, B.M., Wilde, S., 2002. A-type granites in

1244   northeastern china: age and geochemical constraints on their petrogenesis.

1245   Chemical Geology 187, 143–173.

1246 Wu, Y.B., Zheng, Y.F., Zhao, Z.F., Gong, B., Liu, X.M., Wu, F.Y., 2006a. U–Pb, Hf

1247   and O isotope evidence for two episodes of fluid-assisted zircon growth in

1248   marble-hosted eclogites from the Dabie orogen. Geochimica et Cosmochimica

1249   Acta 70, 3743–3761.

1250 Wu, R.X., Zheng, Y.F., Wu, Y.B., Zhao, Z.F., Zhang, S.B., Liu, X.M., Wu, F.Y., 2006b.

1251   Reworking of juvenile crust: element and isotope evidence from Neoproterozoic

1252   granodiorite in South China. Precambrian Research 146, 179–212.

1253 Wu, Y.B., Zheng, Y.F., Tang, J., Gong, B., Zhao, Z.F., Liu, X., 2007. Zircon U–Pb

1254   dating of water–rock interaction during Neoproterozoic rift magmatism in South

1255   China. Chemical Geology 246, 65–86.

1256 Xiao, Y., Hoefs, J., van den Kerkhof, A.M., Li, S.G., 2001. Geochemical constraints of

1257   the eclogite and granulite facies metamorphism as recognized in the Raobazhai

1258   complex from North DabieShan, China. Journal of Metamorphic Geology 19,

1259   3–19.

1260 Xu, S.T., Jiang, L.L., Liu, Y.C., Zhang, Y., 1992a. Tectonic Framework and Evolution

1261   of the Dabie Mountains in Anhui, Eastern China. Acta Geologica Sinica 5,

1262   221–238.

1263 Xu, S.T, Okay, A.I., Ji, S.Y., Sengör, A.M.C., Su, W., Liu, Y.C., Jiang, L.L., 1992b.

1264   Diamond from the Dabie Shan metamorphic rocks and its implication for

1265   tectonic setting. Science 256, 80–82.

1266 Xu, S.T., Liu, Y.C., Su, W., Wang, R.C., Jiang, L.L., Wu, W.P., 2000. Discovery of the

1267   eclogite and its petrography in the Northern Dabie Mountains. Chinese Science

1268   Bulletin 45, 273–278.

1269 Xu, S.T., Liu, Y.C., Chen, G.B., Compagnoni, R., Rolfo, F., He, M.C., Liu, H.F., 2003.

1270   New finding of micro-diamonds in eclogites from Dabie-Sulu region in

1271   central-eastern China. Chinese Science Bulletin 48, 988–994.

1272 Xu, S.T., Liu, Y.C., Chen, G.B., Ji, S.Y., Ni, P., Xiao, W.S., 2005. Microdiamonds,

1273   their classification and tectonic implications for the host eclogites from the Dabie

1274   and Su-Lu regions in central eastern China. Mineralogical Magazine 69,

1275   509–520.

1276 Xue, H.M., Ma, F., Song, Y.Q., 2011. Geochemistry and SHRIMP zircon U-Pb data of

1277   Neoproterozoic meta-magmatic rocks in the Suizhou-Zaoyang area, northern

1278   margin of the Yangtze Craton, Central China. Acta Petrologica Sinica 27,

1279   1116–1130.

1280 Yu, S.Y., Xu, Y.G., Huang, X.L., Ma, J.L., Ge, W.C., Zhang, H.H., Qin, X.F., 2009.

1281   Hf–Nd isotopic decoupling in continental mantle lithosphere beneath Northeast

1282   China: effects of pervasive mantle metasomatism. Journal of Asian Earth Science

1283   35, 554–570.

1284 Yuan, H.L., Gao, S., Liu, X.M., Gunther, D., Wu, F.Y., 2004. Accurate U–Pb age and

1285   trace element determinations of zircon by laser ablation-inductively coupled

1286   plasma mass spectrometry. Geostandards and Geoanalytical Research 28,

1287   353–370.

1288 Zack, T., Moraes, R., Kronz, A., 2004. Temperature dependence of Zr in rutile:

1289   empirical calibration of a rutile thermometer. Contributions to Mineralogy and

1290   Petrology, 148, 471–488.

1291 Zartman, R.E., 1981. PIumbotectonics—the model. Tectonophysics 75, 135–162.

1292 Zhang, H.F., Gao, S., Zhang, Z.Q., Zhang, B.R., Zhang, L., Hu, S.H., 2002.

1293   Geochemical and Sr-Nd-Pb isotopic compositions of Cretaceous granitoids:

1294   constraints on tectonic framework and crustal structure of the Dabieshan

1295   ultrahigh-pressure metamorphic belt, China. Chemical Geology 186, 281–299.

1296 Zhang, R.Y., Liou, J.G., Zheng, Y.F., Fu, B., 2003. Transition of UHP eclogites to

1297   gneissic rocks of low-amphibolite facies during exhumation: evidence from the

1298   dabie terrane, central China. Lithos, 70, 269–291.

1299 Zhang, S.B., Zheng, Y.F., Wu, Y.B., Zhao, Z.F., Gao, S., Wu, F.Y., 2006a. Zircon

1300   isotope evidence for ≥3.5 Ga continental crust in the Yangtze craton of China.

1301   Precambrian Research 146, 16–34.

1302 Zhang, S.B., Zheng, Y.F., Wu, Y.B., Zhao, Z.F., Gao, S., Wu, F.Y., 2006b. Zircon

1303   U–Pb age and Hf–O isotope evidence for Paleoproterozoic metamorphic event in

1304   South China. Precambrian Research 151, 265–288.

1305 Zhang, S.B., Zheng, Y.F., Wu, Y.B., Zhao, Z.F., Gao, S., Wu, F.Y., 2006c. Zircon

1306   U–Pb age and Hf isotope evidence for 3.8 Ga crustal remnant and episodic

1307   reworking of Archean crust in South China. Earth and Planetary Science Letters

1308   252, 56–71.

1309 Zhao, G.C., Cawood, P.A., 2012. Precambrian geology of China. Precambrian

1310   Research 222–223, 13–54.

1311 Zhao, J.H., Zhou, M.F., 2009. Secular evolution of the Neoproterozoic lithospheric

1312   mantle underneath the northern margin of the Yangtze Block, South China.

1313   Lithos 107, 152–168.

1314 Zhao, J.H., Li, Q.W., Liu, H., Wang, W., 2018. Neoproterozoic magmatism in the

1315   western and northern margins of the Yangtze Block (South China) controlled by

1316   slab subduction and subduction-transform-edge-propagator. Earth-Science

1317   Reviews 187, 1–18.

1318 Zheng, Y.F., Zhou, J.B., Wu, Y.B., Xie, Z., 2005. Low-grade metamorphic rocks in the

1319   Dabie-Sulu orogenic belt: a passive-margin accretionary wedge deformed during

1320   continent subduction. International Geology Review 47, 851–871.

1321 Zheng, Y.F., Zhao, Z.F., Wu, Y.B., Zhang, S.B., Liu, X.M., Wu, F.Y., 2006. Zircon

1322   U–Pb age, Hf and O isotope constraints on protolith origin of ultrahigh-pressure

1323   eclogite and gneiss in the Dabie orogen. Chemical Geology 231, 135–158.

1324 Zheng, Y.F., Zhang, S.B., Zhao, Z.F., Wu, Y.B., Li, X.H., Li, Z.X., Wu, F.Y., 2007.

1325   Contrasting zircon Hf and O isotopes in the two episodes of Neoproterozoic

granitoids in South China: implications for growth and reworking of continental crust. Lithos 96, 127–150.

Zheng, Y.F., Wu, R.X., Wu, Y.B., Zhang, S.B., Yuan, H.L., Wu, F.Y., 2008. Rift melting of juvenile arc-derived crust: geochemical evidence from Neoproterozoic volcanic and granitic rocks in the Jiangnan Orogen, South China. Precambrian Research163, 351–383.

Zheng, Y.F., Xia, Q.X., Chen, R.X., Gao, X.Y., 2011. Partial melting, fluid supercriticality and element mobility in ultrahigh-pressure metamorphic rocks during continental collision. Earth Science Reviews 107, 342–374.

Zhou, M.F., Kennedy, A.K., Sun, M., Malpas, J., Lesher, C.M., 2002a. Neoproterozoic arc-related mafic intrusions in the northern margin of South China: implications for accretion of Rodinia. The Journal of Geology 110, 611–618.

Zhou, M.F., Yan, D.P., Kennedy, A.K., Li, Y.Q., Ding, J., 2002b. SHRIMP zircon geochronological and geochemical evidence for Neo-proterozoic arc-related magmatism along the western margin of the Yangtze Block, South China. Earth and Planetary Science Letters 196, 51–67.

Zhou, M.F., Ma, Y.X., Yan, D.P., Xia, X.P., Zhao, J.H., Sun, M., 2006a. The Yanbian Terrane (Southern Sichuan Province, SW China): a Neoproterozoic arc assemblage in the western margin of the Yangtze Block. Precambrian Research 144, 19–38.

Zhou, M.F., Yan, D.P., Wang, C.L., Qi, L., Kennedy, A., 2006b. Subduction related origin of the 750 Ma Xuelongbao adakitic complex (Sichuan Province, China): implications for the tectonic setting of the giant Neoproterozoic magmatic event in South China. Earth and Planetary Science Letters 248, 286–300.

Zindler, A., Hart, S., 1986. Chemical geodynamics. Annual Review of Earth and Planetary Science 14, 493–571.

Figure captions

1354 **Figure 1** Schematic geological map of the Dabie orogen. The inset shows its location

1355 within the Triassic Qinling–Dabie–Sulu collision orogen in central China (modified

1356 from Liu et al., 2007a). Sample locality is marked by a red star. BZ = Beihuaiyang

1357 zone, NDZ = North Dabie high-T/UHP complex zone, CDZ = Central Dabie

1358 mid-T/UHP metamorphic zone, SDZ = South Dabie low-T eclogite zone, SZ =

1359 Susong complex zone, HMZ = Huwan mélange zone, HZ = Hong'an low-T eclogite

1360 zone, DC = amphibolite-facies Dabie complex, XMF = Xiaotian-Mozitan fault, WSF

1361 = Wuhe-Shuihou fault, HMF = Hualiangting-Mituo fault, TSF = Taihu-Shanlong fault,

1362 TLF = Tan-Lu fault.

1363

1364 **Figure 2** Field photograph showing meta-basite lens tectonically enclosed within

1365 meta-granitoid.

1366

1367 **Figure 3** Photomicrographs of plane- and corresponding cross-polarized images for

1368 the meta-basite sample 11LJG7 (a & b), low-Si meta-granitoid sample 1209LJG5 (c

1369 & d), high-Si meta-granitoid sample 1209LJG1 (e & f). Pl: plagioclase; Rt: rutile;

1370 Amp: amphibole; Bt: biotite; Qz: quartz; Ap: apatite; Kfs: K-feldspar; Aln: allanite.

1371

1372 **Figure 4** TAS (total alkalies versus silica) diagram (Le Bas et al., 1986) (a) and

1373 Zr/TiO_2 vs Nb/Y (Winchester and Floyd, 1977) (b) plots for the studied rocks in

1374 Longjingguan. Green circles: meta-basites; red circles: low-Si granitoids; blue circles:

1375 high-Si granitoids; Pc: picrobasalt; B: basalt; O1: basaltic andesite; O2: andesite; O3:

1376 dacite; R: rhyolite; S1: trachybasalt; S2: basaltic trachyandesite; S3: trachyandesite; T:

1377 trachyte; U1: basanite; U2: phonotephrite; U3: tephriphonolite; Ph: phonolite; F:

1378 foidite. Symbols used for different types of samples are the same as in the following

1379 figures.

1380

1381 **Figure 5** Chondrite-normalized REE patterns (a) and primitive mantle-normalized

1382 trace element patterns (b) for the studied rocks in Longjingguan and for the UHP

1383 eclogites (c & d) in the CDZ. Normalized values and the data of the N-MORB and

1384 E-MORB are from Sun and McDonough (1989), the elemental data of the UHP

1385 eclogites are from Tang et al. (2007).

1386

1387 **Figure 6** Representative CL images of zircons from the meta-basites (samples

1388 11LJG3 and 11LJG7), low-Si meta-granitoids (samples 11LJG2, 1209LJG5 and

1389 1202LJG3) and high-Si meta-granitoid (sample 1303LJG2) in Longjingguan. The red

1390 circles locate the SHRIMP analysis spots, and the red numbers are the corresponding

1391 $^{206}Pb/^{238}U$ ages.

1392

1393 **Figure 7** Mineral inclusions within metamorphic zircon domains from samples

1394 11LJG3 (a-i) and 11LJG2 (j-l). Hbl, hornblende; Rt, rutile; Qz, quartz; Ap, apatite;

1395 Kfs, K-feldspar; Mus, muscovite; Ep, epidote; Ttn, titanite; Ilm, ilmenite.

1396

1397 **Figure 8** Zircon rare earth element (REE) patterns for the meta-basites (samples

1398 11LJG3 and 11LJG7) and meta-granitoids (samples 1209LJG5, 11LJG2, 1303LJG2

1399 and 1202LJG3) in Longjingguan. Normalized values are from Sun and McDonough

1400 (1989).

1401

1402 **Figure 9** SHRIMP zircon U-Pb ages for the meta-basites (a & b), low-Si

1403 meta-granitoids (c, d, e, g & h) and high-Si meta-granitoid (f) in Longjingguan. (e)

1404 and (h) correspond to the dashed squares in (d) and (g), respectively.

1405

1406 **Figure 10** Zircon ε_{Hf} (t) vs U-Pb age of the studied meta-basites and meta-granitoids,

1407 as well as the UHP eclogites and gneisses (data from Zheng et al., 2006) from the

1408 CDZ. The evolution trendlines of the depleted mantle (DMM) and chondrite are from

1409 Griffin et al. (2000).

1410

1411

1412 **Figure 11** Plot of Nd vs Sr isotopes for the meta-basites (samples 11LJG3 to 11LJG8)

1413 from Longjingguan. MORB: mid-ocean ridge basalt; UCC: upper continental crust;

1414 LCC: lower continental crust.

1415

1416 **Figure 12** $(^{207}Pb/^{204}Pb)_i$ vs $(^{206}Pb/^{204}Pb)_i$ and $(^{208}Pb/^{204}Pb)_i$ vs $(^{206}Pb/^{204}Pb)_i$ plots for

1417 the meta-basites (samples 11LJG3 to 11LJG8) from Longjingguan. The initial Pb

1418 isotopes data of the meta-basites are calibrated with t=230 Ma, the blue-green and

1419 grey areas in the diagrams represent the UHP orthogneiss and eclogites in the North

1420 Dabie (NDZ) and Central Dabie (CDZ) terranes, respectively (data from Zhang et al.,

1421 2002; Li et al., 2003d). The initial Pb isotope data of MORB, EMI and EMII are from

1422 Zindler and Hart. (1986), and that of lower crust (LC) is from Liu et al. (2004).

1423 $(^{207}Pb/^{204}Pb)_{NHRL}=0.1084\times(^{206}Pb/^{204}Pb)_i + 13.401$; $(^{208}Pb/^{204}Pb)_{NHRL}=1.209\times(^{206}Pb/$

1424 $^{204}Pb)_i + 15.627$.

1425

1426 **Figure 13** Tectonic discrimination diagrams (Velikoslavinsky and Krylov, 2014) for

1427 the meta-basites in Longjingguan. Values of the discriminant functions $DF_1(x)$, $DF_2(x)$,

1428 $DF_3(x)$ and $DF_5(x)$ have been calculated from formula: $D(x) = \Sigma a_i*x_i + constant$,

1429 where a_i is coefficient at corresponding variable; x_i is value of variable (oxide content,

1430 wt %; trace element content, ppm). In the $DF_1(x)-DF_2(x)$ diagram (a), the

1431 meta-basites (green circles) plot in the field of WPB. In the $DF_3(x)$－frequency (%) (b)

1432 and $DF_5(x)$－frequency (%) (c) diagrams, the rocks (the red rectangles with dashed

1433 oblique lines) have function values coincident with the majority population of WPB.

1434

1435 **Figure 14** Plots employing Ga/Al (Whalen et al., 1987) for the meta-granitoids in

1436 Longjingguan. I & S: I-type and S-type granite; A: A-type granite.

1437

1438 **Figure 15** (Sr/Y) vs. Y diagram discriminating adakite and TTG from typical arc

1439 calc-alkaline rocks (Drummond and Defant, 1990).

1440

Figure 1
Click here to download high resolution image
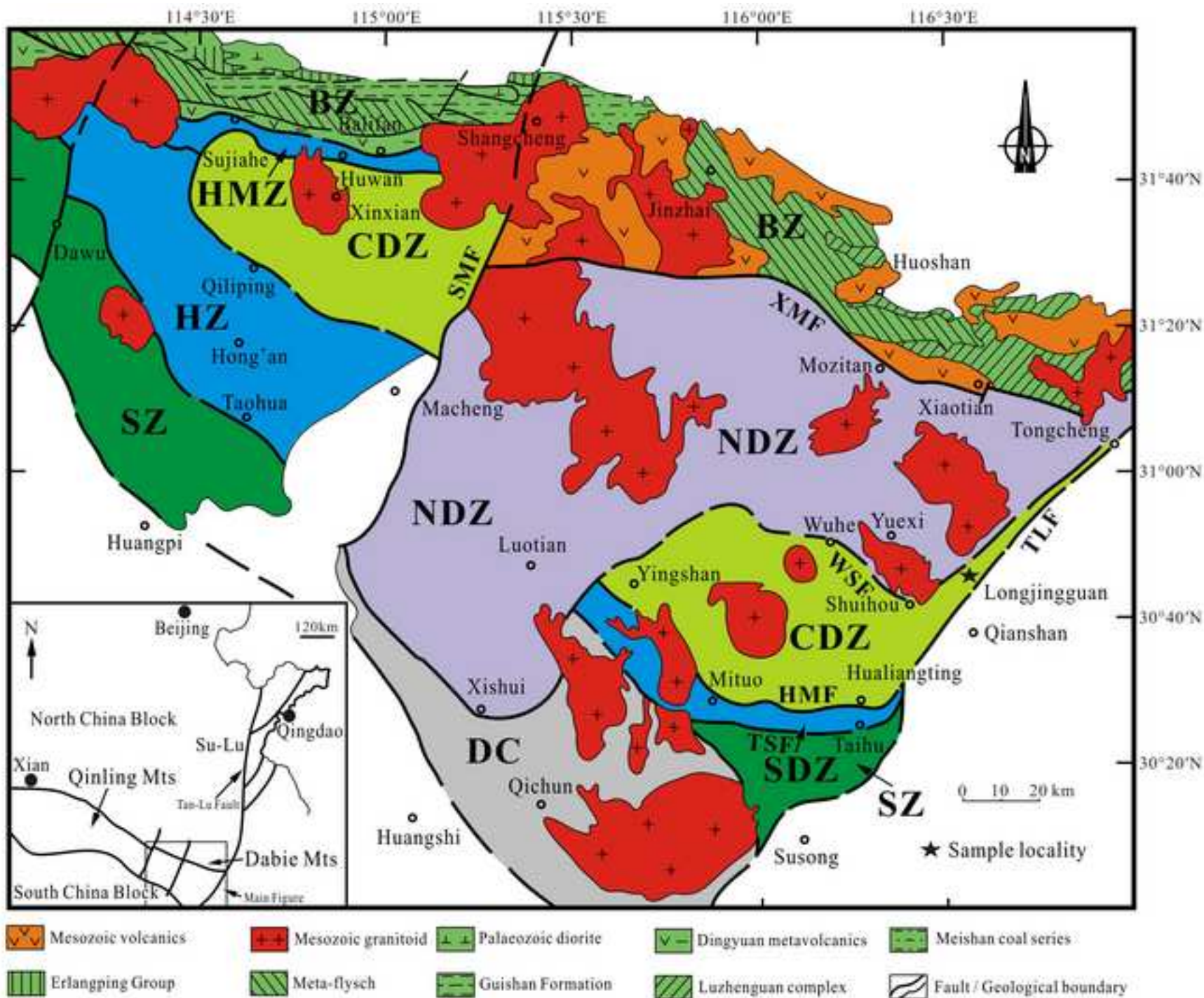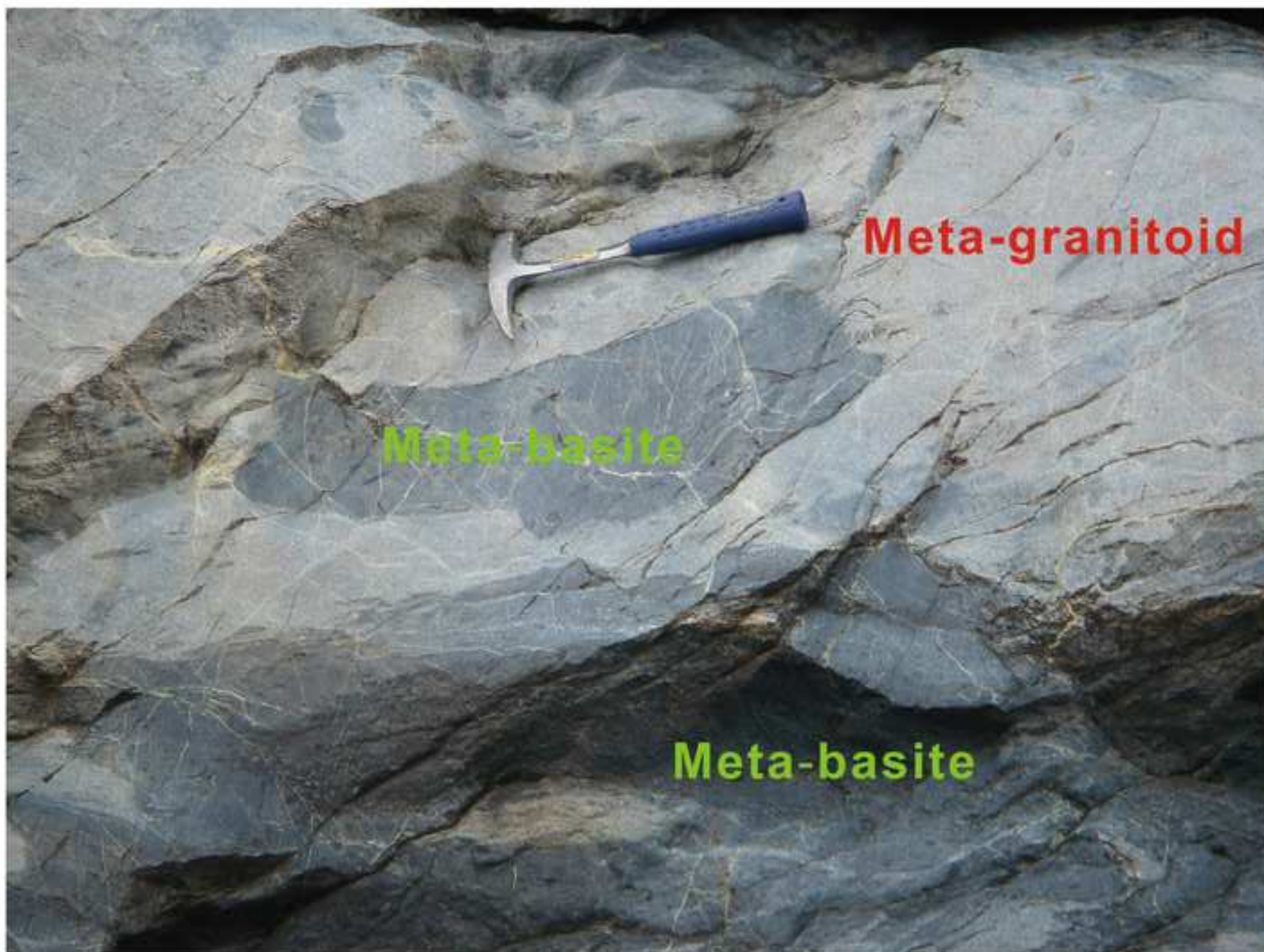
Figure 1

Figure 3
Click here to download high resolution image
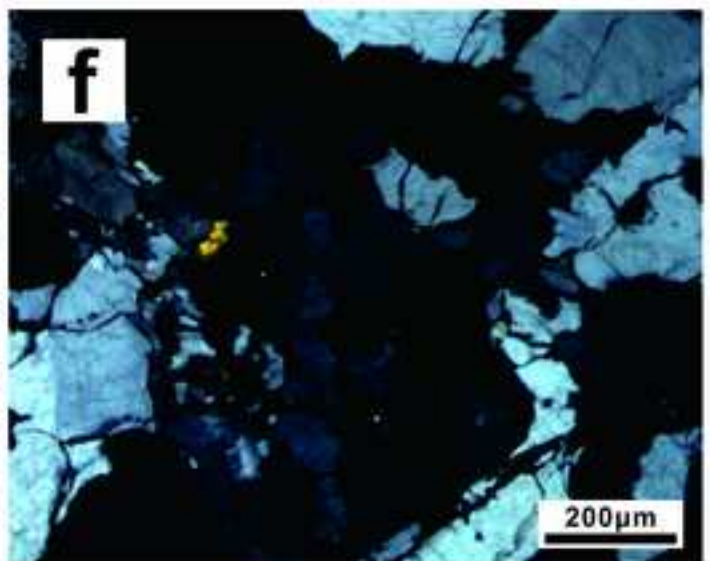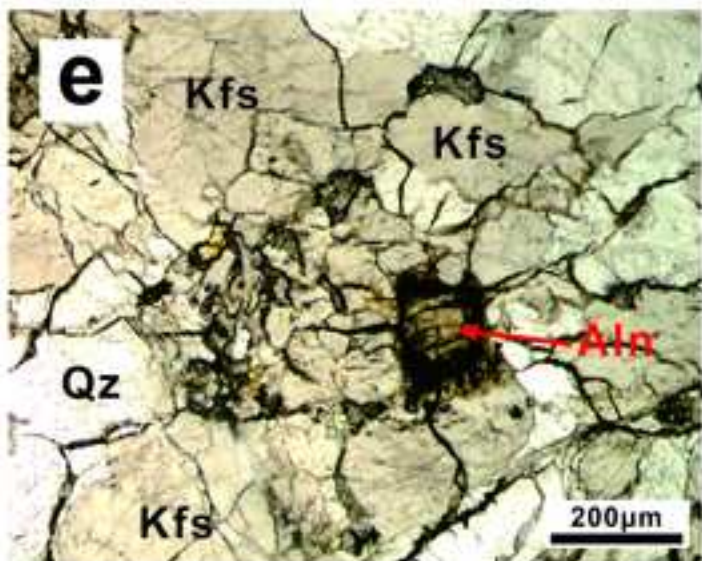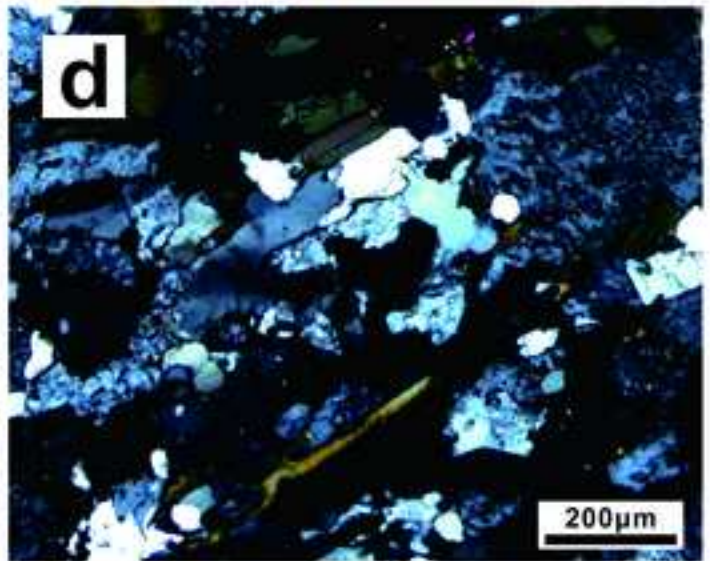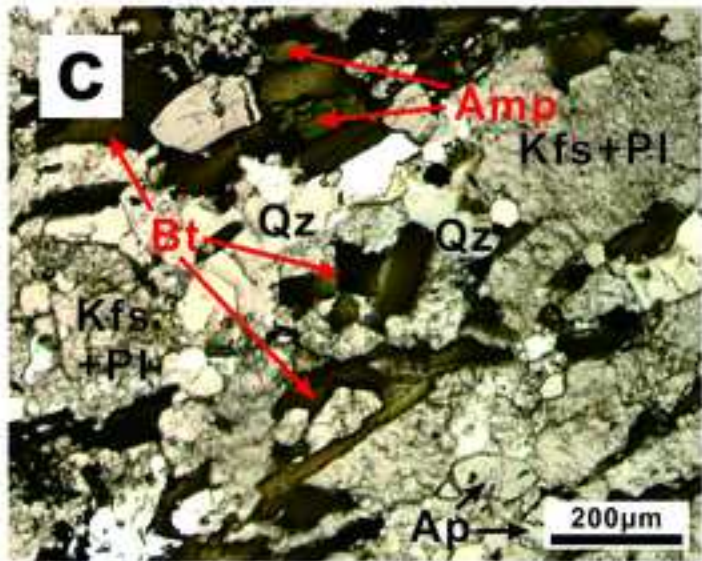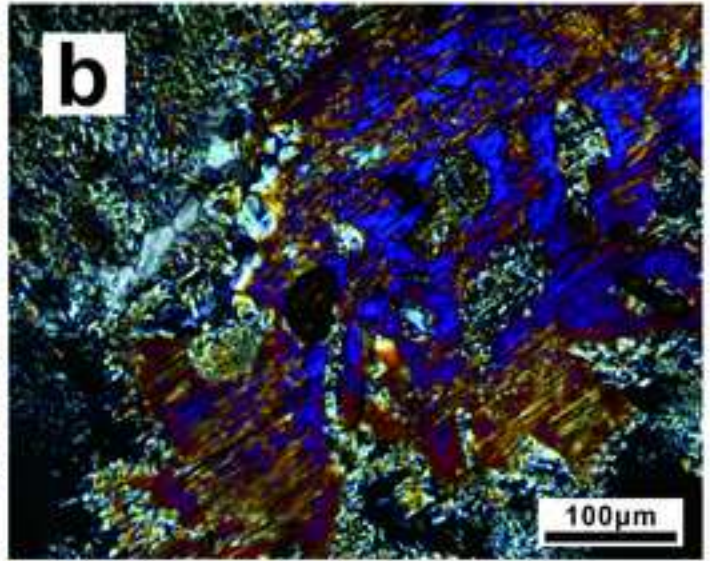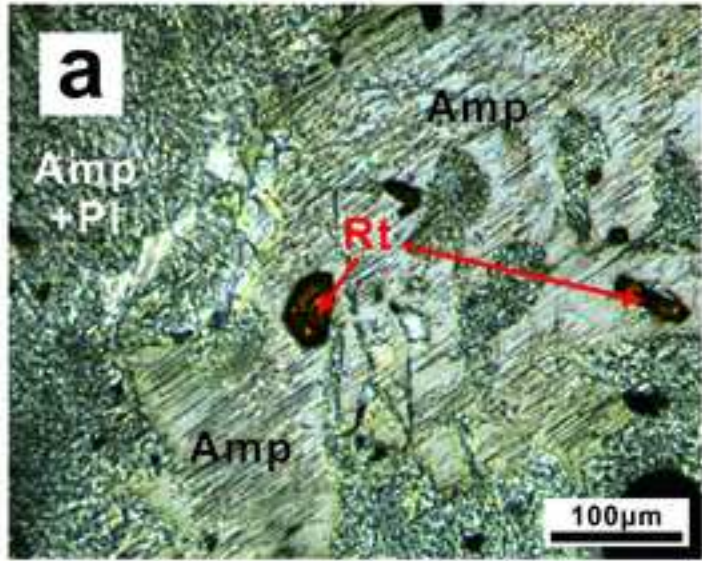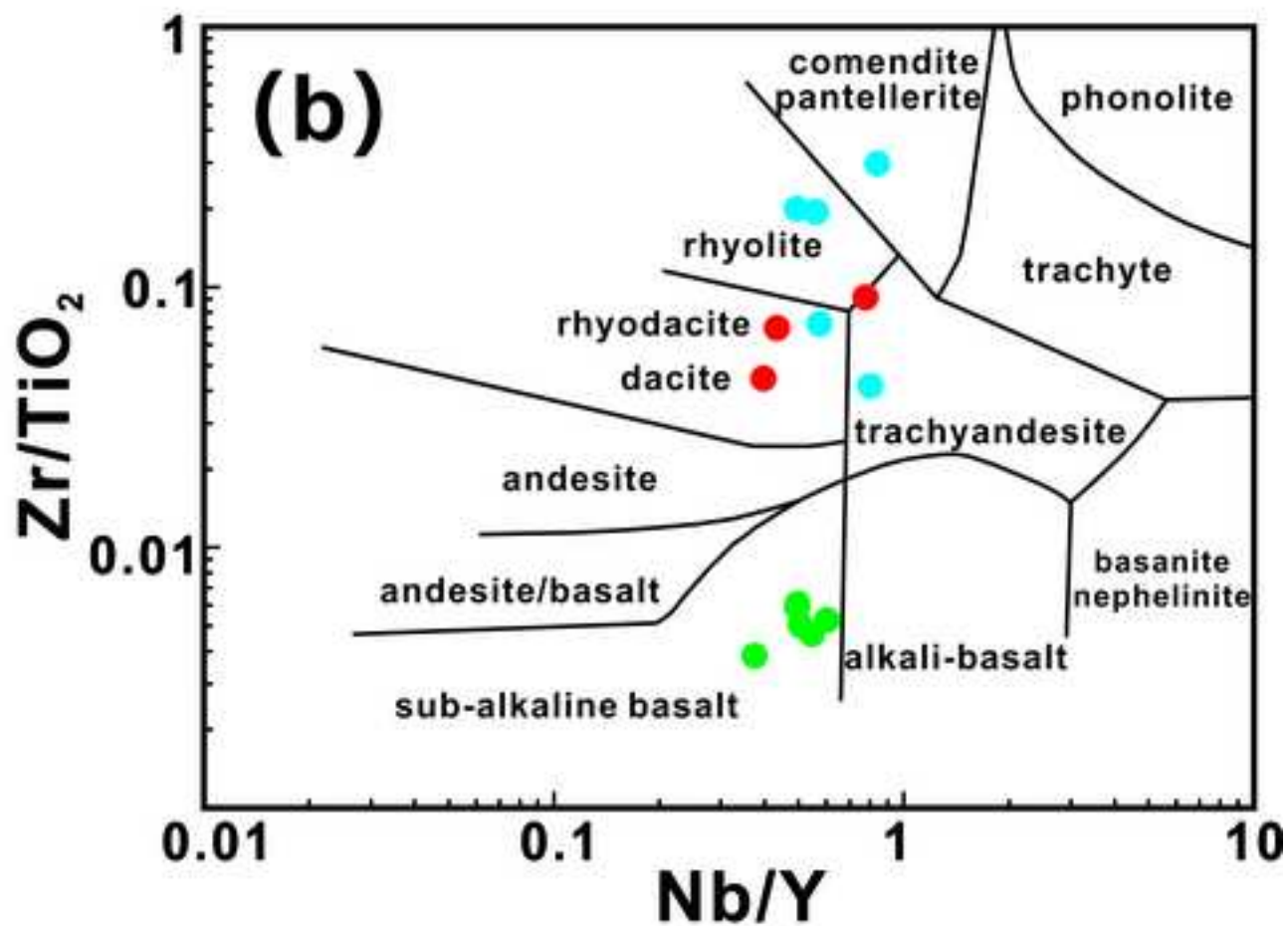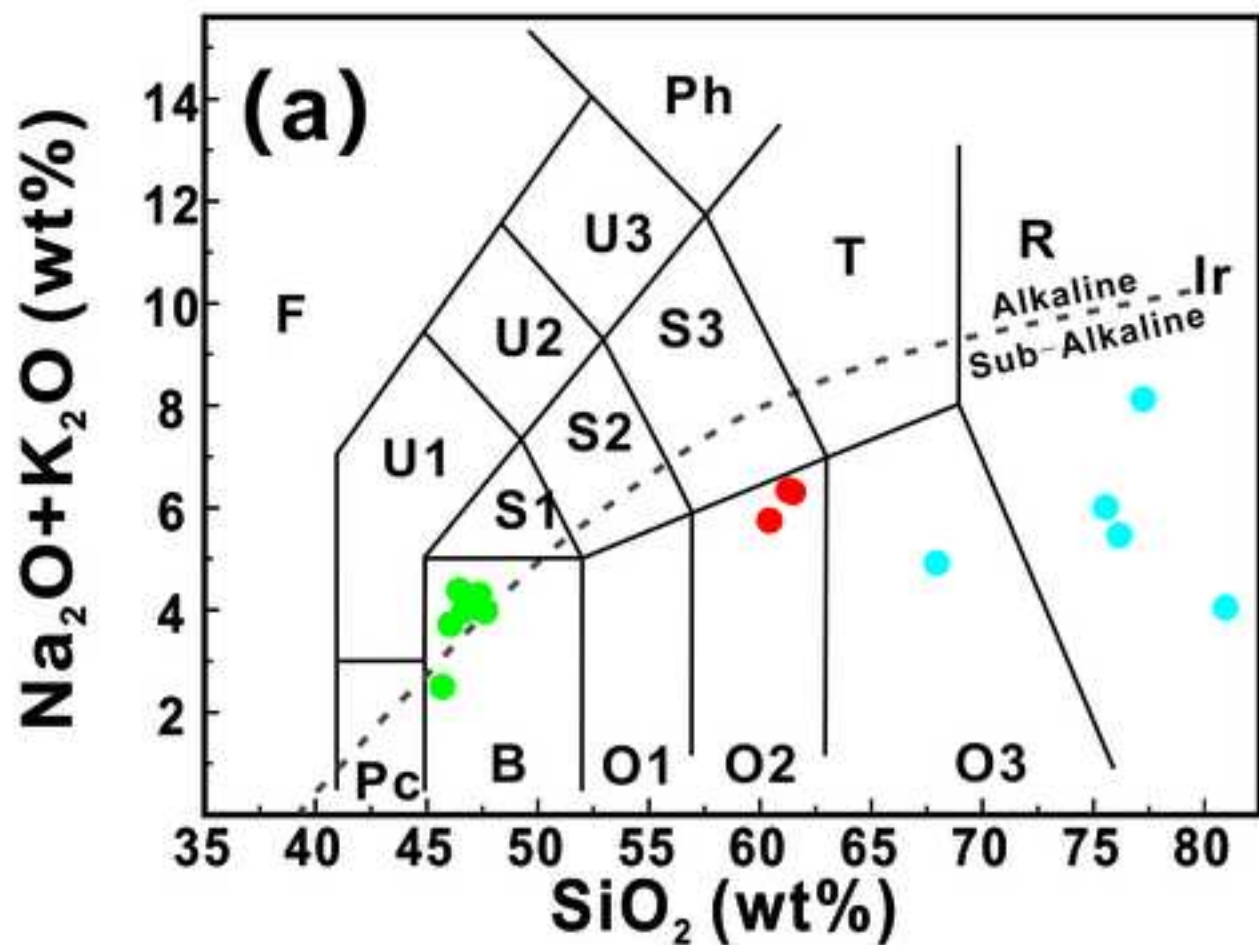
Figure 5
Click here to download high resolution image
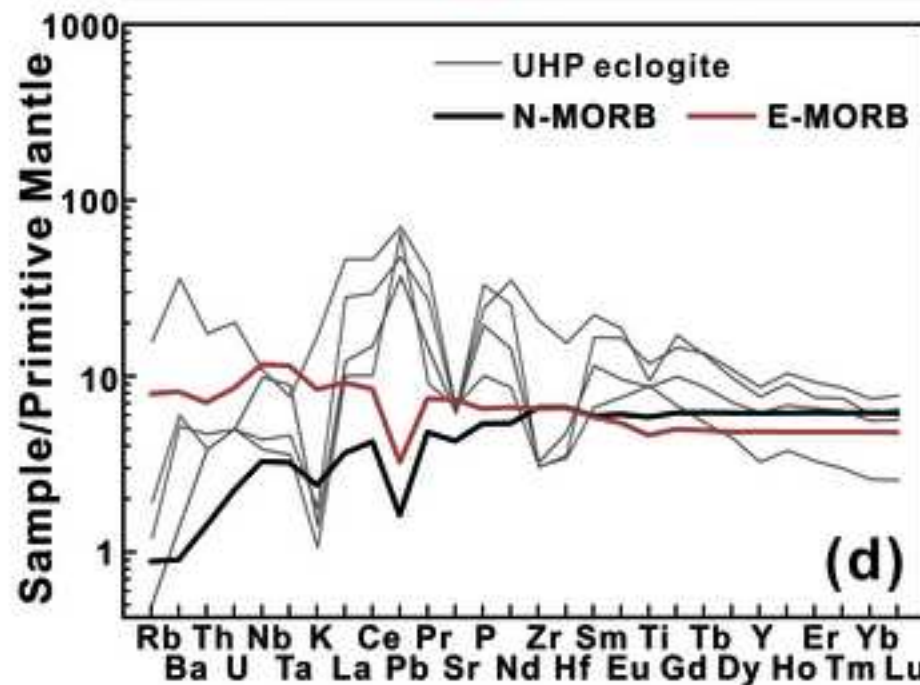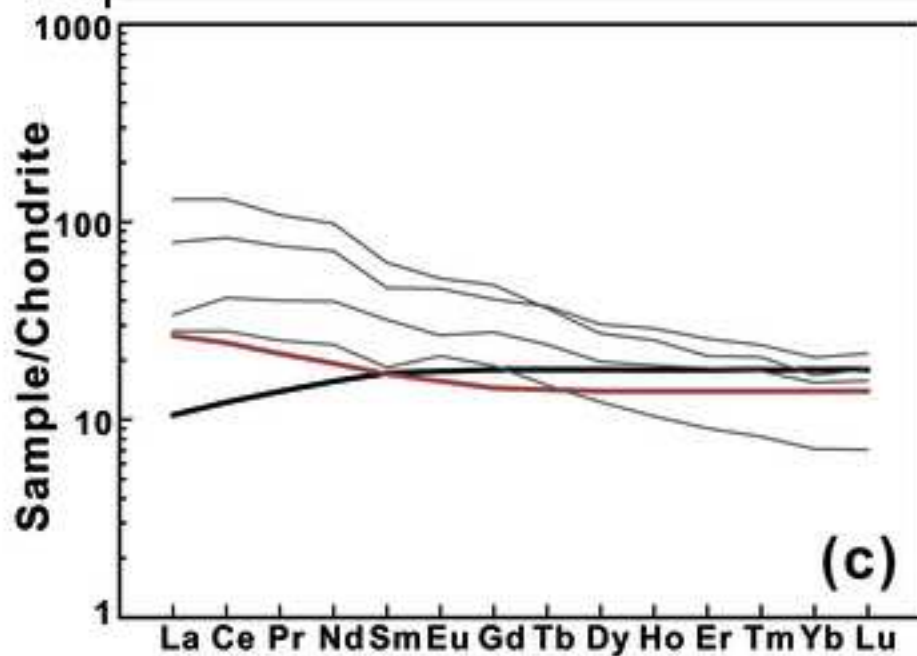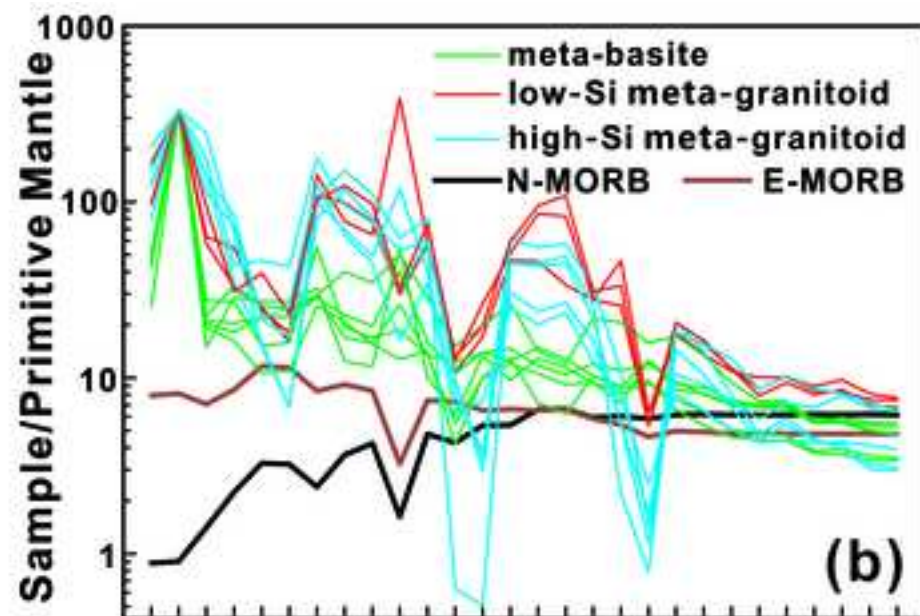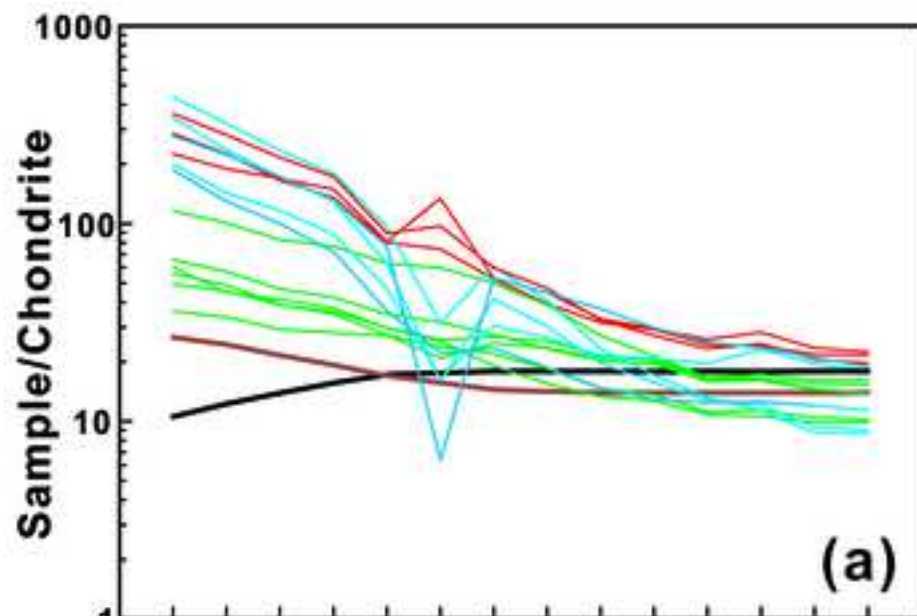
Figure 6
Click here to download high resolution image

11LJG3
768±5 Ma
784±5 Ma
746±2 Ma
50μm

11LJG7
742±3 Ma
766±3 Ma
50μm

11LJG2
756±19 Ma
767±14 Ma
788±6 Ma
50μm

1209LJG5
1922±5 Ma
834±10 Ma
50μm

1202LJG3
802±13 Ma
760±9 Ma
50μm

1303LJG2
811±7 Ma
786±7 Ma
50μm
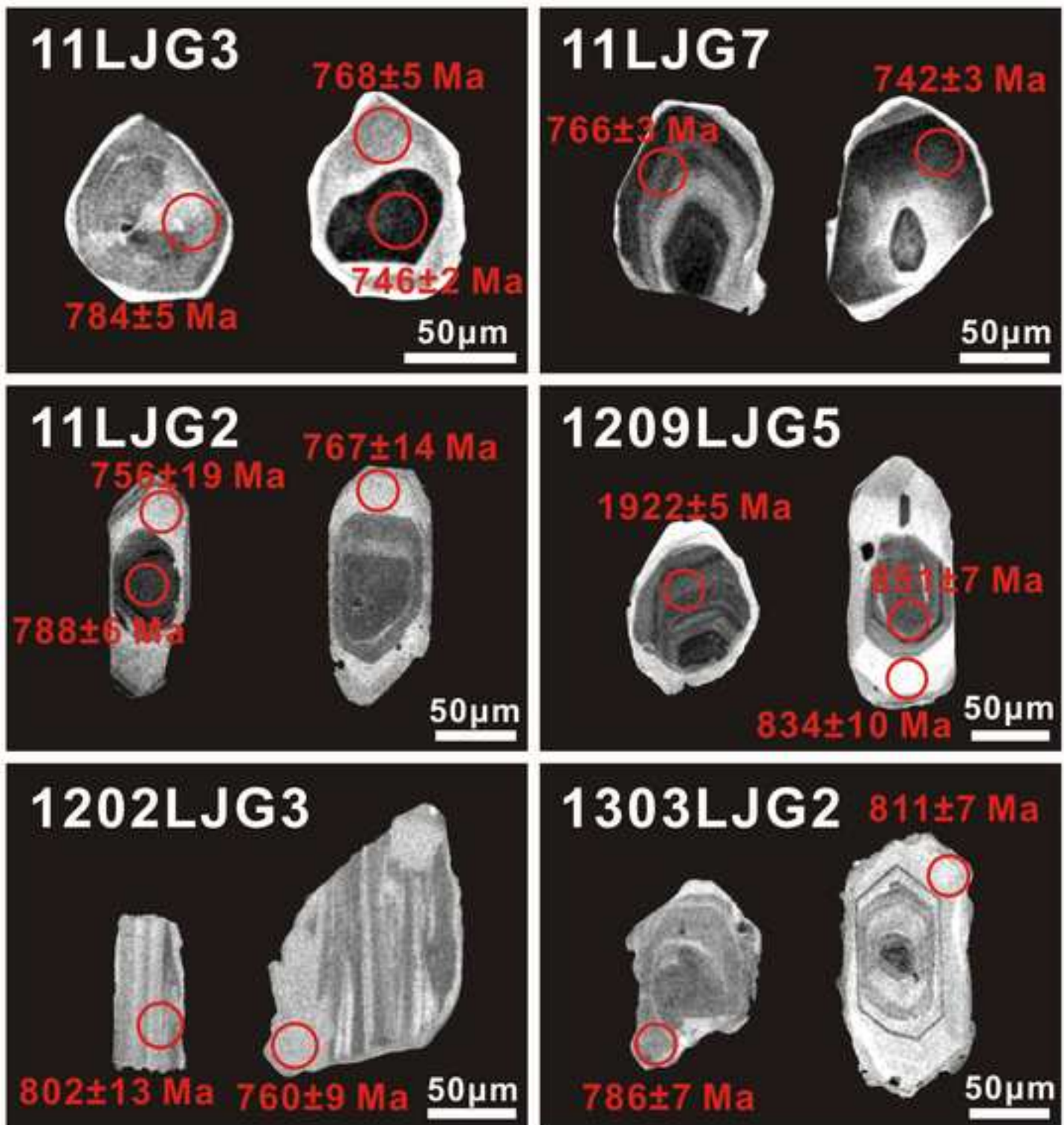
Figure 7
Click here to download high resolution image
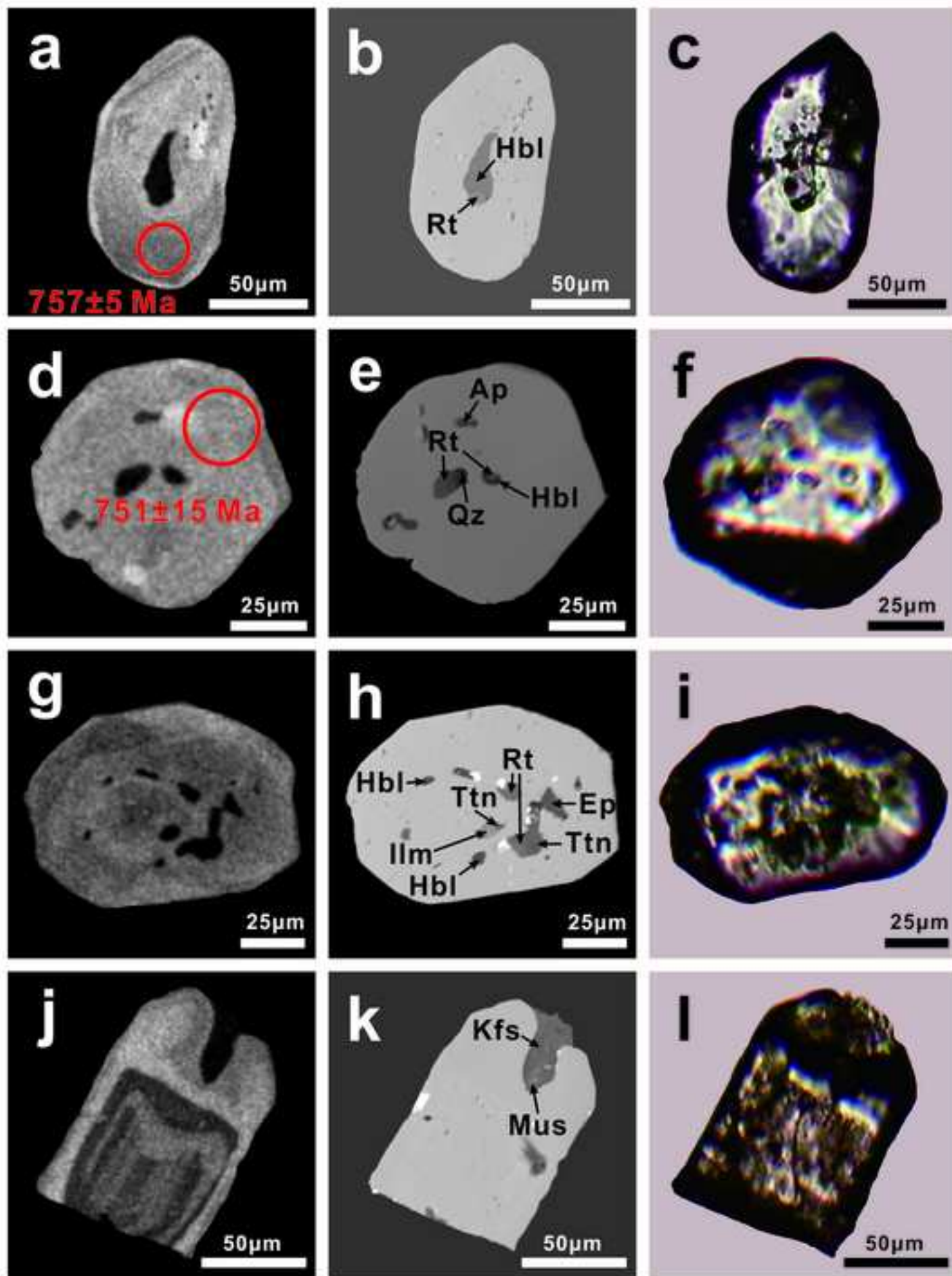
Figure 8
Click here to download high resolution image
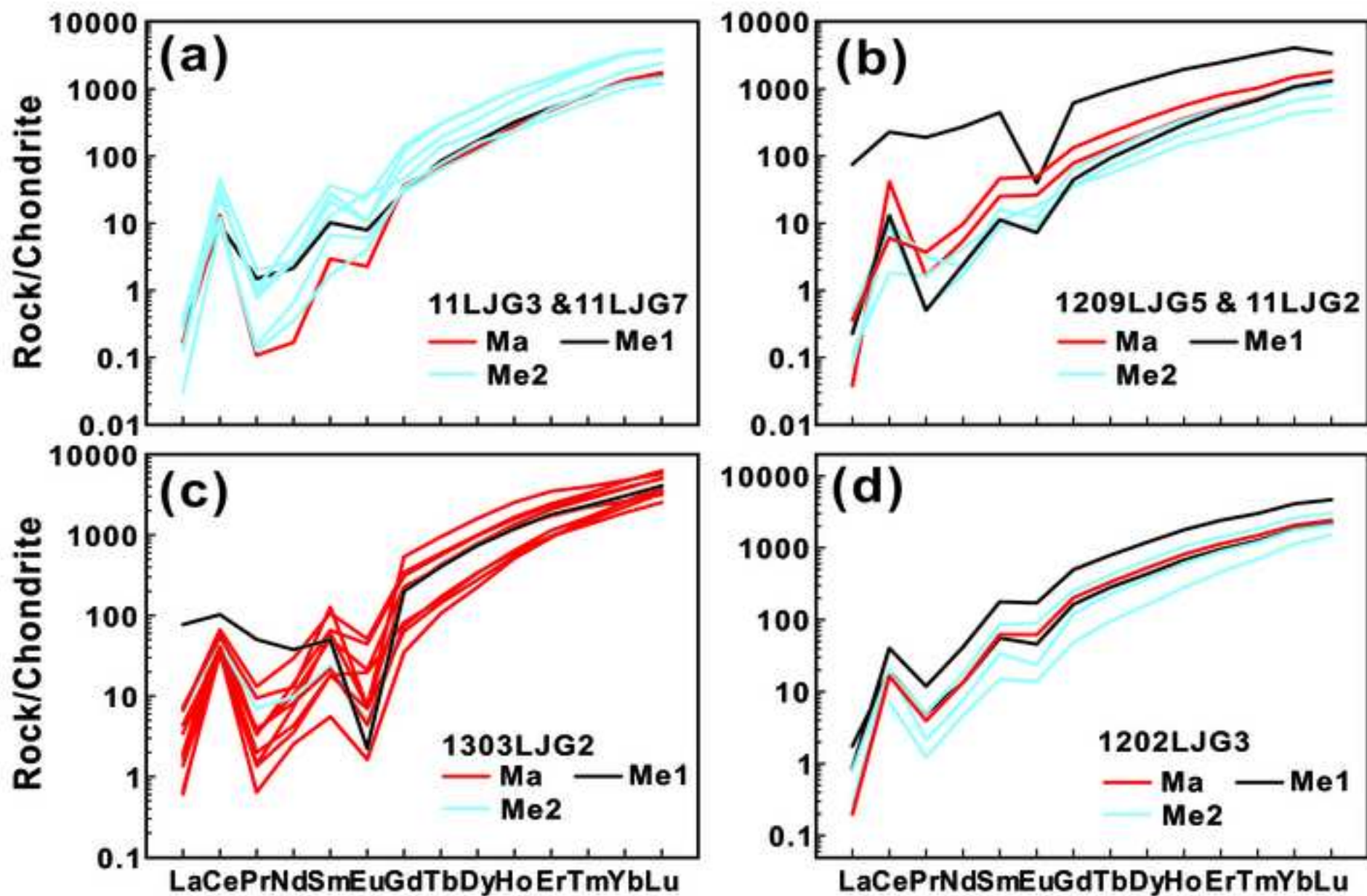
Figure 9
Click here to download high resolution image
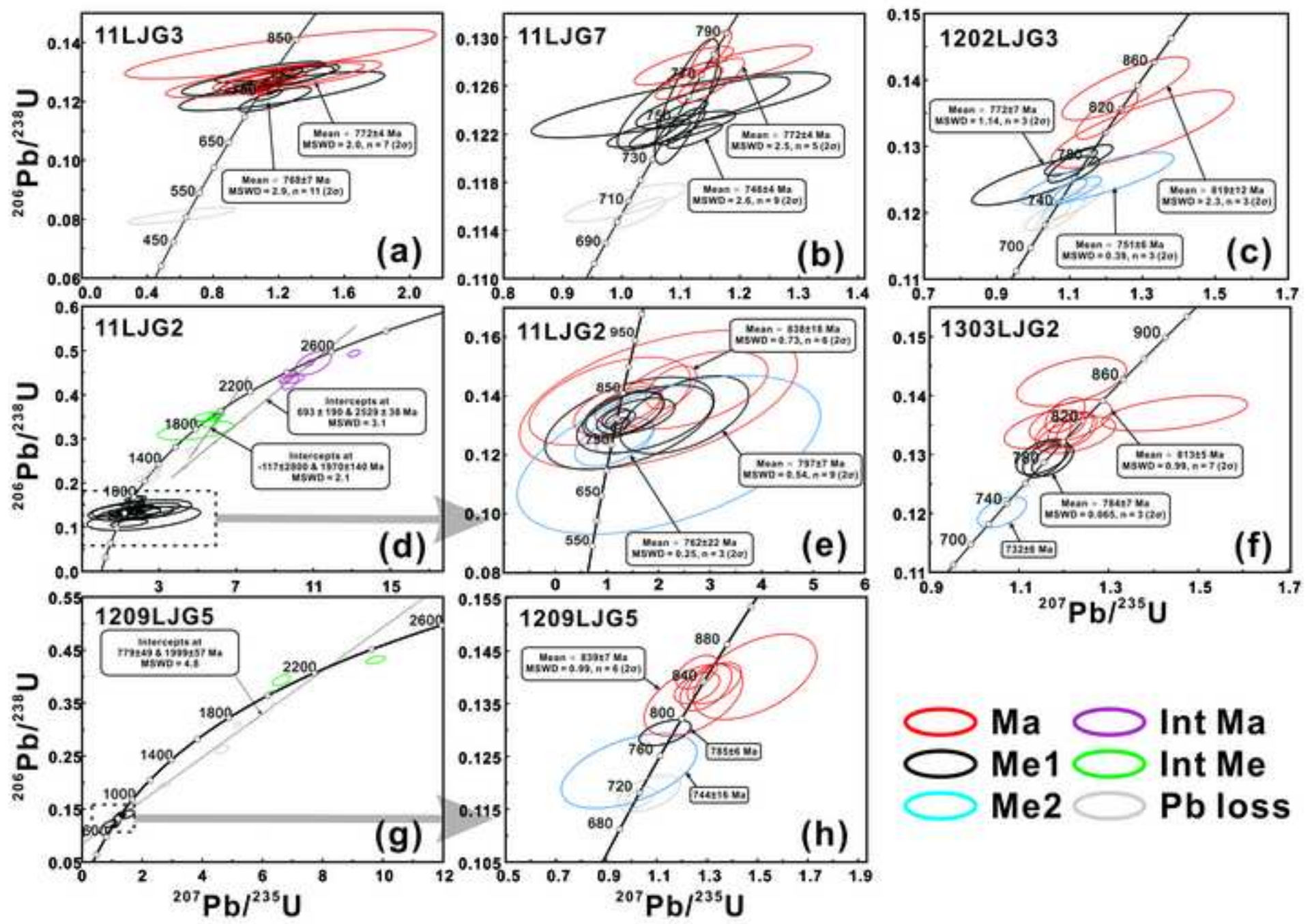
Figure 10
Click here to download high resolution image
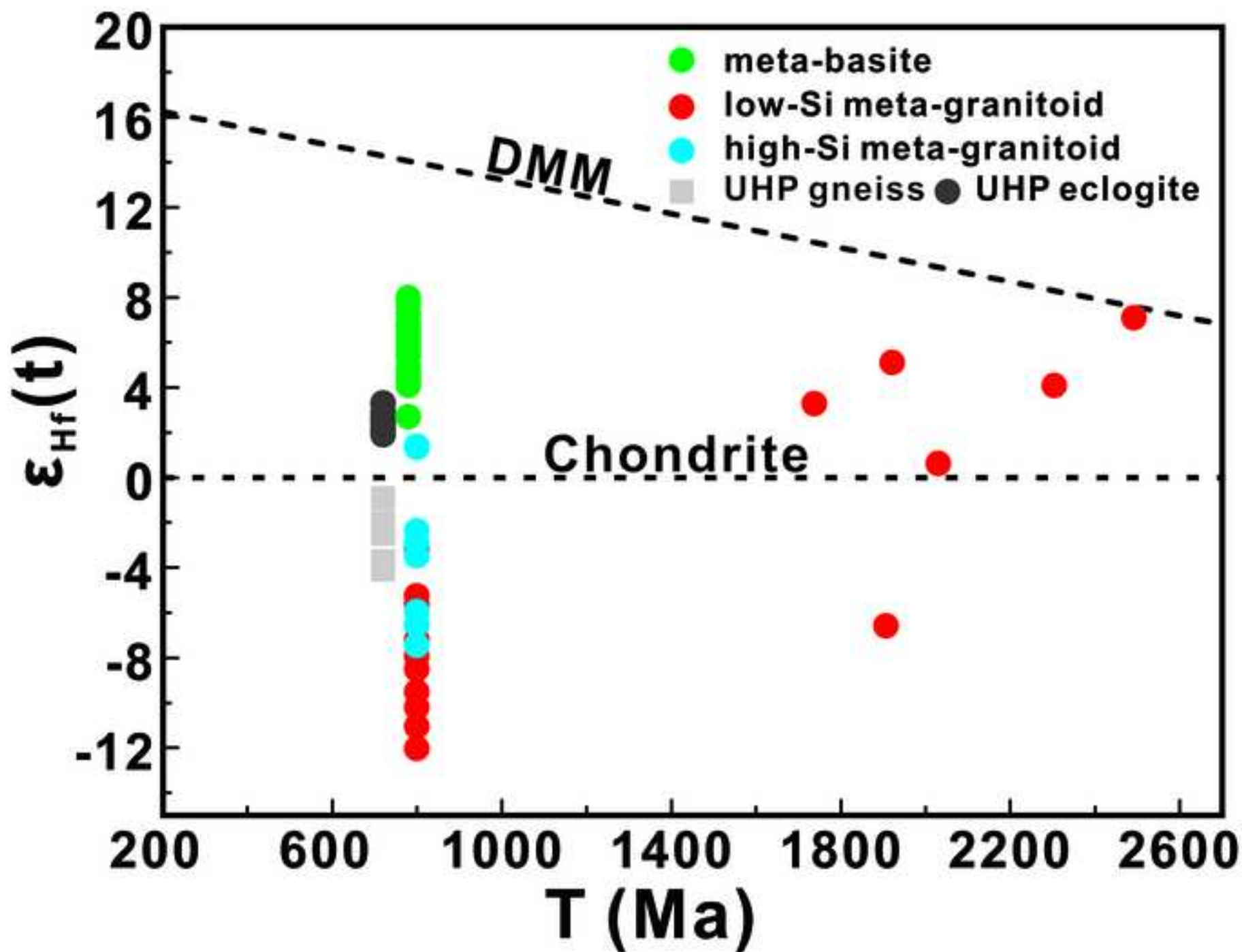
Figure 11
Click here to download high resolution image
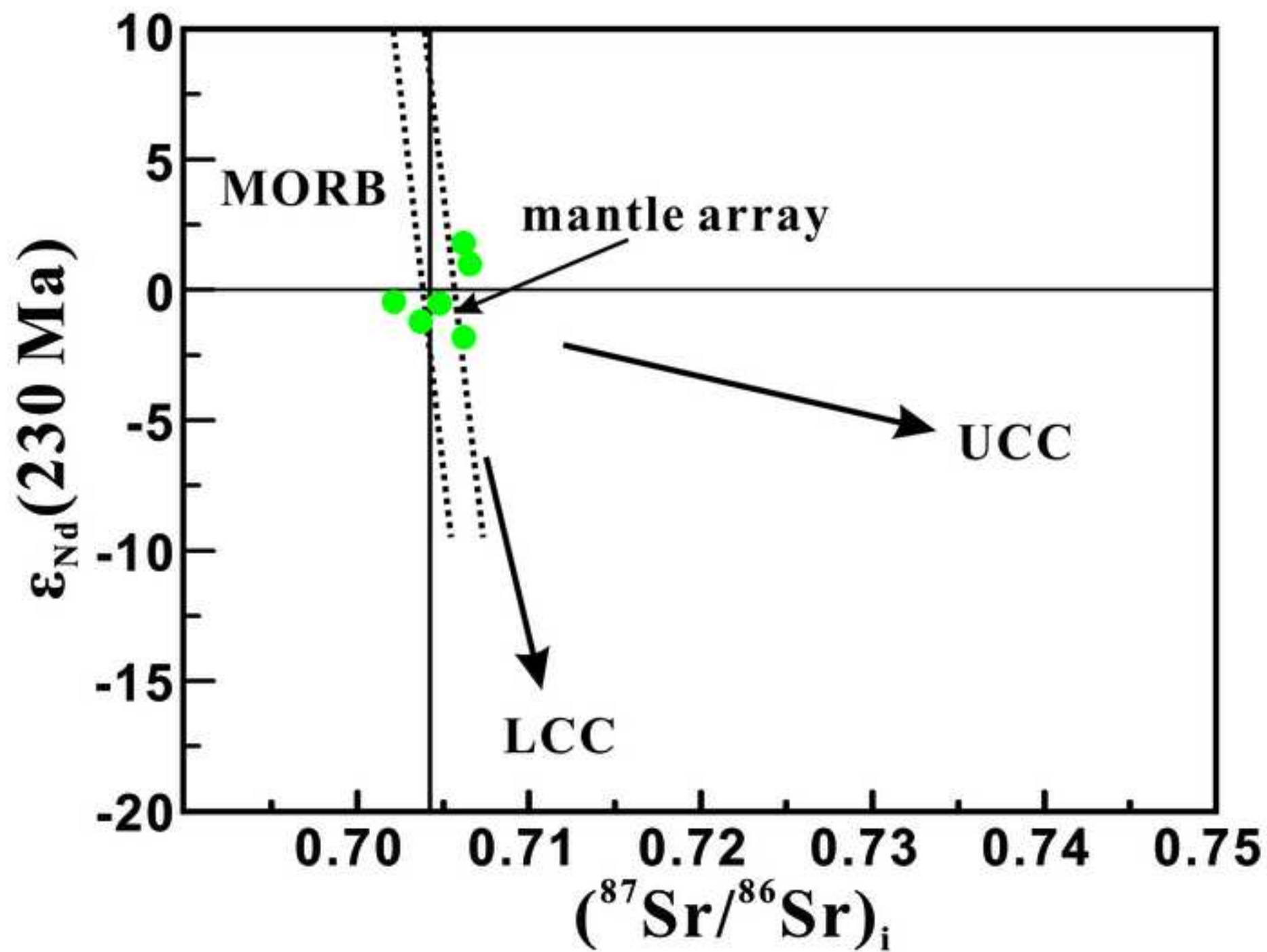
Figure 12
Click here to download high resolution image
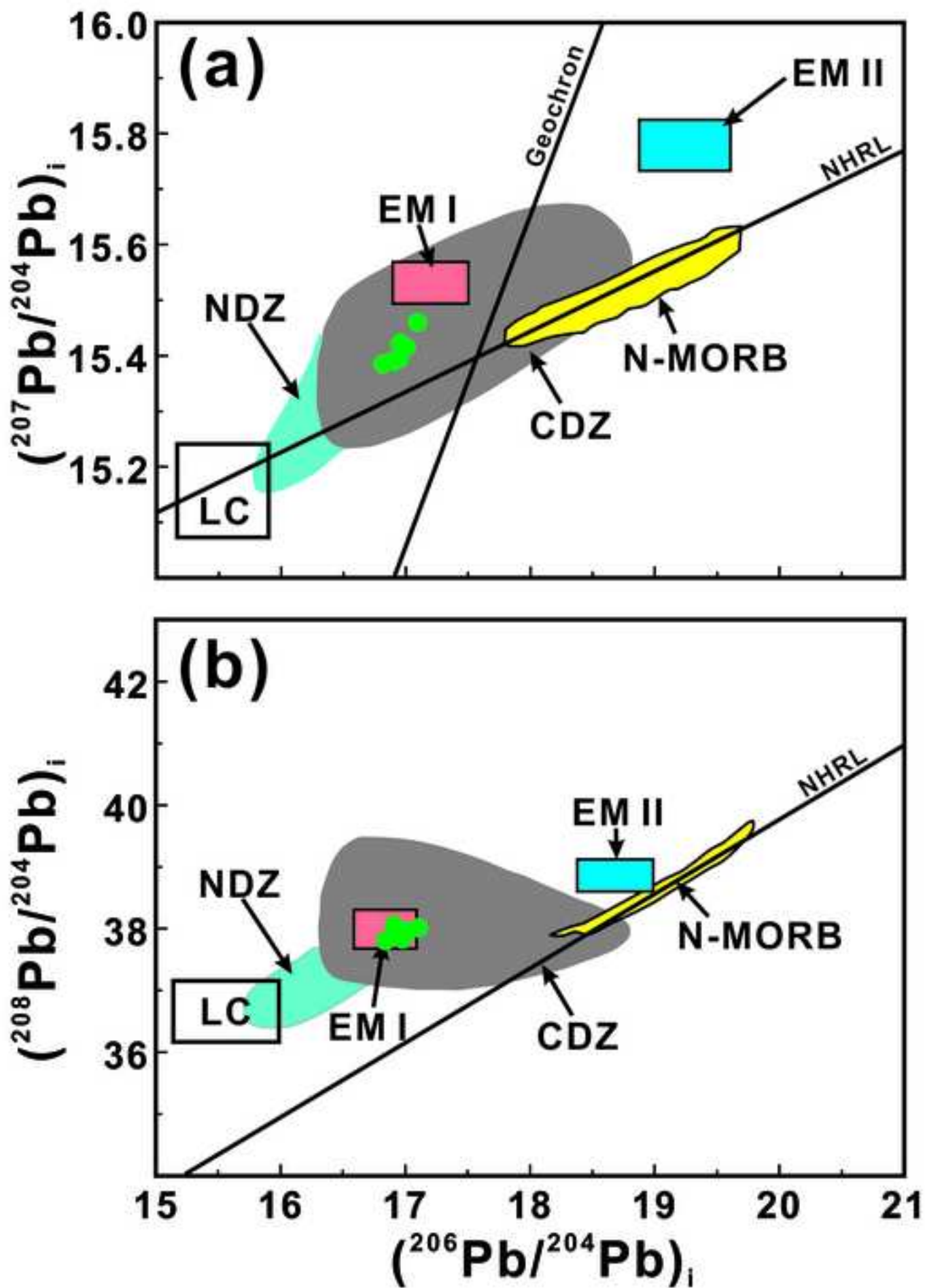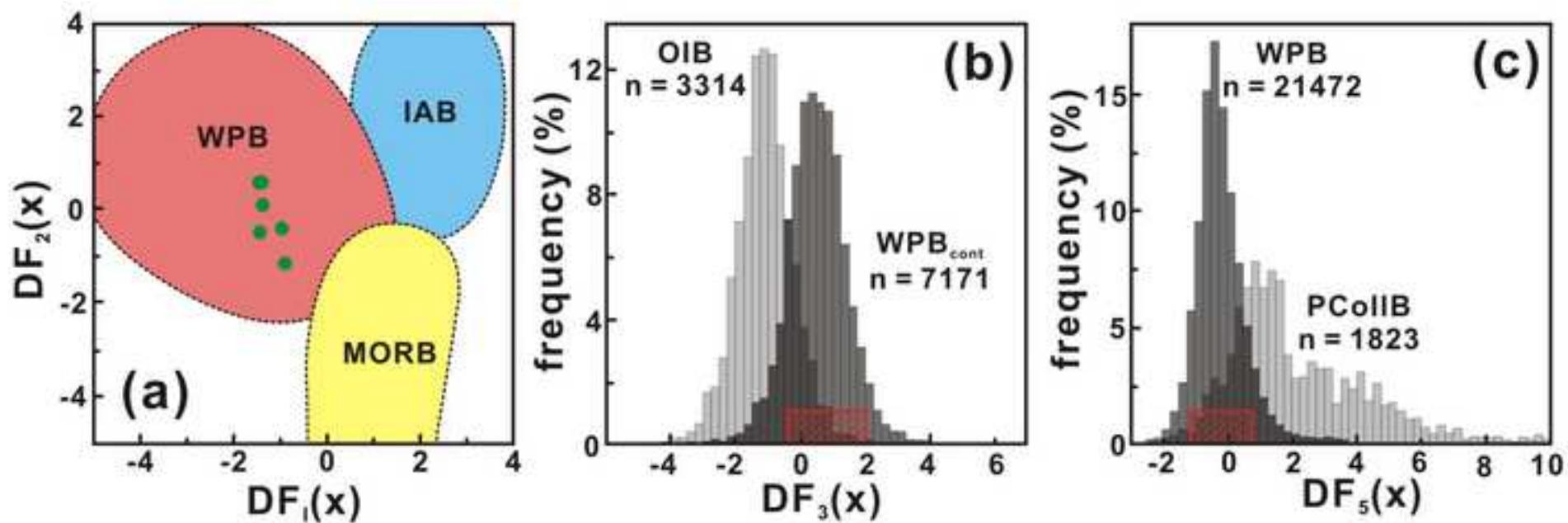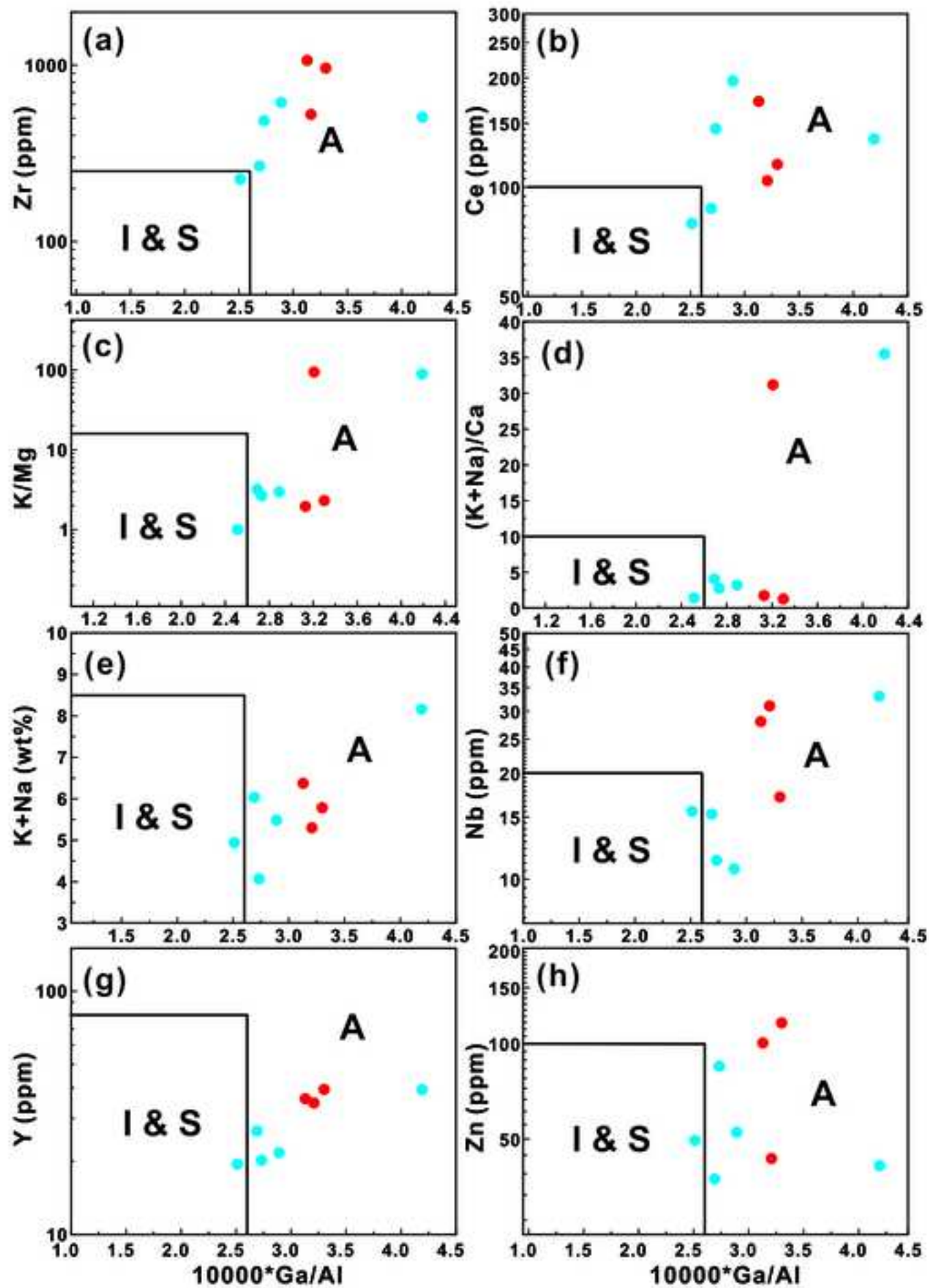
Figure 15
[Click here to download high resolution image](#)

Supplementary Table 1
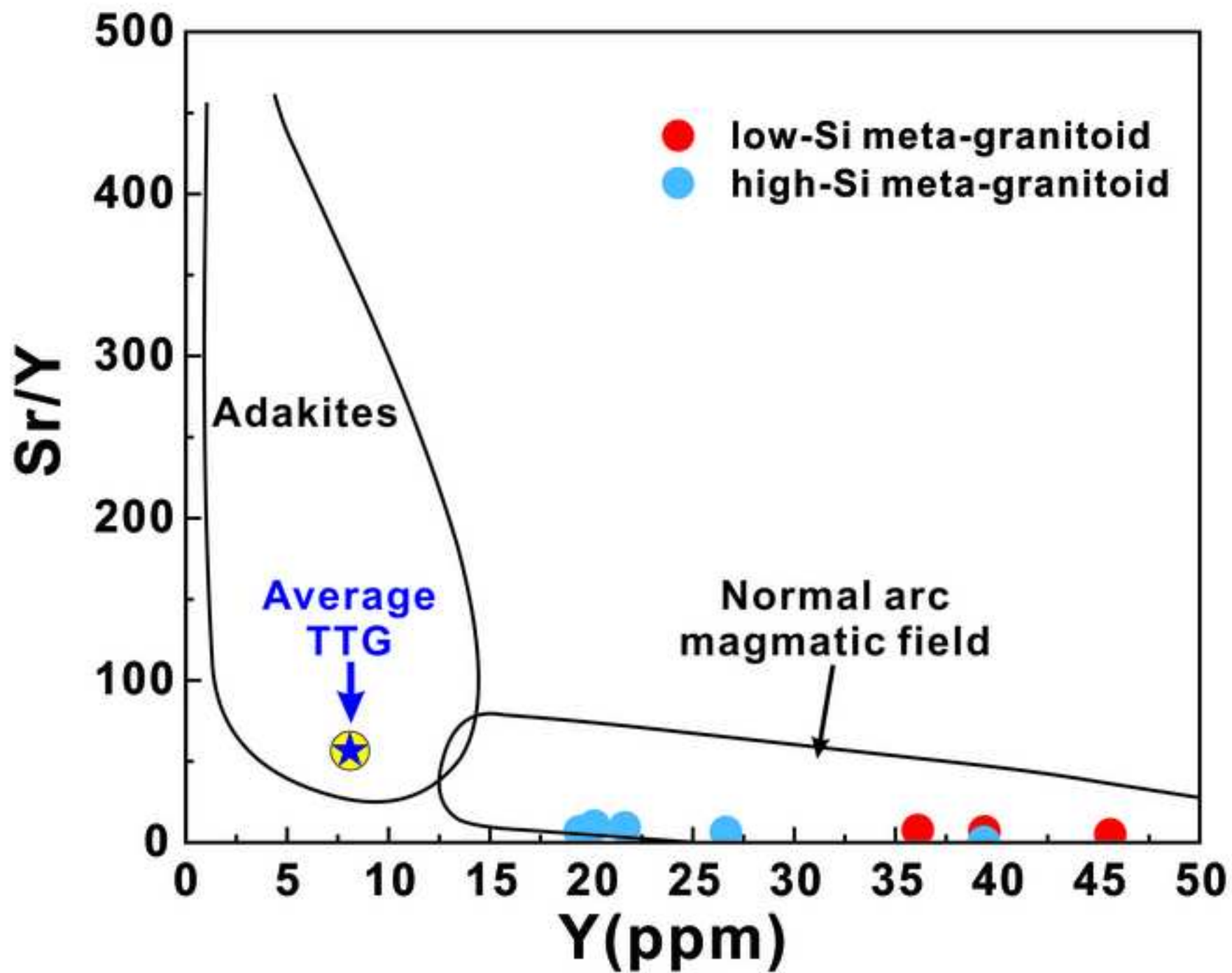
Supplementary Table 1. Electron microprobe analyses of representative minerals from the meta-basites and meta-granitoids in Longjingguan (wt%).

Sample	11LJG7						1209LJG1		1209LJG5			
Mineral	Pl(int)	Pl(ic)	Amp(int)	Amp(porp)	Ru	Ru	Kfs	Aln	Kfs	Pl	Amp	Bt
SiO_2	64.66	66.87	51.87	49.27	0.08	0.04	65.52	34.10	65.90	61.52	40.97	34.86
Al_2O_3	21.11	19.91	5.93	7.94	0.03	0.04	17.63	20.62	17.74	23.59	9.93	14.38
FeO	0.59	0.12	7.63	10.67	0.54	0.39	--	8.64	0.10	0.07	22.65	23.76
MgO	0.33	--	17.94	15.30	0.00	0.04	--	0.32	--	--	6.56	7.41
MnO	0.03	--	0.11	0.27	0.13	0.20	0.03	0.05	--	--	2.99	1.93
CaO	2.94	1.92	11.96	11.82	0.09	0.16	--	14.39	0.02	6.14	11.30	0.03
Na_2O	9.66	10.52	0.76	0.96	0.05	--	0.65	0.19	0.86	7.89	1.03	0.06
K_2O	0.05	0.10	0.21	0.23	--	--	15.75	0.06	15.15	0.14	1.28	9.64
TiO_2	0.02	--	0.13	0.35	97.93	98.10	--	--	0.03	--	0.89	4.12
Cr_2O_3	0.05	0.01	0.09	0.11	0.30	0.21	0.06	--	0.02	0.00	0.08	0.01
NiO	0.02	--	--	--	0.03	0.04	--	0.01	--	0.03	--	--
Cl	--	--	0.02	0.02	--	--	--	--	--	--	0.22	0.22
ZrO_2	--	--	--	--	0.04	0.10	--	--	--	--	--	--
Ce_2O_3	--	--	--	--	--	--	--	4.57	--	--	--	--
Total	99.47	99.44	96.64	96.94	99.31	99.21	99.63	82.94	99.81	99.37	97.84	96.36

int: intergrowth; ic: inclusion; porp: porphyroblast; --: not detected.

Supplementary Table 2

Supplementary Table 2. Major and trace elements compositions of the meta-basites and meta-granitoids from Longjingguan.

Lithology	Meta-basite						Low-Si meta-granitoid			High-Si meta-granitoid				
Sample	11LJG3	11LJG4	11LJG5	11LJG6	11LJG7	11LJG8	11LJG2	1209LJG5	1202LJG3	1209LJG1	1303LJG4	1209LJG3	1303LJG2	1209LJG4
Major elements (wt%)														
SiO_2	46.72	47.64	47.38	46.08	45.72	46.48	61.50	61.30	60.45	75.57	67.98	76.20	77.26	80.98
Al_2O_3	13.32	13.55	14.30	12.83	12.46	13.72	14.76	14.96	14.18	11.24	11.78	10.48	10.90	8.96
TiO_2	3.42	2.74	2.73	2.01	2.10	2.61	1.16	1.17	1.38	0.37	0.54	0.31	0.17	0.25
Fe_2O_3	4.86	3.87	5.94	3.91	3.47	7.56	3.06	3.60	1.60	1.15	0.84	1.32	1.83	0.46
FeO	8.24	8.50	7.07	8.12	8.86	8.19	5.03	4.78	6.85	1.56	3.54	1.84	1.08	1.68
CaO	10.85	9.14	9.35	8.14	8.34	10.50	3.52	3.63	4.53	1.49	3.50	1.71	0.23	1.47
MgO	6.43	7.73	5.92	11.41	13.29	4.37	1.93	1.60	1.86	0.95	3.82	1.08	0.06	0.92
K_2O	0.89	0.97	0.89	1.66	0.77	0.86	3.28	3.11	4.28	3.05	3.82	3.20	5.35	2.44
Na_2O	3.12	3.02	3.44	2.08	1.74	3.55	3.05	3.26	1.50	2.99	1.12	2.29	2.81	1.63
MnO	0.18	0.18	0.17	0.19	0.19	0.19	0.15	0.21	0.45	0.06	0.06	0.03	0.05	0.02
P_2O_5	0.43	0.29	0.30	0.22	0.22	0.30	0.37	0.43	0.57	0.08	0.16	0.08	0.01	0.06
H_2O	1.13	1.75	1.83	2.66	2.39	1.12	1.17	1.24	1.56	0.92	1.99	1.18	0.06	0.97
LOI	1.63	2.31	2.14	3.25	3.22	1.53	1.48	1.51	1.79	1.22	2.85	1.29	0.17	1.04
Total	100.08	99.95	99.62	99.89	100.38	99.86	99.30	99.56	99.45	99.72	100.01	99.81	99.92	99.89
Trace elements (ppm)														
Li	6.61	15.00	13.00	45.20	38.80	17.30	27.80	26.88	39.41	18.62	47.53	14.95	1.39	12.93
Be	1.39	1.48	1.00	1.97	0.52	2.21	1.63	1.62	1.67	2.01	1.88	0.75	2.37	0.95
Sc	30.40	37.00	28.30	26.20	23.10	27.90	18.80	28.04	40.21	6.14	9.75	4.51	1.20	3.63
V	326.00	352.00	289.00	213.00	155.00	279.00	86.80	61.20	65.20	52.80	68.10	43.60	9.30	24.20
Cr	172.00	142.00	126.00	292.00	282.00	113.00	31.30	20.00	13.90	29.20	42.70	19.10	2.10	20.90
Co	41.90	54.70	46.30	58.70	44.60	54.60	13.10	16.40	12.40	6.00	13.30	11.10	0.20	5.20
Ni	113.00	95.60	104.00	317.00	228.00	115.00	49.40	12.20	7.70	15.00	35.30	18.80	0.60	7.10
Cu	15.00	60.90	289.00	28.10	8.40	12.40	24.00	80.60	30.10	12.00	26.90	5.00	3.50	3.20
Zn	143.00	146.00	145.00	164.00	113.00	120.00	108.00	100.40	116.20	37.40	49.50	52.50	41.20	84.80
Ga	24.30	19.00	22.70	17.70	14.10	20.40	24.90	24.79	24.78	16.01	15.67	16.04	24.19	12.96
Rb	16.00	29.60	27.00	62.90	32.90	27.70	63.00	61.50	105.40	78.60	131.40	80.90	96.20	50.40
Sr	320.00	129.00	261.00	116.00	87.30	225.00	227.00	275.50	266.70	169.80	134.00	201.00	13.40	209.30
Y	33.50	32.20	31.80	21.80	20.20	30.80	45.60	36.10	39.39	26.64	19.43	21.65	39.36	20.15
Zr	159.00	144.00	166.00	118.00	80.50	131.00	518.00	1064.00	960.40	267.40	225.50	614.00	506.60	483.90
Nb	18.30	19.40	15.80	10.80	7.57	15.60	18.10	28.02	17.11	15.29	15.58	10.69	33.03	11.30
Cs	0.20	0.46	0.34	1.06	0.58	0.25	1.44	1.35	4.52	0.79	2.38	0.59	0.83	0.61
Ba	189.00	215.00	221.00	411.00	126.00	135.00	2324.00	2298.00	4001.00	945.70	979.50	802.80	78.30	503.30
La	27.50	8.55	11.70	13.30	14.30	15.60	67.70	85.09	53.34	47.47	44.30	103.60	65.94	80.87
Ce	61.60	20.60	27.90	29.90	27.50	35.00	138.00	172.30	115.60	87.41	79.41	196.30	135.80	144.80
Pr	7.88	2.78	3.68	3.72	3.93	4.43	15.70	20.52	16.11	11.08	9.49	22.39	16.42	16.40
Nd	35.90	13.10	16.80	16.30	17.50	19.80	63.20	80.66	69.52	41.33	33.80	83.58	61.52	60.76
Sm	9.64	4.15	4.54	4.17	4.53	5.32	12.30	13.67	12.44	7.17	5.55	14.73	11.68	9.65
Eu	3.47	1.21	1.50	1.38	1.47	1.84	4.31	5.62	7.78	0.95	1.29	1.82	0.37	0.93

Gd	10.30	5.10	5.49	4.50	3.93	5.64	10.80	12.26	10.87	6.27	4.80	12.44	10.91	8.55
Tb	1.45	0.88	0.95	0.69	0.58	0.87	1.47	1.76	1.68	0.99	0.70	1.53	1.67	1.13
Dy	6.91	5.32	5.50	3.74	3.39	5.13	8.02	8.25	8.37	5.46	3.75	5.91	9.44	4.99
Ho	1.21	1.16	1.14	0.77	0.72	1.10	1.65	1.54	1.67	1.18	0.73	0.97	1.68	0.89
Er	2.77	2.77	2.70	1.85	1.79	2.64	4.05	3.86	4.30	3.25	2.05	2.18	4.17	2.11
Tm	0.42	0.44	0.41	0.29	0.27	0.41	0.61	0.63	0.72	0.59	0.32	0.29	0.60	0.31
Yb	2.63	2.74	2.49	1.78	1.68	2.46	3.72	3.49	3.99	3.31	2.04	1.49	3.58	1.59
Lu	0.39	0.41	0.35	0.26	0.25	0.35	0.55	0.50	0.57	0.46	0.29	0.22	0.48	0.23
Hf	3.72	3.54	3.97	2.83	1.93	3.23	10.40	33.54	25.66	8.29	7.23	17.92	15.15	13.91
Ta	1.02	1.12	0.91	0.65	0.45	0.91	0.65	0.95	0.74	0.70	1.04	0.28	1.75	0.28
Pb	9.34	10.20	4.83	3.45	2.36	7.48	5.51	6.00	72.30	22.10	3.00	11.50	9.90	5.90
Th	1.91	1.27	1.73	2.34	1.65	1.80	4.95	7.98	5.39	9.59	11.73	20.91	14.98	11.95
U	0.70	0.60	0.38	0.57	0.34	0.43	0.69	0.65	1.15	1.53	1.76	1.40	0.91	0.73

wt%: weight percentage; ppm: part per million; --: not detected.

Supplementary Table 3. Electron microprobe analyses of typical mineral inclusions within zircon from the meta-basites and meta-granitoids from Longjingguan (wt%).

Sample	11LJG3								11LJG2					11LJG3		
Mineral	Ep	Ap	Hbl	Kfs	Bi	Ttn	Ilm	Pl	Ep	Bi	Kfs	Mus		Rt	Rt	Rt
SiO_2	40.86	0.15	44.01	63.57	57.18	30.55	0.20	63.52	37.62	34.03	60.31	46.31	SiO_2	0.11	0.16	0.15
TiO_2	0.68	0.00	0.82	0.00	0.68	36.88	49.40	0.03	0.23	3.17	0.00	0.16	Al_2O_3	0.01	0.02	0.02
Al_2O_3	24.72	0.00	9.07	17.71	24.22	0.98	0.00	22.98	15.66	14.15	23.63	30.51	MgO	0.00	0.00	0.00
FeO^T	8.39	0.00	18.10	0.00	2.27	0.52	44.40	0.07	22.90	25.14	0.54	7.05	TiO_2	99.53	99.69	99.83
MnO	0.05	0.00	0.21	0.02	0.00	0.02	1.79	0.00	0.51	0.48	0.08	0.09	FeO^T	0.34	0.48	0.35
MgO	1.07	0.00	10.31	0.01	2.25	0.00	0.65	0.00	3.76	8.55	0.05	0.89	Cr_2O_3	0.06	0.02	0.11
Na_2O	0.06	0.01	1.26	0.31	0.09	0.00	0.00	7.97	1.14	0.00	0.48	0.10	Nb_2O_5	0.14	0.09	0.07
CaO	17.25	54.03	11.66	0.07	0.15	27.90	0.00	4.23	11.15	0.52	0.01	0.01	V_2O_3	0.54	0.56	0.51
K_2O	2.48	0.01	0.96	17.42	8.77	0.00	0.00	0.25	2.38	6.97	15.65	10.66	MnO	0.01	0.01	0.01
P_2O_5	0.02	40.59	0.00	0.02	0.14	0.01	0.01	0.00	0.00	0.00	0.00	0.00	ZrO_2	0.30	0.29	0.35
Cr_2O_3	0.01	0.02	0.10	0.00	0.00	0.06	0.09	0.00	0.04	0.02	0.00	0.01	F	--	--	--
NiO	0.00	0.00	0.01	0.01	0.02	0.02	0.06	0.00	0.00	0.02	0.01	0.00	Cl	--	--	--
F	0.07	4.18	0.06	--	--	--	--	--	--	--	--	--	Total	101.04	101.32	101.40
Cl	0.00	0.25	0.15	--	--	--	--	--	--	--	--	--	Zr(ppm)	2197	2107	2519
Total	95.62	97.42	96.65	99.14	95.76	96.94	96.60	99.05	95.38	93.05	100.75	95.79	T(°C)	843	839	860

The temperatures of sample 11LJG3 were estimated according to the Zr-in-rutile thermometer (Tomkins et al., 2007; P=10 kbar). --: not detected.

Supplementary Table 4. Electron microprobe analytical results of the rutile inclusions in zircon from the sample 11LJG3

Spot No.	1	2	3	4	5	6	7
SiO_2	0.18	0.29	1.80	0.75	0.11	0.16	0.15
Al_2O_3	0.03	0.02	0.28	0.01	0.01	0.02	0.02
MgO	0.01	0.00	0.02	0.00	0.00	0.00	0.00
TiO_2	86.96	84.77	95.46	99.47	99.53	99.69	99.83
FeO	0.19	0.31	0.35	0.36	0.34	0.48	0.35
Cr_2O_3	0.11	0.04	0.05	0.07	0.06	0.02	0.11
Nb_2O_5	0.06	0.14	0.06	0.15	0.14	0.09	0.07
V_2O_3	0.56	0.57	0.48	0.55	0.54	0.56	0.51
MnO	0.00	0.00	0.00	0.00	0.01	0.01	0.01
ZrO_2	0.26	0.66	0.57	0.73	0.30	0.29	0.35
Total	88.39	86.80	99.08	102.09	101.04	101.32	101.40
Zr(ppm)	2196	5595	4235	5307	2197	2107	2519
T(°C)	843	966	926	958	843	839	860

Supplementary Table 5. LA-ICPMS trace element analysis for zircons in the meta-basites and meta-granitoids from Longjingguan (ppm).

Spot No.	11LJG2_5.1	11LJG2_16.1	11LJG2_2.1	11LJG2_20.1	11LJG2_41.1	11LJG3_5.2	11LJG3_12.1	11LJG3_12.2	1209LJG5_9.1	1209LJG5_4.1	1202LJG3_4.1
Age(Ma)	2385	1938	845	797	730	771	768	746	845	785	750.4
Nb	2.87	3.57	1.6	1.43	1.67	3.07	1.05	2.11	0.53	2.71	0.96
La	1.57	0.04	0.01	0.00	0.03	0.00	0.00	0.03	0.09	0.05	0.19
Ce	17.26	12.02	25.39	3.25	1.11	16.30	9.15	18.82	3.70	7.88	12.33
Pr	0.99	0.08	0.15	0.07	0.16	0.00	0.08	0.07	0.35	0.05	0.20
Nd	6.59	0.77	2.54	0.65	1.99	0.35	0.00	1.29	4.54	1.13	3.54
Sm	3.57	1.26	3.86	1.23	1.64	0.44	0.45	1.98	7.04	1.72	5.17
Eu	0.73	0.11	1.52	0.75	1.05	0.64	0.05	1.67	2.87	0.42	1.37
Gd	11.49	12.25	16.06	7.98	7.34	12.88	4.70	9.17	27.31	9.12	24.75
Tb	3.63	4.25	4.98	2.85	2.06	5.67	2.36	5.10	8.40	3.49	8.57
Dy	42.67	51.37	55.84	32.45	23.00	64.94	23.88	56.85	92.57	42.06	93.47
Ho	15.94	18.12	20.47	12.99	8.53	27.62	11.10	23.59	31.97	16.69	34.53
Er	71.57	75.47	85.50	52.47	33.25	130.13	49.13	122.95	133.76	79.02	146.95
Tm	17.38	16.30	18.21	11.96	7.31	32.18	12.89	28.91	26.26	17.37	30.25
Yb	169.57	142.90	180.62	116.04	74.14	340.23	135.43	311.40	254.93	183.06	299.98
Lu	25.21	21.77	34.26	18.28	12.41	54.98	23.71	62.04	45.84	33.54	52.71
Hf	8290	8531	7250	5229	4281	8091	7839	8882	6063	8163	7269
Ta	0.88	1.16	0.27	0.20	0.09	0.70	0.41	0.73	0.22	0.96	0.54
Th	105.63	62.35	71.78	15.49	4.99	450.74	192.76	698.54	28.37	57.38	111.16
U	256.61	94.95	42.44	22.84	8.33	507.06	295.99	927.89	31.14	120.39	290.04
ΣREE	388.17	356.71	449.41	260.97	174.02	686.36	272.93	643.87	639.63	395.6	714.01

Supplementary Table 6. LA-ICPMS rare earth element analysis for zircons in the meta-basites and meta-granitoids from Longjingguan.

Spot No.	Age(Ma)	La	Ce	Pr	Nd	Sm	Eu	Gd	Tb	Dy	Ho	Er	Tm	Yb	Lu
11LJG2															
1.1	2492	0.00	4.77	0.04	1.29	3.26	1.19	14.34	5.38	61.10	22.22	91.62	21.86	207.84	35.66
2.1	8834	0.01	25.39	0.15	2.54	3.86	1.52	16.06	4.98	55.84	20.47	85.50	18.21	180.62	34.26
4.1	2304	0.06	7.30	0.00	0.10	0.83	0.45	3.75	1.32	17.59	6.55	31.57	8.88	99.09	16.57
5.1	2385	1.57	17.26	0.99	6.59	3.57	0.73	11.49	3.63	42.67	15.94	71.57	17.38	169.57	25.21
6.1	1786	0.00	2.48	0.05	1.08	2.13	1.16	12.87	3.74	42.35	14.39	55.60	11.92	107.63	16.10
7.1	1237	0.00	8.09	0.07	1.97	4.20	1.46	19.55	7.31	84.47	30.87	123.43	26.36	239.12	37.55
9.1	798	17.82	139.16	17.98	127.83	68.17	2.30	127.06	35.71	348.52	110.48	408.51	81.89	696.48	85.67
10.1	1325	0.01	34.35	0.08	1.75	5.93	0.80	36.79	15.99	215.02	82.14	337.69	71.47	612.21	76.61
11.1	1366	0.03	8.00	0.19	6.42	8.55	3.64	25.86	10.13	107.59	32.20	129.81	28.88	235.54	39.16
12.1	2492	3.79	26.83	2.76	16.93	9.70	2.22	28.90	9.63	91.03	30.40	126.42	27.96	269.74	35.52
13.1	810	0.00	32.70	0.20	4.27	6.42	1.33	38.66	14.40	174.13	63.68	253.10	54.57	489.55	69.90
15.1	2327	1.36	43.20	1.57	16.92	17.56	4.83	45.07	12.42	110.37	31.55	110.28	20.84	186.31	26.49
16.1	1938	0.04	12.02	0.08	0.77	1.26	0.11	12.25	4.25	51.37	18.12	75.47	16.30	142.90	21.77
18.1	837	0.00	3.32	0.22	2.84	5.07	3.35	20.59	7.74	74.48	27.76	109.03	21.62	214.26	39.59
19.1	1907	0.04	38.80	0.04	1.26	1.38	0.70	9.29	3.46	46.62	19.78	104.10	26.88	301.12	55.16
20.1	792	0.00	3.25	0.07	0.65	1.23	0.75	7.98	2.85	32.45	12.99	52.47	11.96	116.04	18.28
24.1	1936	0.04	27.21	0.10	2.04	4.32	0.52	13.83	5.09	53.37	17.44	68.95	14.38	136.53	18.00
24.2	1566	0.04	16.17	0.09	0.70	2.02	0.19	7.00	2.95	37.69	14.55	58.57	14.43	138.73	20.76
26.1	1325	0.03	29.14	0.09	2.39	4.59	0.11	26.17	9.88	123.99	46.50	194.82	42.32	394.55	58.12
27.1	1952	0.00	23.92	0.01	0.56	2.68	0.11	11.75	4.36	49.63	17.52	72.21	16.11	149.99	22.53
28.1	808	0.00	2.74	0.00	0.03	1.67	1.36	7.99	2.36	32.56	11.09	48.25	11.57	106.90	17.17
29.1	1645	0.10	4.66	0.07	0.30	0.25	0.11	3.37	1.58	21.89	9.63	47.03	13.14	145.33	26.07

32.1	826	0.00	5.62	0.06	0.90	1.71	0.33	7.24	3.35	34.93	13.83	63.25	14.07	125.54	23.69
32.2	803	0.00	7.01	0.01	0.68	2.50	0.77	17.98	6.89	83.06	30.97	121.93	26.03	225.50	35.89
40.1	2332	0.02	9.50	0.00	0.25	0.95	0.20	8.36	3.50	45.85	17.52	77.66	18.85	190.92	31.05
41.1	730	0.03	1.11	0.16	1.99	1.64	1.05	7.34	2.06	23.00	8.53	33.25	7.31	74.14	12.41
11LJG3															
1.1	778	0.09	6.75	0.00	0.13	0.39	0.09	5.76	2.23	26.12	11.81	53.73	12.38	128.72	25.52
5.1	783	0.00	7.24	0.00	0.00	0.47	0.17	4.95	1.94	28.85	11.71	61.68	16.48	173.34	37.48
5.2	771	0.00	16.30	0.00	0.35	0.44	0.64	12.88	5.67	64.94	27.62	130.13	32.18	340.23	54.98
6.1	774	0.00	12.89	0.00	0.00	2.07	0.42	8.46	2.28	42.05	18.31	104.26	27.15	290.78	63.06
6.2	774	0.00	8.25	0.01	0.94	0.68	0.14	5.31	2.27	26.47	9.62	45.12	13.16	128.84	22.32
7.1	773	0.00	1.56	0.00	0.06	0.26	0.09	1.71	0.48	6.97	4.05	22.04	6.64	83.20	18.05
9.1	750	0.00	17.17	0.00	1.07	2.20	0.80	10.06	4.49	58.61	24.55	123.36	31.65	330.57	59.19
10.1	503	0.03	9.68	0.00	0.22	1.97	0.55	7.21	2.27	35.05	15.95	69.58	19.06	192.64	33.52
12.1	768	0.00	9.15	0.08	0.00	0.45	0.05	4.70	2.36	23.88	11.10	49.13	12.89	135.43	23.71
12.2	746	0.03	18.82	0.07	1.29	1.98	1.67	9.17	5.10	56.85	23.59	122.95	28.91	311.40	62.04
13.1	774	0.18	4.37	0.00	0.00	0.65	0.17	3.73	1.77	16.36	8.12	35.97	8.75	107.37	18.92
14.1	766	0.00	8.35	0.11	0.00	0.43	0.57	5.21	2.40	33.42	16.68	79.62	20.03	224.73	41.44
17.1	823	0.00	10.08	0.00	0.69	2.21	0.84	8.30	3.23	43.68	17.57	80.05	21.07	216.18	36.32
24.1	774	0.00	7.26	0.00	0.00	0.68	0.05	3.01	1.25	22.54	9.40	42.24	11.05	116.73	21.41
11LJG7															
1.1	766	0.07	5.80	0.14	1.01	1.56	0.46	6.06	3.14	42.21	18.13	85.89	20.83	226.74	41.82
2.1	744	0.00	18.08	0.08	0.65	2.72	0.31	18.65	8.29	110.24	47.37	223.05	55.88	556.22	99.67
3.1	752	0.09	17.50	0.09	1.38	3.14	0.62	14.73	7.14	88.88	38.84	197.39	51.55	543.82	98.95
4.1	704	0.01	5.52	0.01	0.30	1.02	0.35	6.06	2.38	30.75	13.39	64.17	16.14	170.65	31.05
10.1	741	0.07	27.27	0.19	1.24	4.33	0.62	24.74	11.20	134.53	54.68	246.96	59.07	580.02	100.26
14.1	757	0.05	5.56	0.00	0.00	0.86	0.09	4.87	1.95	23.86	10.25	54.89	15.76	161.20	33.50

17.1	775	0.04	7.96	0.01	0.08	0.45	0.13	7.38	2.74	33.70	15.64	79.95	21.26	229.73	44.38
17.2	755	0.08	7.31	0.01	0.16	0.26	0.24	7.08	2.90	39.92	13.64	83.23	21.58	209.66	37.95
19.1	756	0.00	6.34	0.03	0.71	1.26	0.38	7.44	3.17	40.87	17.32	84.00	21.69	236.26	42.71
22.1	757	0.03	15.21	0.10	2.85	5.60	1.38	29.29	11.65	140.15	55.44	233.64	52.79	541.69	93.06
1209LJG5															
1.1	744	8.10	23.02	2.39	12.01	3.93	1.27	9.88	3.09	36.24	13.75	59.59	12.58	121.59	20.54
2.1	715	0.02	6.28	0.30	1.04	2.44	0.71	12.93	4.45	54.34	19.59	83.56	17.26	167.74	29.24
3.1	719	0.12	5.35	0.05	0.80	1.36	0.54	7.43	2.67	32.29	12.23	53.00	11.26	112.92	20.13
4.1	785	0.05	7.88	0.05	1.13	1.72	0.42	9.12	3.49	42.06	16.69	79.02	17.37	183.06	33.54
9.1	845	0.09	3.70	0.35	4.54	7.04	2.87	27.31	8.40	92.57	31.97	133.76	26.26	254.93	45.84
1202LJG3															
1.1	771	0.42	11.72	0.48	6.17	8.51	2.66	33.64	10.54	110.08	38.27	157.74	32.12	308.48	55.58
2.1	740	0.07	11.30	0.49	8.34	13.02	5.23	51.75	15.87	169.64	58.73	233.48	46.98	443.22	77.08
3.1	731	<0.01	4.44	0.12	2.18	2.28	0.81	9.90	3.58	40.93	15.88	76.43	17.86	191.16	38.75
4.1	750	0.19	12.33	0.20	3.54	5.17	1.37	24.75	8.57	93.47	34.53	146.95	30.25	299.98	52.71
9.1	760	0.20	24.51	1.13	19.45	27.05	9.90	102.12	29.57	304.04	100.81	397.44	76.58	695.61	118.29
11.1	837	0.05	10.07	0.38	6.28	9.53	3.59	41.40	12.45	133.20	45.85	187.42	37.81	350.54	61.25

Note: Ages are collected from Supplementary Table 7.

Supplementary Table 7. SHRIMP zircon U-Pb isotope data for the meta-basites and meta-granitoids from Longjingguan.

Spot	Domain	Element (ppm)			Th/U	Isotopic ratio								Age (Ma)					
		U	Th	Pb		$^{207}Pb/^{206}Pb$	1σ	$^{207}Pb/^{235}U$	1σ	$^{206}Pb/^{238}U$	1σ	$^{206}Pb/^{238}U$	1σ	$^{207}Pb/^{206}Pb$	1σ	$^{208}Pb/^{232}Th$	1σ
11LJG2																	
1.1	C	25.3	8.2	10.3	0.33	0.1689	0.0046	10.9900	0.3847	0.4720	0.0109	2492	47	2547	45	2727	270
2.1	C	24.6	12.2	3.2	0.51	0.0560	0.0336	1.0600	0.6360	0.1382	0.0061	834	35	450	1300	675	430
3.1	M	86.8	34.7	10.8	0.41	0.1140	0.0100	2.2500	0.2025	0.1429	0.0030	861	17	1869	160	1733	170
4.1	C	351.9	177.9	130.0	0.52	0.1652	0.0014	9.7800	0.1858	0.4295	0.0073	2304	33	2510	14	2235	58
5.1	C	673.5	301.9	259.0	0.46	0.1602	0.0010	9.8880	0.0811	0.4478	0.0025	2385	11	2457	10	2334	39
6.1	M	46.5	37.2	13.3	0.83	0.1110	0.0178	4.9000	0.8330	0.3193	0.0089	1786	43	1820	300	1798	350
7.1	C	155.0	113.8	28.8	0.76	0.0811	0.0089	2.3700	0.2607	0.2115	0.0032	1237	17	1224	220	1225	130
9.1	C	343.0	210.0	39.3	0.63	0.0695	0.0067	1.2600	0.1222	0.1318	0.0013	798	7	914	200	807	68
10.1	C	472.1	184.3	92.5	0.40	0.0950	0.0013	2.9880	0.0478	0.2282	0.0015	1325	8	1528	27	1446	19
11.1	M	734.9	292.5	149.0	0.41	0.1320	0.0021	4.2960	0.0730	0.2359	0.0013	1366	7	2125	28	994	30
12.1	C	447.2	155.2	182.0	0.36	0.1661	0.0010	10.8080	0.0908	0.4719	0.0029	2492	13	2519	9	2481	42
13.1	C	139.4	111.8	16.4	0.83	0.0730	0.0168	1.3500	0.3105	0.1339	0.0029	810	17	1023	460	774	130
14.1	M	227.7	73.2	30.3	0.33	0.0948	0.0045	2.0020	0.0961	0.1532	0.0017	919	9	1524	88	1192	100
15.1	C	331.3	411.3	124.0	1.28	0.1596	0.0021	9.5600	0.1434	0.4346	0.0032	2327	14	2451	22	2223	41
16.1	C	204.6	145.2	62.9	0.73	0.1131	0.0054	5.4700	0.2680	0.3508	0.0039	1938	18	1849	87	1752	120
17.1	M	122.1	94.4	13.9	0.80	0.0770	0.0131	1.3500	0.2295	0.1263	0.0025	767	14	1128	330	934	100
18.1	M	30.1	24.3	4.1	0.83	0.1040	0.0582	2.0000	1.1200	0.1387	0.0096	837	54	1700	1000	--	--
19.1	C	814.6	613.6	242.0	0.78	0.1556	0.0009	7.3870	0.0554	0.3443	0.0017	1907	8	2409	9	1744	26
20.1	M	44.7	31.0	5.5	0.72	0.0800	0.0368	1.4400	0.6624	0.1307	0.0064	792	37	1201	910	1143	330
21.1	M	169.1	60.4	24.6	0.37	0.0784	0.0067	1.7700	0.1540	0.1635	0.0020	976	11	1157	170	954	110
23.1	M	77.7	58.8	22.8	0.78	0.1220	0.0031	5.6900	0.1707	0.3379	0.0054	1877	26	1986	45	1938	86

24.1	C	379.4	325.1	115.0	0.89	0.1247	0.0017	6.0240	0.0964	0.3504	0.0025	1936	12	2025	25	1895	55
25.1	C	497.8	37.7	212.0	0.08	0.1927	0.0015	13.1100	1.3110	0.4934	0.0031	2585	13	2765	13	2104	400
26.1	C	601.9	381.8	119.0	0.66	0.0855	0.0033	2.6900	0.1049	0.2281	0.0015	1325	8	1327	75	1209	54
27.1	C	401.6	301.3	123.0	0.78	0.1227	0.0033	5.9900	0.1677	0.3537	0.0027	1952	13	1996	47	1884	72
28.1	M	31.4	24.2	3.8	0.80	0.1360	0.0272	2.5000	0.5000	0.1336	0.0055	808	31	2172	350	1343	240
29.1	C	1715.1	229.4	429.0	0.14	0.1476	0.0007	5.9140	0.0337	0.2906	0.0010	1645	5	2318	7	1700	60
30.1	M	156.9	106.8	18.0	0.70	0.0660	0.0185	1.1400	0.3192	0.1245	0.0034	756	19	814	580	772	150
31.1	M	268.7	72.3	36.7	0.28	0.0760	0.0122	1.5900	0.2544	0.1524	0.0024	914	13	1085	310	692	310
32.1	M	147.8	94.0	17.9	0.66	0.0750	0.0135	1.4100	0.2538	0.1367	0.0026	826	15	1064	370	927	140
33.1	M	70.1	45.6	8.5	0.67	0.0650	0.0189	1.2200	0.3538	0.1355	0.0037	819	21	777	600	749	180
34.1	M	178.6	73.4	26.0	0.42	0.0780	0.0101	1.7700	0.2301	0.1638	0.0026	978	14	1158	260	1383	190
37.1	M	145.5	44.2	18.6	0.31	0.0950	0.0295	1.7400	0.5394	0.1321	0.0048	800	27	1534	580	1413	610
40.1	C	233.1	108.1	87.7	0.48	0.1674	0.0027	10.0600	0.1911	0.4358	0.0038	2332	17	2532	27	2331	110
32.2	C	421.0	333.9	48.7	0.82	0.0639	0.0062	1.1700	0.1147	0.1326	0.0013	803	8	737	210	738	50
35.1	M	44.0	34.4	5.6	0.81	0.1350	0.0297	2.6500	0.6095	0.1420	0.0054	856	30	2167	390	1431	310
36.1	M	121.4	75.7	12.6	0.64	0.0960	0.0269	1.4400	0.4032	0.1090	0.0034	667	20	1544	520	1027	210
38.1	M	112.6	68.6	13.2	0.63	0.0850	0.0170	1.5600	0.3120	0.1331	0.0025	805	14	1319	390	868	120
39.1	M	96.6	68.6	11.7	0.73	0.0720	0.0173	1.3200	0.3168	0.1338	0.0033	809	19	978	480	916	160
41.1	M	20.0	8.9	2.3	0.46	0.1360	0.0694	2.2000	1.1440	0.1200	0.0108	730	62	2174	890	1749	920
24.2	M	330.5	193.8	78.2	0.61	0.1240	0.0030	4.7000	0.1222	0.2750	0.0022	1566	11	2015	43	1694	39
30.2	C	504.9	499.2	56.9	1.02	0.0702	0.0037	1.2590	0.0680	0.1301	0.0010	788	6	934	110	775	24
11LJG3																	
1.1	M	140.4	86.3	16.0	0.64	0.0710	0.0107	1.2600	0.1890	0.1283	0.0019	778	11	966	310	827	120
2.1	M	141.5	80.4	14.8	0.59	0.0706	0.0054	1.1770	0.0906	0.1208	0.0017	735	10	947	150	739	55
3.1	M	778.5	475.2	82.0	0.63	0.0678	0.0018	1.1410	0.0319	0.1220	0.0007	742	4	863	57	737	20
4.1	C	657.9	472.6	71.6	0.74	0.0658	0.0022	1.1390	0.0387	0.1254	0.0008	762	4	801	71	711	19

5.1	M	527.1	361.2	58.5	0.71	0.0711	0.0018	1.2660	0.0329	0.1291	0.0009	783	5	961	52	802	16
6.1	C	308.2	171.1	34.6	0.57	0.0670	0.0154	1.1700	0.2691	0.1276	0.0026	774	15	826	480	737	180
7.1	M	188.7	106.6	21.1	0.58	0.0620	0.0112	1.0900	0.1962	0.1274	0.0022	773	12	679	380	721	120
8.1	M	415.2	292.8	44.4	0.73	0.0683	0.0010	1.1730	0.0188	0.1245	0.0009	757	5	878	30	776	12
9.1	C	1330.0	927.5	142.0	0.72	0.0625	0.0013	1.0620	0.0212	0.1233	0.0005	750	3	690	42	711	12
10.1	M	237.7	131.6	17.5	0.57	0.0550	0.0116	0.6100	0.1342	0.0812	0.0011	503	7	405	480	430	59
11.1	M	1138.3	881.6	123.0	0.80	0.0648	0.0020	1.1150	0.0346	0.1247	0.0007	758	4	769	65	755	20
12.1	M	777.7	511.8	84.8	0.68	0.0645	0.0032	1.1250	0.0563	0.1264	0.0008	768	5	759	100	733	29
13.1	M	648.8	452.7	71.9	0.72	0.0635	0.0058	1.1200	0.1030	0.1276	0.0012	774	7	724	200	727	52
14.1	M	622.0	404.1	68.0	0.67	0.0642	0.0044	1.1170	0.0771	0.1263	0.0009	766	5	747	140	730	36
17.1	C	148.4	84.5	18.2	0.59	0.0640	0.0205	1.2100	0.3872	0.1361	0.0034	823	19	756	680	871	230
18.1	C	735.1	657.0	82.3	0.92	0.0654	0.0033	1.1660	0.0583	0.1293	0.0008	784	5	788	100	758	22
19.1	C	260.8	168.9	28.8	0.67	0.0636	0.0062	1.1100	0.1077	0.1270	0.0014	771	8	729	200	744	65
20.1	C	677.0	815.5	12.6	1.24	0.0472	0.0066	0.1350	0.0189	0.0208	0.0002	133	1	60	340	131	9
21.1	C	36.8	29.6	4.8	0.83	0.0750	0.0608	1.4000	1.1340	0.1308	0.0085	793	48	1080	1600	693	420
22.1	M	400.0	286.3	45.6	0.74	0.0642	0.0077	1.1500	0.1380	0.1300	0.0014	788	8	750	260	794	62
6.2	M	201.2	130.3	22.3	0.67	0.0677	0.0081	1.1900	0.1428	0.1276	0.0018	774	11	859	260	727	78
4.2	M	2380.3	1485.2	258.0	0.64	0.0653	0.0065	1.1340	0.0147	0.1260	0.0010	765	6	783	21	729	9
12.2	C	2566.9	1856.4	271.0	0.75	0.0653	0.0065	1.1050	0.0111	0.1227	0.0004	746	2	785	21	710	5
23.1	C	3803.9	2568.4	73.6	0.70	0.0487	0.0030	0.1505	0.0093	0.0224	0.0001	143	1	133	140	144	6
24.1	M	526.9	320.2	58.1	0.63	0.0662	0.0015	1.1640	0.0279	0.1276	0.0009	774	5	812	48	728	15
5.2	C	968.1	1034.1	106.0	1.10	0.0639	0.0021	1.1200	0.0370	0.1271	0.0007	771	4	739	69	745	13
27.1	M	150.6	107.3	16.6	0.74	0.0710	0.0149	1.2200	0.2562	0.1235	0.0027	751	15	970	420	875	130
11LJG7																	
1.1	C	1380.3	1025.4	151.0	0.77	0.0640	0.0013	1.1140	0.0234	0.1262	0.0006	766	3	741	44	715	11
2.1	M	1493.7	925.5	158.0	0.64	0.0642	0.0026	1.0840	0.0444	0.1224	0.0006	744	4	749	86	716	26

3.1	C	1878.2	983.2	200.0	0.54	0.0646	0.0010	1.1020	0.0176	0.1237	0.0005	752	3	762	33	713	11
4.1	M	1424.2	931.4	142.0	0.68	0.0646	0.0012	1.0290	0.0185	0.1155	0.0005	704	3	763	38	673	10
5.1	M	1186.2	519.5	131.0	0.45	0.0628	0.0019	1.1050	0.0343	0.1277	0.0007	775	4	700	66	724	28
6.1	M	957.2	616.4	101.0	0.67	0.0651	0.0009	1.1010	0.0165	0.1226	0.0006	746	4	778	30	749	10
7.1	M	2184.0	1838.7	230.0	0.87	0.0633	0.0013	1.0650	0.0213	0.1220	0.0005	742	3	719	42	728	10
8.1	M	238.4	351.6	5.7	1.52	0.0970	0.0922	0.2800	0.2688	0.0209	0.0023	133	14	1560	1800	151	63
9.1	M	723.0	386.9	80.0	0.55	0.0649	0.0007	1.1520	0.0138	0.1288	0.0007	781	4	770	23	807	16
10.1	M	2808.3	2269.3	294.0	0.83	0.0669	0.0011	1.1230	0.0191	0.1219	0.0004	741	2	834	34	710	9
14.1	M	572.1	314.9	61.8	0.57	0.0671	0.0031	1.1540	0.0531	0.1246	0.0009	757	5	842	96	740	36
15.1	C	477.1	1364.0	8.8	2.95	0.0430	0.0323	0.1180	0.0885	0.0197	0.0007	126	5	-140	1900	118	10
17.1	C	1142.6	518.9	126.0	0.47	0.0681	0.0029	1.1990	0.0504	0.1277	0.0007	775	4	872	86	751	37
24.1	M	1674.6	1030.9	182.0	0.64	0.0660	0.0013	1.1510	0.0230	0.1265	0.0008	768	4	807	39	750	13
19.1	C	785.7	352.8	84.9	0.46	0.0641	0.0060	1.1000	0.1034	0.1244	0.0011	756	6	746	200	711	82
8.2	C	1611.5	4107.5	28.4	2.63	0.0451	0.0044	0.1260	0.0122	0.0202	0.0002	129	1	-49	240	121	2
22.1	M	2006.5	1767.6	216.0	0.91	0.0646	0.0006	1.1100	0.0222	0.1247	0.0021	757	12	760	20	723	13
17.2	M	651.2	358.1	70.2	0.57	0.0630	0.0020	1.0800	0.0356	0.1243	0.0015	755	9	708	66	707	22
25.1	M	1205.6	363.9	122.0	0.31	0.0628	0.0026	1.0060	0.0423	0.1163	0.0007	709	4	700	88	698	48
1303LJG2																	
1.1	C	301.4	252.9	34.8	0.87	0.0664	0.0009	1.2280	0.0184	0.1341	0.0012	811	7	820	26	776	10
2.1	C	194.8	311.4	22.3	1.65	0.0668	0.0018	1.2280	0.0356	0.1333	0.0013	807	7	831	57	774	10
3.1	C	312.7	147.1	32.4	0.49	0.0641	0.0012	1.0620	0.0223	0.1202	0.0011	732	6	745	39	853	16
4.1	M	352.2	388.5	42.4	1.14	0.0766	0.0034	1.4470	0.0666	0.1370	0.0012	828	7	1111	90	874	18
5.1	C	298.2	144.2	35.1	0.50	0.0638	0.0008	1.2030	0.0180	0.1367	0.0012	826	7	735	26	818	12
6.1	C	164.1	125.6	19.0	0.79	0.0625	0.0019	1.1580	0.0371	0.1343	0.0013	812	8	693	64	800	18
7.1	C	69.7	55.1	8.6	0.82	0.0620	0.0025	1.2170	0.0499	0.1424	0.0017	858	10	673	85	833	24
8.1	M	505.3	321.1	56.2	0.66	0.0650	0.0008	1.1570	0.0197	0.1292	0.0013	783	7	774	28	841	13

9.1	C	221.9	251.9	25.6	1.17	0.0657	0.0009	1.2150	0.0207	0.1342	0.0012	812	7	797	30	787	10
10.1	C	100.3	100.5	11.7	1.03	0.0649	0.0019	1.2150	0.0377	0.1357	0.0015	821	9	773	62	827	21
11.1	C	368.7	353.1	41.0	0.99	0.0660	0.0009	1.1750	0.0188	0.1291	0.0011	783	6	807	27	763	9
12.1	M	208.3	140.8	23.2	0.70	0.0645	0.0012	1.1530	0.0242	0.1296	0.0012	786	7	759	39	779	19
13.1	C	515.1	523.8	59.1	1.05	0.0640	0.0007	1.1760	0.0165	0.1334	0.0011	807	6	740	23	782	9
1202LJG3																	
1.1	C	221.0	78.7	24.2	0.37	0.0632	0.0015	1.1070	0.0277	0.1271	0.0010	771	6	715	50	769	22
2.1	C	166.9	152.9	17.5	0.95	0.0660	0.0020	1.1080	0.0343	0.1216	0.0010	740	6	808	62	734	15
3.1	C	139.3	34.1	14.4	0.25	0.0650	0.0016	1.0770	0.0280	0.1201	0.0012	731	7	776	52	682	28
4.1	C	373.9	55.0	39.8	0.15	0.0648	0.0011	1.1020	0.0187	0.1235	0.0007	750	4	767	35	712	33
5.1	C	214.5	55.0	23.7	0.27	0.0638	0.0021	1.1250	0.0383	0.1279	0.0009	776	5	735	70	670	38
6.1	C	38.4	56.8	4.4	1.53	0.0712	0.0056	1.3000	0.1027	0.1326	0.0024	802	13	963	160	854	31
7.1	C	82.8	73.6	9.0	0.92	0.0585	0.0041	1.0070	0.0715	0.1248	0.0015	758	9	550	150	769	29
8.1	C	195.4	42.5	20.1	0.22	0.0631	0.0015	1.0390	0.0260	0.1195	0.0009	728	5	711	50	746	32
9.1	M	68.0	35.2	7.4	0.54	0.0682	0.0049	1.1760	0.0858	0.1251	0.0016	760	9	874	150	812	56
10.1	M	98.7	106.8	10.4	1.12	0.0550	0.0253	0.7900	0.3634	0.1043	0.0023	640	14	400	1000	702	97
11.1	M	57.2	29.5	6.9	0.53	0.0656	0.0036	1.2540	0.0715	0.1387	0.0019	837	11	793	120	932	46
12.1	C	209.8	51.9	22.3	0.26	0.0649	0.0019	1.1040	0.0342	0.1233	0.0009	749	5	772	63	756	55
13.1	M	71.9	61.5	8.3	0.88	0.0648	0.0017	1.2030	0.0349	0.1347	0.0015	815	9	768	56	860	19
1209LJG5																	
1.1	M	19.1	10.6	2.0	0.57	0.0586	0.0064	0.9900	0.1089	0.1223	0.0028	744	16	554	230	651	65
2.1	M	147.4	145.1	14.9	1.02	0.0640	0.0014	1.0340	0.0238	0.1172	0.0008	715	5	741	47	682	10
3.1	M	46.5	38.8	4.7	0.86	0.0657	0.0031	1.0690	0.0513	0.1180	0.0014	719	8	797	98	747	18
4.1	M	117.9	47.9	13.2	0.42	0.0635	0.0023	1.1330	0.0419	0.1295	0.0010	785	6	724	76	800	55
5.1	C	121.1	107.1	14.4	0.91	0.0662	0.0019	1.2600	0.0365	0.1380	0.0012	833	7	813	58	841	17
6.1	M	55.8	30.7	12.6	0.57	0.1283	0.0021	4.6460	0.0976	0.2626	0.0032	1503	17	2075	29	1100	33

7.1	M	64.7	26.7	7.7	0.43	0.0680	0.0020	1.2950	0.0414	0.1381	0.0018	834	10	869	62	1071	32
8.1	M	61.8	45.3	20.9	0.76	0.1225	0.0018	6.6300	0.1193	0.3927	0.0043	2135	20	1994	26	2143	44
9.1	C	20.1	17.5	2.4	0.90	0.0769	0.0050	1.4900	0.1028	0.1401	0.0032	845	19	1118	130	906	40
10.1	C	581.2	725.1	184.0	1.29	0.1238	0.0006	6.2930	0.0422	0.3686	0.0017	2023	8	2012	9	2106	17
11.1	M	82.7	41.7	9.9	0.52	0.0694	0.0022	1.3280	0.0438	0.1389	0.0017	838	9	910	64	810	27
12.1	M	132.9	76.6	22.5	0.60	0.1013	0.0030	2.7280	0.0846	0.1953	0.0019	1150	10	1648	55	1198	53
13.1	M	27.8	18.8	3.3	0.70	0.0666	0.0041	1.2460	0.0797	0.1357	0.0028	820	16	825	130	805	39
14.1	C	926.4	371.1	277.0	0.41	0.1327	0.0006	6.3540	0.0343	0.3474	0.0010	1922	5	2133	8	1885	20
15.1	C	648.9	666.5	173.0	1.06	0.1209	0.0011	5.1610	0.0568	0.3095	0.0017	1738	8	1970	16	1612	26
6.2	C	198.9	27.8	73.7	0.14	0.1641	0.0018	9.7600	0.1269	0.4314	0.0030	2312	13	2498	19	2198	56
7.2	C	197.6	138.1	24.0	0.72	0.0647	0.0017	1.2590	0.0340	0.1410	0.0013	851	7	766	54	836	18

C: core; M: mantle; --: no data. Common Pb corrected using measured [204]Pb.

Supplementary Table 8

Supplementary Table 8. MC-ICPMS zircon Hf isotope data for the meta-basites and meta-granitoids from Longjingguan.

Sample	$^{176}Yb/^{177}Hf$	$^{176}Lu/^{177}Hf$	$^{176}Hf/^{177}Hf$	±(2s)	Age (Ma)	$\varepsilon_{Hf}(t)$	±(2σ)	T_{DM1}(Ma)	±(2σ)	$f_{Lu/Hf}$	T_{DM2}(Ma)	±(2σ)
	0.0387	0.001604	0.282230	0.000043	783	-2.4	0.8	1466	61	-0.95	1853	95
	0.0806	0.001937	0.282118	0.000033	807	-6.5	0.6	1640	48	-0.94	2114	74
	0.0398	0.001477	0.282127	0.000033	783	-6.0	0.6	1607	47	-0.96	2079	73
	0.0988	0.002446	0.282211	0.000031	807	-3.5	0.6	1527	45	-0.93	1923	68
1303LJG2	0.0377	0.001614	0.282215	0.000030	811	-2.9	0.5	1488	43	-0.95	1889	67
	0.0593	0.002007	0.282092	0.000028	828	-7.5	0.5	1679	40	-0.94	2172	62
	0.0557	0.001634	0.282337	0.000023	858	1.4	0.4	1316	33	-0.95	1618	51
	0.0345	0.001251	0.282329	0.000019	811	1.3	0.3	1313	26	-0.96	1622	42
	0.1109	0.002578	0.282078	0.000041	749	-8.3	0.7	1727	59	-0.92	2213	91
	0.0269	0.001198	0.282069	0.000041	731	-7.9	0.7	1676	57	-0.96	2186	90
	0.0548	0.001727	0.282058	0.000039	802	-8.5	0.7	1715	55	-0.95	2227	86
1202LJG3	0.0238	0.000765	0.282017	0.000035	758	-9.5	0.6	1729	49	-0.98	2287	78
	0.0392	0.001070	0.282130	0.000032	728	-5.6	0.6	1585	45	-0.97	2047	71
	0.0490	0.001369	0.282025	0.000031	776	-9.5	0.6	1746	44	-0.96	2290	69
	0.0981	0.002896	0.282131	0.000034	771	-6.6	0.6	1663	49	-0.91	2104	75
	0.0226	0.000939	0.282059	0.000042	744	-8.1	0.8	1678	58	-0.97	2199	93
	0.0150	0.000460	0.281940	0.000028	715	-12.0	0.5	1820	39	-0.99	2446	62
1209LJG5	0.0295	0.001109	0.281978	0.000025	820	-11.0	0.5	1799	35	-0.97	2384	56
	0.0154	0.000590	0.282013	0.000024	845	-9.5	0.4	1726	33	-0.98	2289	52
	0.0241	0.000735	0.281304	0.000041	1738	3.3	0.8	2702	56	-0.98	2823	90

	0.0277	0.000773	0.281558	0.000039	2030	0.6	0.7	2359	54	-0.98	2574	86
	0.0266	0.000877	0.281363	0.000030	1922	5.1	0.6	2631	41	-0.97	2710	65
	0.0388	0.001323	0.282144	0.000024	798	-5.3	0.4	1575	34	-0.96	2023	54
	0.0136	0.000572	0.282078	0.000028	834	-7.2	0.5	1636	39	-0.98	2145	63
	0.0407	0.001459	0.282071	0.000026	810	-7.9	0.5	1685	36	-0.96	2191	57
11LJG2	0.0184	0.000737	0.281996	0.000029	837	-10.2	0.5	1756	41	-0.98	2332	65
	0.0740	0.002359	0.282219	0.000022	803	-3.2	0.4	1513	32	-0.93	1893	49
	0.0156	0.000652	0.281418	0.000022	2492	7.1	0.4	2542	30	-0.98	2506	48
	0.0067	0.000306	0.281316	0.000022	2304	4.1	0.4	2656	29	-0.99	2690	48
	0.0237	0.001066	0.281363	0.000019	1907	-6.6	0.4	2643	26	-0.97	3758	42
	0.009640	0.000425	0.282450	0.000019	778	5.6	0.3	1118	26	-0.99	1326	41
	0.031623	0.001417	0.282520	0.000018	746	7.6	0.3	1049	25	-0.96	1203	40
11LJG3	0.015560	0.000686	0.282458	0.000018	774	5.8	0.3	1114	26	-0.98	1316	41
	0.018829	0.000831	0.282519	0.000020	762	7.9	0.4	1033	28	-0.97	1184	45
	0.017119	0.000886	0.282411	0.000021	774	4.0	0.4	1187	30	-0.97	1429	48
	0.030741	0.001317	0.282453	0.000020	750	5.3	0.4	1140	29	-0.96	1347	45
	0.011368	0.000510	0.282476	0.000014	766	6.5	0.3	1085	20	-0.98	1271	32
	0.018567	0.000814	0.282433	0.000017	741	4.8	0.3	1153	24	-0.98	1377	39
11LJG7	0.027072	0.001152	0.282425	0.000018	775	4.3	0.3	1175	26	-0.97	1405	40
	0.023857	0.001042	0.282428	0.000019	744	4.5	0.3	1168	27	-0.97	1396	43
	0.041313	0.001769	0.282501	0.000020	752	6.7	0.4	1085	29	-0.95	1256	45

0.021598	0.000954	0.282501	0.000022	746	7.1	0.4	1062	30	-0.97	1229	48
0.031613	0.001363	0.282378	0.000018	742	2.6	0.3	1248	25	-0.96	1518	39
0.017878	0.000776	0.282469	0.000020	781	6.1	0.4	1101	28	-0.98	1294	44

$\varepsilon_{Hf}(t)$ values are calculated at 780 Ma and 800 Ma for meta-basites and meta-granitoids, respectively, and at the zircon U-Pb ages for the older inherited zircon domains. Age data were obtained by in-situ zircon SHRIMP U-Pb analyses.

Supplementary Table 9. Sr-Nd isotope compositions for the meta-basites from Longjingguan.

Sample	Rb (ppm)	Sr(ppm)	^{87}Rb/^{86}Sr	^{87}Sr/^{86}Sr	(^{87}Sr/^{86}Sr)$_i$	Sm (ppm)	Nd (ppm)	^{147}Sm/^{144}Nd	^{143}Nd/^{144}Nd	ε_{Nd}(t)	T_{DM1} (Ma)	T_{DM2} (Ma)
11LJG3	16.0	320	0.1423	0.705386	0.7049	9.64	35.9	0.1626	0.512559	-0.5	1768	1051
11LJG4	29.6	129	0.7176	0.708677	0.7063	4.15	13.1	0.1888	0.512532	-1.8	3773	1156
11LJG5	27	261	0.2865	0.707254	0.7063	4.54	16.8	0.1606	0.512674	1.8	1368	862
11LJG6	62.9	116	1.6997	0.709376	0.7038	4.17	16.3	0.1541	0.512511	-1.2	1634	1106
11LJG7	32.9	87	1.2153	0.706262	0.7023	4.53	17.5	0.1515	0.512546	-0.5	1483	1044
11LJG8	27.7	225	0.3828	0.707910	0.7067	5.32	19.8	0.1611	0.512634	1.0	1498	927

Supplementary Table 10. Pb isotopic compositions for the meta-basites from Longjingguan.

Sample	$^{206}Pb/^{204}Pb$	$^{207}Pb/^{204}Pb$	$^{208}Pb/^{204}Pb$	Pb(ppm)	Th(ppm)	U(ppm)	$(^{206}Pb/^{204}Pb)_i$	$(^{207}Pb/^{204}Pb)_i$	$(^{208}Pb/^{204}Pb)_i$
11LJG3	17.127	15.403	38.119	9.34	1.91	0.70	16.959	15.394	37.969
11LJG4	17.046	15.397	38.149	10.20	1.27	0.60	16.914	15.391	38.058
11LJG5	17.192	15.424	38.209	4.83	1.73	0.38	17.015	15.415	37.946
11LJG6	17.216	15.405	38.304	3.45	2.34	0.57	16.843	15.386	37.806
11LJG7	17.308	15.440	38.344	2.36	1.65	0.34	16.982	15.424	37.829
11LJG8	17.235	15.467	38.190	7.48	1.80	0.43	17.105	15.460	38.013